International Journal of Antennas and Propagation

Compact Microstrip Antenna Structures with Multiband, Broadband, and Band-Notched Properties, for Portable Devices

Guest Editors: Alistair P. Duffy, Mohammad Naser-Moghadasi, Jalil Rashed-Mohassel, and Bal Singh Virdee

Compact Microstrip Antenna Structures with Multiband, Broadband, and Band-Notched Properties, for Portable Devices

International Journal of Antennas and Propagation

Compact Microstrip Antenna Structures with Multiband, Broadband, and Band-Notched Properties, for Portable Devices

Guest Editors: Alistair P. Duffy, Mohammad Naser-Moghadasi, Jalil Rashed-Mohassel, and Bal Singh Virdee

Editorial Board

Contents

Hindawi Publishing Corporation
International Journal of Antennas and Propagation
Volume 2014, Article ID 419565, 1 page
http://dx.doi.org/10.1155/2014/419565

Editorial

Compact Microstrip Antenna Structures with Multiband, Broadband, and Band-Notched Properties, for Portable Devices

Alistair P. Duffy,[1] Mohammad Naser-Moghadasi,[2] Jalil Rashed-Mohassel,[3] and Bal Singh Virdee[4]

[1] *De Montfort University, Leicester LE1 9BH, UK*
[2] *Islamic Azad University, Science and Research Branch, Tehran, Iran*
[3] *University of Tehran, Iran*
[4] *London Metropolitan University, UK*

Correspondence should be addressed to Alistair P. Duffy; apd@dmu.ac.uk

Received 18 March 2014; Accepted 18 March 2014; Published 14 April 2014

It is difficult to list all the current applications for microstrip antennas; it could be said that they are the transducers that control modern life. Yet, every year, new applications are required which challenge the performance limits of current designs. Some of those challenges are associated with controlling the spectrum performance and continuing to seek techniques to tailor the shape to the applications.

This special issue brings some of the latest thinking in compact microstrip antenna design. However, the variety of approaches presented in the papers shows the possibilities that exist for future developments: this special issue is as much about setting out possibilities as it is about presenting new thinking.

The papers in this special issue are as follows. An approach to design microstrip antennas is presented in *"Design of arbitrarily shaped planar microstrip antenna arrays with improved efficiency"* which considers improved radiation efficiency. Focusing on the application areas of Bluetooth and WLAN, a dual-band planar inverted-E antenna (PIEA) is presented in *"Compact dual-band planar inverted-e-shaped antenna using defected ground structure"* with a novel ground. A mesh grid structure planar wideband zero index metamaterial (ZIM) antenna is presented in *"Zero index metamaterial for designing high-gain patch antenna"* that provides a bandwidth of 9.9 GHz to 11.4 GHz.An arc H-shaped slot on the radiating patch provides dual band-notched characteristics which is discussed in *"Design and analysis of a novel dual band-notched UWB antenna."* The paper entitled *"Printed modified bow-tie dipole antenna for DVB/WLAN applications"* presents a printed modified bow-tie dipole antenna which consists of asymmetric feed and inserted slots. A frequency range of 3.1–10.6 GHz is achieved by an antenna of only 30 mm × 36 mm and is discussed in *"A compact UWB diversity antenna."* A modified compact planar ultrawideband (UWB) monopole antenna with triple controllable band-notched characteristics is presented in *"A compact planar UWB antenna with triple controllable band-notched characteristics,"* which consists of a modified staircased V-shaped radiating element and partial ground plane. The radiation pattern is controlled using elliptical and rectangular patches, which is discussed in *"A compact size 4–19.1 GHz heart shape UWB antenna with triangular patches."*

Acknowledgments

The editors would like to extend their gratitude to the many anonymous referees and to the authors for responding so positively to the questions asked and the suggestions made by those referees.

Alistair P. Duffy
Mohammad Naser-Moghadasi
Jalil Rashed-Mohassel
Bal Singh Virdee

Hindawi Publishing Corporation
International Journal of Antennas and Propagation
Volume 2014, Article ID 848062, 10 pages
http://dx.doi.org/10.1155/2014/848062

Research Article

A Compact Planar UWB Antenna with Triple Controllable Band-Notched Characteristics

Chaabane Abdelhalim[1] and Djahli Farid[2]

[1] *Laboratoire des Télécommunications, Faculté des Sciences et de la Technologie, Université 8 mai 1945 Guelma, 24000 Guelma, Algeria*
[2] *Laboratoire LIS, Faculté de Technologie, Université Ferhat Abbas Sétif, 19000 Sétif, Algeria*

Correspondence should be addressed to Chaabane Abdelhalim; chaabaneabdelhalim@yahoo.fr

Received 27 May 2013; Revised 14 December 2013; Accepted 22 December 2013; Published 6 February 2014

Academic Editor: Rashed Mohassel

A modified compact planar ultrawideband (UWB) monopole antenna with triple controllable band-notched characteristics is presented in this paper. The proposed antenna consists of a modified stair cased V-shaped radiating element and partial ground plane. The triple band-notched characteristics are achieved by embedding two different vertical up C-shaped slots with a vertical down C-shaped slot in the radiating patch and in the ground plane, respectively. Besides, the bandwidth of each rejected band can be independently controlled by adjusting the dimensions of the corresponding band notched structure. The proposed antenna with rejected bands characteristics is successfully simulated, prototyped, and measured. The measured results show that the antenna operates until upper 11 GHz for voltage standing wave ratio (VSWR) is less than 2, and exhibits bands rejection of 1.6–2.66 GHz (49.76%), 3-4 GHz (28.57%), and 5.13–6.03 GHz (16.12%). Moreover, the proposed antenna shows a near omnidirectional radiation patterns, stable peak gain, and with small group delay and transfer function variation on the whole UWB frequency range except in the notched frequency bands, which makes it suitable for being used in the future UWB applications.

1. Introduction

Ultrawideband (UWB) is specified in the Federal Communication Commission (FCC) [1] as the frequency band that ranges from 3.1 GHz to 10.6 GHz, which is a 7.5 GHz bandwidth (BW). Several planar UWB monopole antennas, which have the potential to meet such requirements, were reported in [2–5]. Due to the overlap of the currently allocated UWB frequency band with the communication systems such as Wireless Local Area Network (WLAN) bands in the 2.4 GHz (2.4–2.484 GHz), 5.2 GHz (5.15–5.35 GHz), and 5.8 GHz (5.725–5.825 GHz) bands, and the World Interoperability for Microwave Access (WiMAX) system bands 2.5 GHz (2.5–2.69 GHz), 3.5 GHz (3.4–3.69 GHz), and 5.8 GHz (5.25–5.825 GHz) [6]. Now, many systems operate across several frequency bands, requiring a band-notched or band-rejected function. Thus, it is desirable to design UWB antennas with band notch characteristics to avoid potential interferences from the other frequency bands. To overcome problems caused by this electromagnetic interference, several designs of UWB antennas with single or multiple notch functions have been proposed in recent literature [6–39]. Reviewing the literature shows that there are few ways for monopole planar antennas to achieve band-notched characteristics. The most popular approach is cutting different shaped slots from the radiating patch, from the ground plane, or from the feed line, that is, U-shaped slot [7], a Hilbert-curve shaped slot [8], cutting a wide line [9], T-shaped slot [10], defected ground structure (DGS) [11], semicircular slot [12], a bent slot or C-shaped slot [13–15], split ring in the ground plane [16], and slot line in the feed line [17]). Another way consists of loading diverse parasitic elements on the antenna, such as parasitic elements rear or near the radiating element [18–23], and near the feed line [24–33], to generate the band-notched

feature, which acts as resonator when the length of strip is about a half or a quarter of the guided wavelength at the desired notch frequency. In reference [31], a band-notched characteristic has been achieved by coupling a pair of open-loop resonators beside the feed line, in this reference, the author just notched the band for WLAN system. In reference [32], one set of band rejected structure with two C-shaped slots has been adopted to reject the lower WLAN band (5.15–5.35 GHz) and another one with two splits inverted resonators has been employed to reject the upper WLAN band (5.725–5.825 GHz). In reference [33], two splits rectangular ring resonators have been placed close to the microstrip line to reject the band 5.02–6.05 GHz. Additionally, a straight line slit has been etched on the radiating patch to reject the band 2.52–3.66 GHz; by using this technique, the control of this rejected band is limited by few key design parameters, and by the space restriction of the radiating patch to avoid this drawback and to get more freedom in designing, it is better to use another shape slit. In reference [34], only one notched band centered at 5.5 GHz is achieved by etching a partial annular slot in the lower portion of a ring radiator. Most of UWB antennas have no more than two notched bands, and few of them have three notched bands [35–37], which reveal that potential interference from other narrow bands may still exist. So, to design an antenna for UWB applications with notching all the bands for WiMAX and WLAN systems is necessary. In reference [35], three parasitic resonant elements are placed near the ground plane to generate three notch frequency bands 3.26–3.71 GHz, 5.15–5.37 GHz, and 5.78–5.95 GHz; in this reference, the bands 2.4/2.5 GHz corresponding to WLAN and WiMAX have not been rejected, and the use of parasitic resonators leads to a more complex structure. In reference [36], a compact UWB antenna with triple band rejected characteristics is achieved with using a meander line split ring resonator, with using this technique three bands 3.15–3.75, 4.85–6.08, and 7.98–8.56 GHz are rejected. The meander line split ring resonator used in this reference is complex compared to a conventional C-shaped slot structure. In reference [37], a pair of spiral loop resonators have been merged with radiating patch to create the first notched band in 3.3–3.7 GHz, in addition, two integrated microstrip resonators have been coupled with ground plane to generate the second and the third-notched bands in 5.2–5.4 GHz and 5.7–6 GHz. All the techniques can achieve good band notch characteristics, but some of the notched band structures are complex and difficult to design. In the designing of triple or multiband notch antenna, it is difficult to adjust and to control the frequency center of the notch bands in a limited space. Moreover, strong couplings between the band-notched characteristics designs for adjacent frequencies are the complication in achieving efficient triple band-notched UWB antenna. There are a lot of researches on UWB antennas with band-notched characteristics [6–39], but how to obtain high efficient band-notched characteristics is still a challenging issue. The main problem of the band rejected function design is the difficulty of controlling bandwidth and the shifting of the notched band, especially for the case of antennas with several rejected band structures, without infecting other rejected bands.

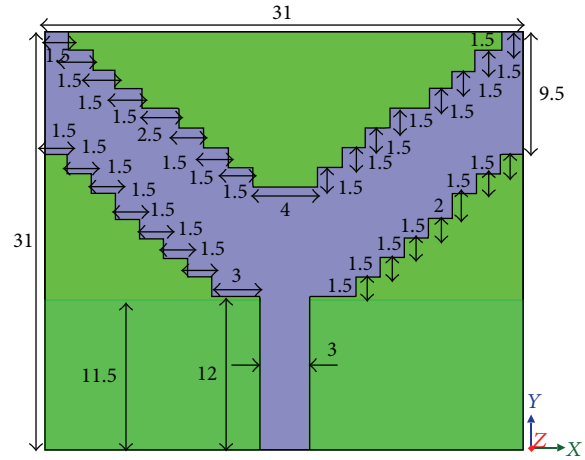

Figure 1: Geometry of the proposed UWB antenna without band rejected structure.

In the future, we expect that the shifting and the control of the frequency center and the bandwidth of the band-notched frequency can be both important and useful in wireless communication systems. So, the aim of this paper is to design a low cost and simple structure UWB antenna with controllable triple band-notched characteristics and an independent control of the width and the shifting of the rejected bands. We propose a compact microstrip-fed planar UWB antenna with modified stair cased V-shaped radiating elements and partial ground plane. To simplify the adjustment of the parameters of the rejected band structures and to obtain high efficient band-notched characteristics, three simple rejected band structures are investigated in this paper. So, three frequency bands notched are achieved with the investigation of these structures; the first rejected band (1.6–2.66 GHz) is achieved by inserting the vertical down C-shaped slot in the ground plane, two others rejected bands (3-4 GHz and 5.13–6.03 GHz) are realized by inserting two vertical up C-shaped slots in the radiator patch. The desired frequency notched bands can be easily achieved and flexibly controlled by adjusting the total length of the corresponding band-notched structure. The designed antenna with optimal dimensions was prototyped and measured. A comparison between experimental and simulated results of the voltage standing wave ratio is achieved. The remaining of this paper is organized as follows. Section 2 presents the configuration of the proposed antenna; parametric study is investigated in Section 3. The simulated and measured results are discussed in Section 4, and finally the conclusion is provided in Section 5.

2. Antenna Configuration

Figure 1 shows the geometry of the proposed compact planar UWB monopole antenna without rejecting band structures. The proposed UWB antenna is located on the x–y plane and the normal direction is parallel to z-axis. This antenna is fabricated on a low-cost FR4 epoxy substrate with the

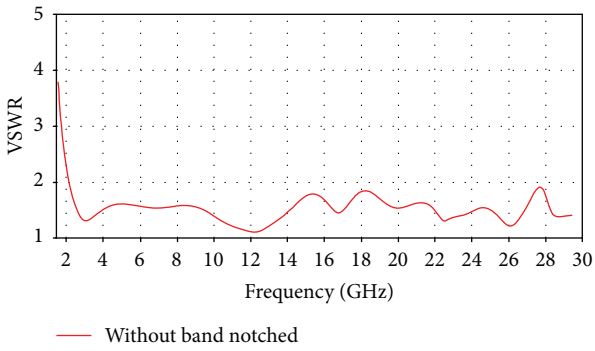

Figure 2: Simulated VSWR of the reference antenna without band-rejected characteristics.

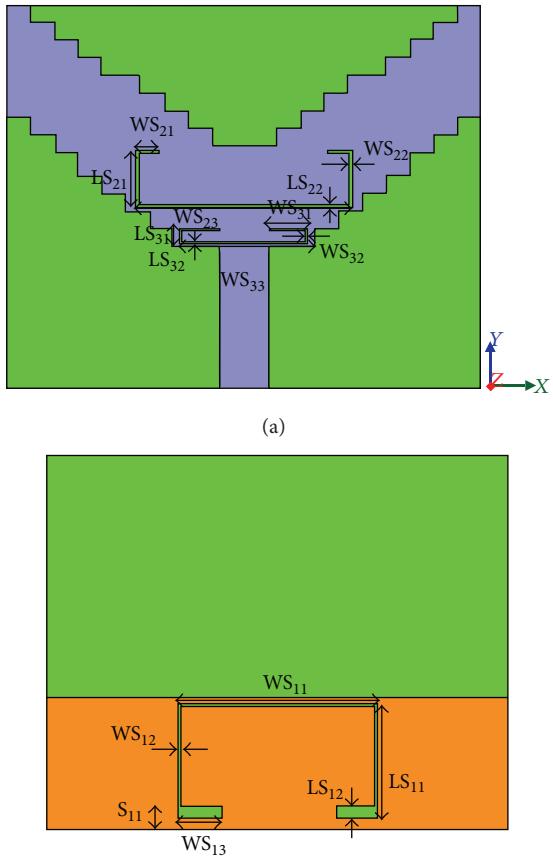

Figure 3: The geometry of the proposed triple band-notched antenna: (a) top view and (b) bottom view.

thickness of 1.6 mm, relative dielectric constant of 4.4, and loss tangent of 0.008. On the front surface of the substrate of each UWB antenna, a modified stair cased V-shaped radiating element is printed, fed by a microstrip line 50 Ω with 3 mm of width. The ground plane size is $31 \times 11.5\ \text{mm}^2$, and the distance between the radiating patch to the ground plane printed on the back surface substrate is 0.5 mm.

The simulated voltage standing wave ratio (VSWR) of the reference UWB antenna without band-rejected is presented in Figure 2. The parameters of the reference antenna are

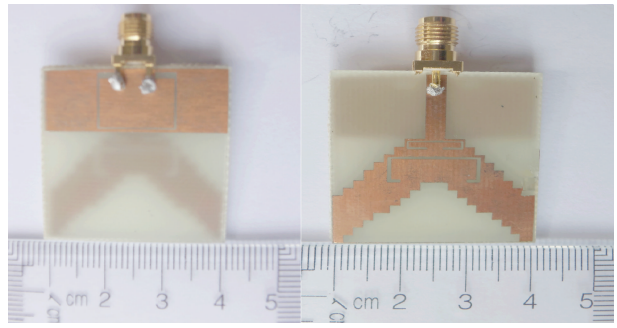

Figure 4: Top and bottom view of the fabricated sample of the proposed antenna.

optimized to get a VSWR that is less than 2 and to get stable radiation characteristics throughout the frequency band 2.1 GHz to upper than 30 GHz.

To overcome the unwanted electromagnetic interferences of UWB communication systems with WLAN and WiMAX frequencies band, two half wavelength vertical up C-shaped slots are inserted in the radiating patch with a half wavelength vertical down C-shaped slot that is embedded in the ground plane. The geometry of the proposed triple band-notched antenna is depicted in Figure 3. The HFSS software is employed to perform the design process.

The total length of each slot can be deduced by (1), which is based on the author's previous works like in [18]. The slots resonate at the corresponding band notching frequency, where its total length is equal to a half wavelength as follows:

$$L_{\text{Total}} = \frac{c}{2 f_{\text{notch}} \sqrt{\varepsilon_{\text{eff}}}}, \tag{1}$$

where

$$\varepsilon_{\text{eff}} = \frac{\varepsilon_r + 1}{2}. \tag{2}$$

And L_{Total} denotes the total length of the corresponding slot; ε_{eff} is the effective dielectric constant of the substrate; and c is the speed of light in free space.

3. Parametric Study

A parametric study of the proposed triple band-notched UWB antenna was carried out in order to control the band rejection operation. It is necessary to control the notched bandwidths in practical application to obtain an effective band-notched UWB antenna. Therefore, the rejected bandwidths based on the dimensions of the corresponding notched band structure are studied. By adjusting the total length of each slot to be about a half-wavelength at the desired notched frequency, a destructive interference can take place, and triple band-notched characteristics at 2.2/3.54/5.68 GHz frequencies center are achieved. Details of the influence of each parameter on the proposed triple band-notched antenna will be studied in this section. The discussed parameter is changed, and the other parameters are kept unchanged.

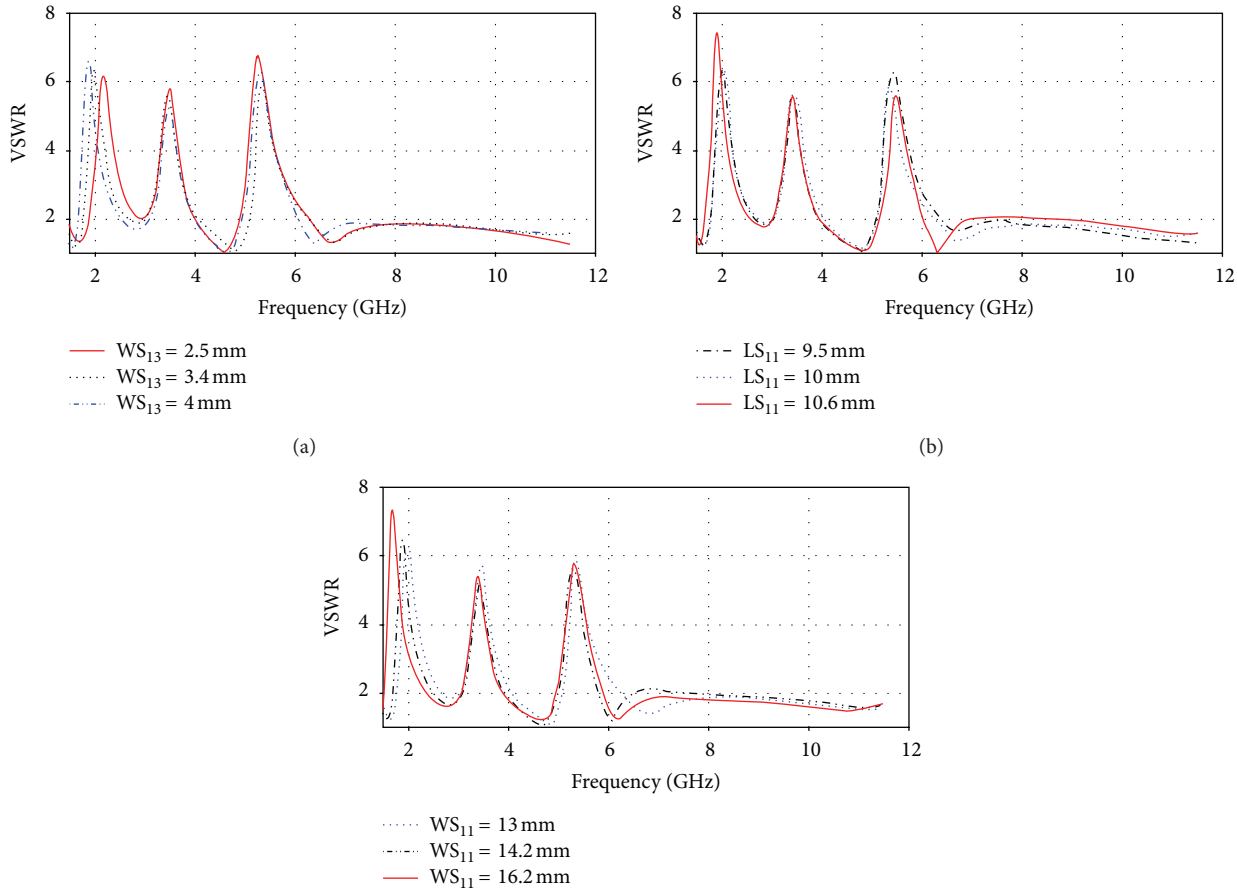

FIGURE 5: The simulated VSWR of the proposed antenna: effects of some parameters on the 2.2 GHz band-notched function, (a) WS_{13}, (b) LS_{11}, (c) WS_{11}.

3.1. Controlling the First Rejected Band Generated by the Vertical down C-Shaped Slot. Figures 5(a), 5(b), and 5(c) show the simulated VSWR with changing WS_{13}, LS_{11}, and WS_{11} on the 2.2 GHz frequency center band. When WS_{13} increases, the center of the first rejected band 2.2 GHz shifts slightly for lower frequencies side: from 2.37 GHz for WS_{13} = 2.5 mm to 2.1 GHz for WS_{13} = 4 mm. We observe the same effect when LS_{11} increases: the center of the first rejected band shifts slightly from 2.2 GHz for LS_{11} = 9.5 mm to 2.16 GHz for LS_{11} = 10.6 mm. In addition, the lower rejected bandwidth shifts slightly for lower frequencies side with increasing WS_{11}: from 2.2 GHz for WS_{11} = 13 mm to 2 GHz for WS_{11} = 16.2 mm. The first notched band width is decided by WS_{13}, LS_{11}, and WS_{11}. On the other hand, we can observe that the parameters WS_{13}, LS_{11}, and WS_{11} have small influences for the two other rejected bands 3.54 GHz and 5.68 GHz.

3.2. Controlling the Second Rejected Band Generated by the Upper Vertical up C-Shaped Slot. Figures 6(a), 6(b), and 6(c) show the simulated VSWR with changing WS_{21}, LS_{21}, and WS_{23} on the second rejected band 3.54 GHz. When WS_{21} increases, the center of the second rejected band 3.54 GHz shifts for lower frequencies side: from 3.54 GHz for WS_{21} = 1.4 mm to 2.6 GHz for WS_{21} = 5.9 mm. We observe the same effect when LS_{21} increases: the center of the second rejected band 3.54 GHz shifts from 3.9 GHz for LS_{21} = 2.2 mm to 3.54 GHz for LS_{21} = 4.7 mm. In addition, the second rejected bandwidth becomes wider when WS_{23} increases, and the center of the lower rejected band shifts for lower frequencies side: the width of the lower rejected band increases from 0.45 GHz for WS_{23} = 10.8 mm to 1 GHz for WS_{23} = 13.8 mm. From the discussion above, the parameters WS_{21}, LS_{21}, and WS_{23} are the most important parameters of second notched bandwidth 3.54 GHz, and it can be independently adjusted by changing these three parameters. On the other hand, we can observe that the parameters WS_{21}, LS_{21}, and WS_{23} have very small influences for the 2.2 GHz and 5.68 GHz rejected bands.

3.3. Controlling the Third Rejected Band Generated by the Lower Vertical up C-Shaped Slots. Figures 7(a), 7(b), and 7(c) show the simulated VSWR with changing WS_{31}, LS_{31}, and WS_{33} on the third rejected band 5.68 GHz. When WS_{31} increases the center of the third rejected band shifts for lower frequencies side: from 5.91 GHz for WS_{31} = 2.4 mm to 5.48 GHz for WS_{31} = 3 mm. We observe the same effect when LS_{31} increases: the center of the third rejected band shifts from 5.82 GHz for LS_{31} = 0.65 mm to 5.42 GHz for LS_{31} = 1.55 mm. In addition, the third rejected bandwidth

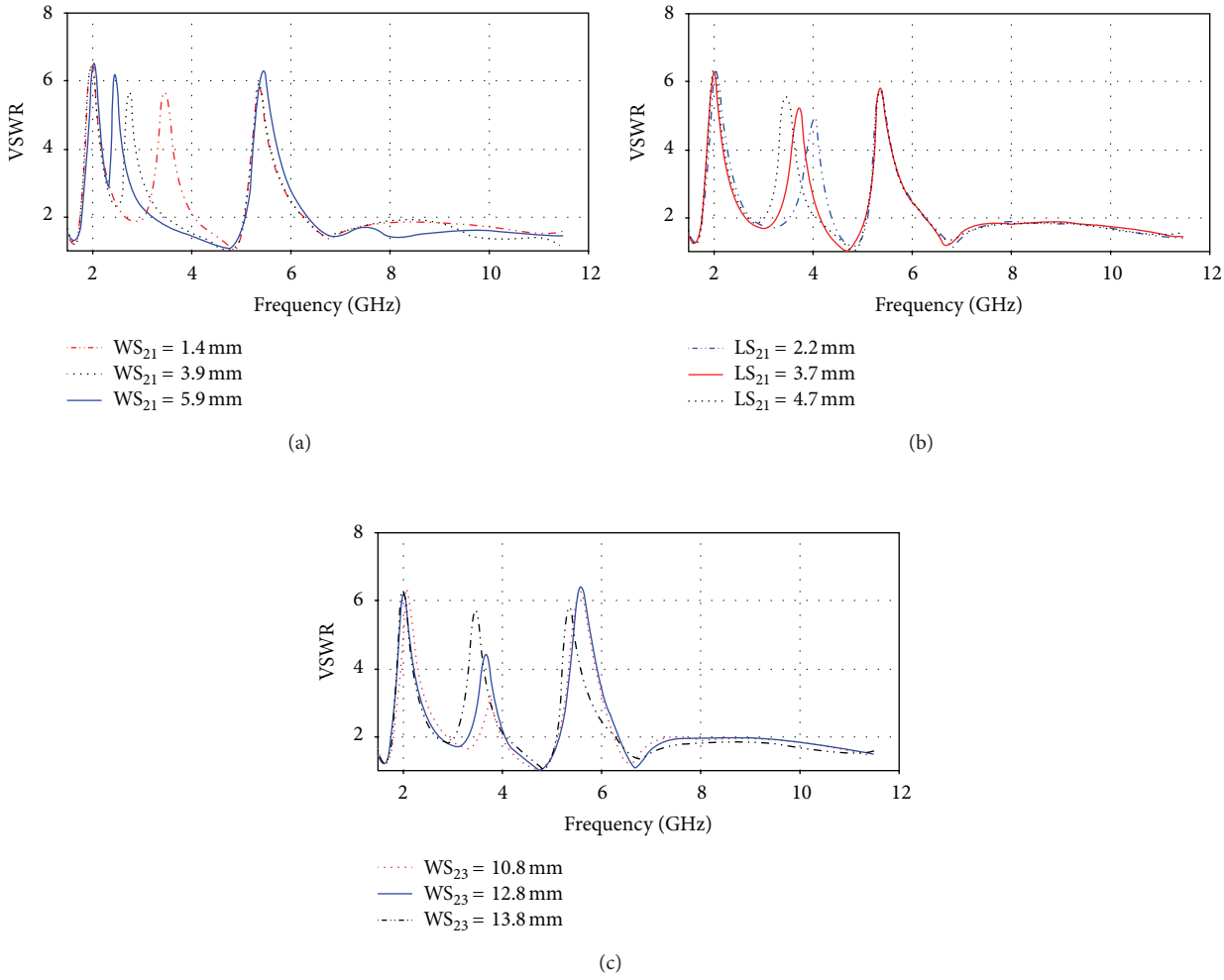

Figure 6: The simulated VSWR of the proposed antenna: effects of some parameters on the 3.54 GHz band-notched function, (a) WS_{21}, (b) LS_{21}, (c) WS_{23}.

Table 1: The optimized dimensions of the slots investigated in the proposed antenna.

Parameter	WS_{13}	LS_{11}	WS_{11}	WS_{21}	LS_{21}	WS_{23}	WS_{31}	LS_{31}	WS_{33}
Value (mm)	3.4	10	13	1.4	4.7	13.8	2.7	1.25	8.3

becomes wider when WS_{33} increases, and the center of the third rejected band shifts for lower frequencies side: the width of the lower rejected band increases from 0.44 GHz for WS_{33} = 7.3 mm to 1.18 GHz for WS_{33} = 8.3 mm. From the discussion above, we can control the shifted band-notched frequency and the enhanced width of the third band notch 5.68 GHz by varying the parameters WS_{31}, LS_{31}, and WS_{33}, and it can be independently adjusted by changing these parameters. On the other hand, we can observe that the parameters WS_{31}, LS_{31}, and WS_{33} have very small influences for the two lower rejected bands 2.2 GHz and 3.54 GHz. In summary, the longer the length of the slots and resonators gets, the lower the notched band frequency becomes.

4. Results and Discussion

The proposed UWB antenna with triple band-notched characteristics has been fabricated and measured. The photograph of the prototyped antenna is shown in Figure 4. The optimized dimensions of the band-notched structures used in measurement are depicted in Table 1.

4.1. VSWR Measurement. Figure 8 shows the measured and simulated voltage standing wave ratio (VSWR) results for the proposed antenna with bands notched characteristics, an excellent agreement between them is observed. It can be seen that the measured notched frequencies and the

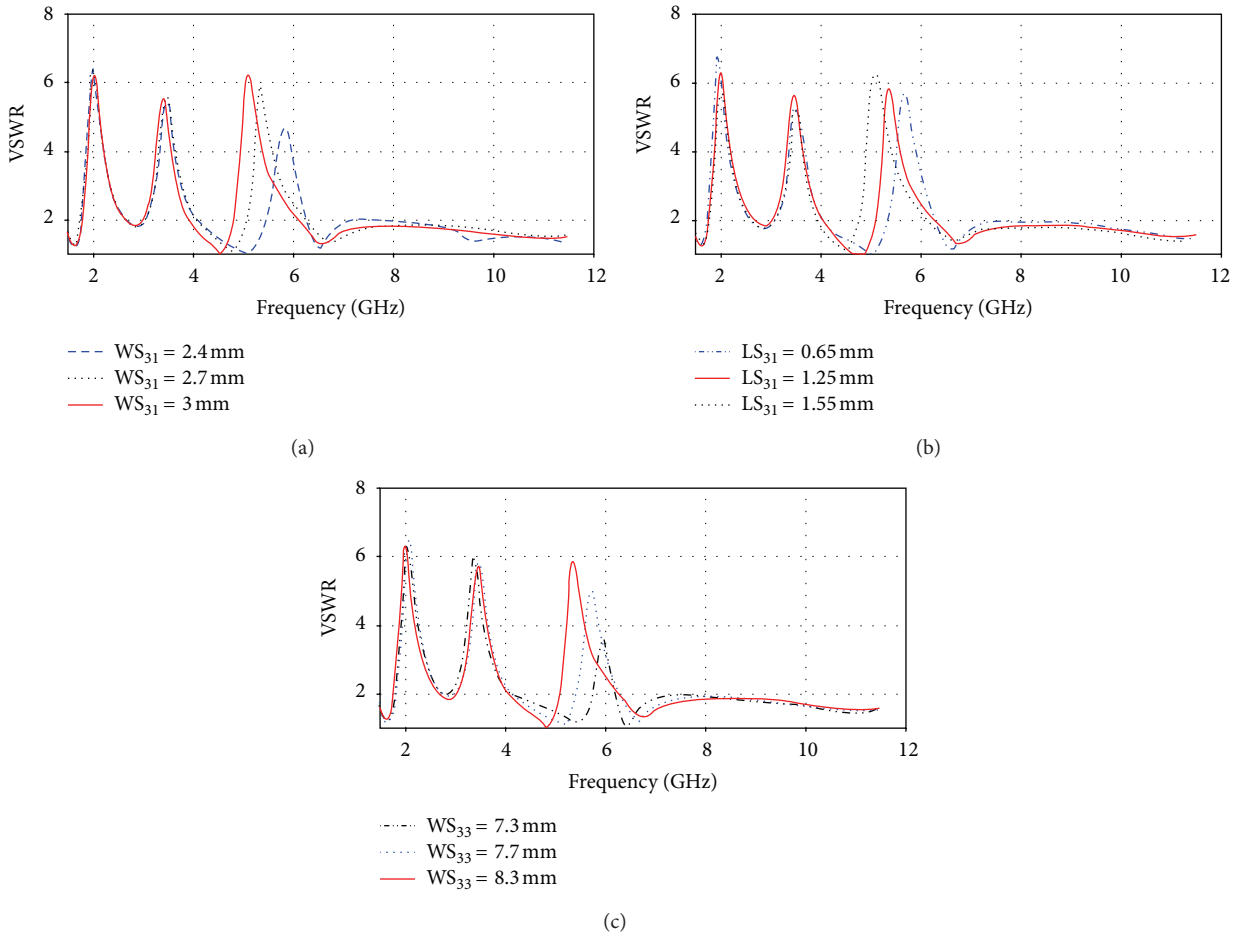

Figure 7: The simulated VSWR of the proposed antenna: effects of some parameters on the 5.68 GHz band-notched function, (a) WS_{31}, (b) LS_{31}, (c) WS_{33}.

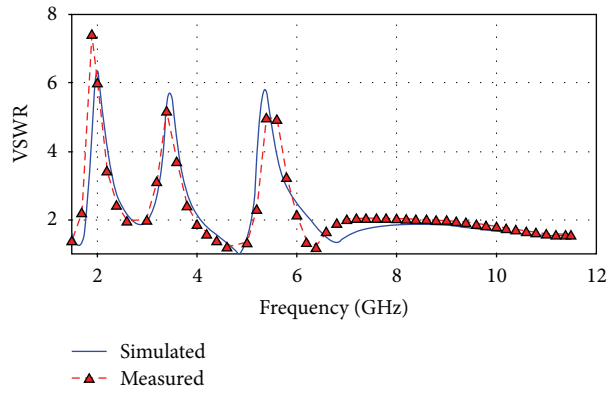

Figure 8: The measured and simulated VSWR of the proposed triple band-notched antenna.

Table 2: The rejected bands achieved with the proposed antenna.

Results	Frequency bands		
	1st rejected band	2nd rejected band	3rd rejected band
Simulated	1.7–2.7 GHz	3.04–4.04 GHz	5.09–6.27 GHz
Measured	1.6–2.66 GHz	3-4 GHz	5.13–6.03 GHz

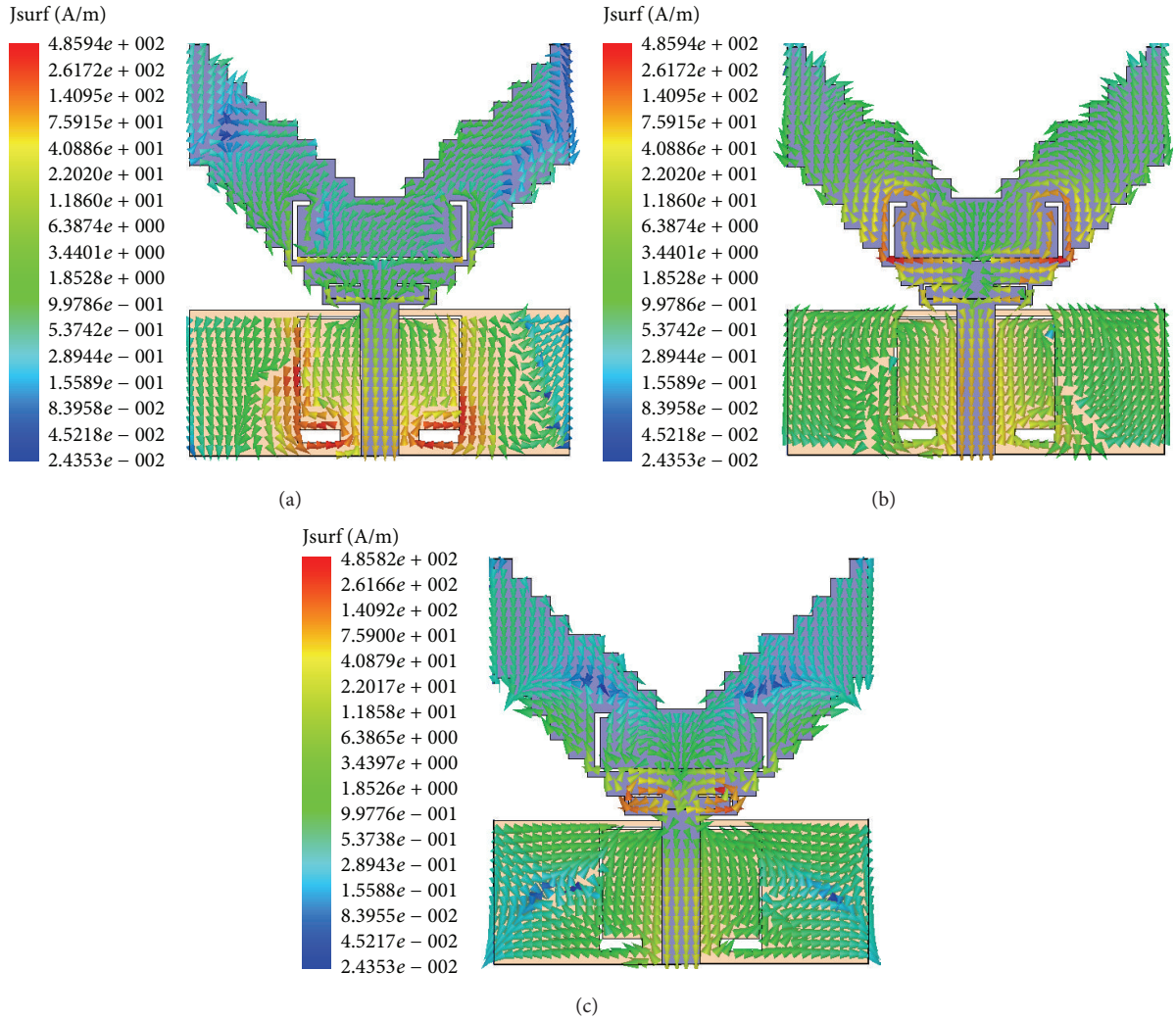

Figure 9: The current distribution on the proposed antenna at (a) 2.2 GHz, (b) 3.54 GHz, (c) 5.68 GHz.

bandwidths for each of the notched band are very suitable to suppress the disturbances from WLAN and WiMAX systems. The measured frequency range covers commercial UWB band (3.1–10.6 GHz) and rejects three frequencies bands 1.6–2.66 GHz (49.76%), 3-4 GHz (28.57%), and 5.13–6.03 GHz (16.12%); see Table 2.

4.2. Current Distribution. Figures 9(a), 9(b), and 9(c) show the current distribution on our proposed antenna with triple band-notched characteristics at frequencies 2.2 GHz, 3.54 GHz, and 5.68 GHz for the optimal design. A large current distribution around the edges of the slots is observed. In this case, destructive interference for the excited surface currents in the antenna will occur, which causes the antenna to be nonresponsive at those frequencies. At 2.2 GHz, a large current that is distributed around the vertical down C-shaped slot and a very small current that flowed along the two other slots with vertical up C-shaped are seen, which indicates that the changed dimensions of the vertical down C-shaped slot embedded in the ground plane have no effects on the two other upper rejected bands 3.54 GHz and 5.68 GHz. At 3.54 GHz, the current distribution mainly flows along the longest vertical up C-shaped slot embedded in the radiating element, while the currents around the two other slots are very small. In this way, the adjusted size for the longest vertical up C-shaped slot embedded in the radiating element does not affect the 2.2 GHz and 5.68 GHz frequency bands. At 5.68 GHz, the current distributions mainly flow along the shortest vertical up C-shaped slot embedded in the radiating element, while the currents around the other two are very small. In this way, the adjusted size for the shortest vertical up C-shaped slot embedded in the radiating element does not affect the 2.2 GHz and 3.54 GHz frequency bands.

4.3. Radiation Pattern. Figure 10 shows the normalized far-field radiation patterns for the proposed antenna in two principle planes at different operating frequencies 1.5 GHz, 4.5 GHz, 7.5 GHz, 8.5 GHz, and 10 GHz. At higher frequencies, the radiation pattern deteriorates because the equivalent radiating area changes with frequency over UWB; unequal phase distribution and significant magnitude of

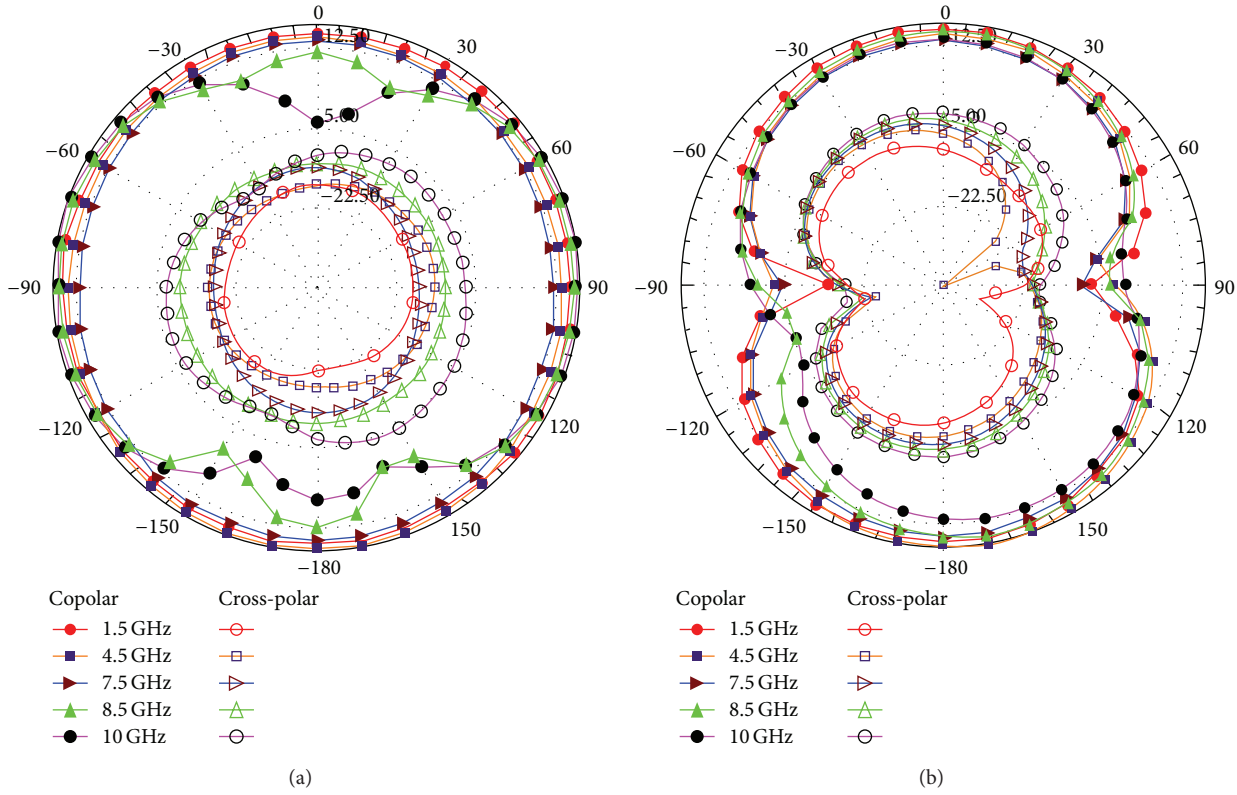

FIGURE 10: Radiation patterns at some frequencies: (a) x-z plane (H plane) and (b) y-z plane (E plane).

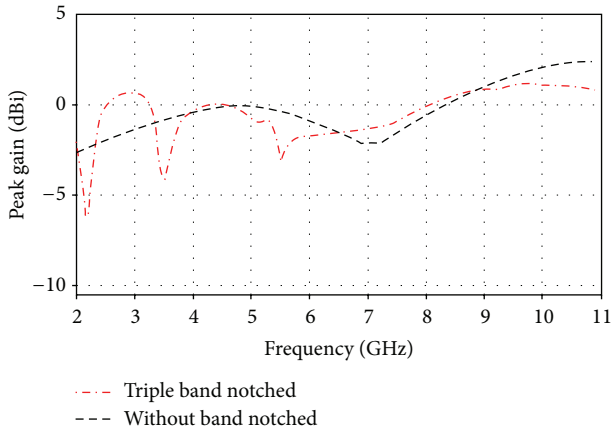

FIGURE 11: Peak gain of the proposed antenna with and without notched band structure.

higher order modes also play a part in the deterioration of the radiation pattern. Omnidirectional characteristics and radiation bandwidth can be improved if the ground plane length is approximately the same size as that of the radiating structure width. Also they can be further improved by using a thin substrate or a substrate with low dielectric constant [38]. The proposed triple band-notched antenna has nearly omnidirectional radiation characteristic in the H plane copolar radiation pattern and becomes faintly directional with increasing the frequency. The E-plane copolar radiation patterns over operating frequencies are roughly symmetric and have two main lobes. In addition, we can note that the cross-polarization level plane increases marginally with increasing the frequency.

4.4. Peak Gain. The comparison of the peak gain of the proposed antenna with that of the one without band-notched structures is shown in Figure 11. The peak gain of the proposed triple band-notched antenna almost follows the peak gain of the reference antenna without band-notched structures over the UWB frequency band, except in the notched bands. Three significant drops of the peak gain can be observed in the operating frequency. The peak gain decreases drastically to −6.23/−5.06/−3.20 dBi at around the notched bands which demonstrates that the band-notched function is good.

4.5. Group Delay and Transfer Function. Group delay is an important parameter to characterize the degree of distortion of the pulse signal for UWB impulse-based system. It is desired that the group delay response is stable over the UWB frequency band. In addition, the shape of the transmitted pulse should not be distorted [39]. Two identical antennas are arranged face to face at a distance of 30 cm which achieves the far-field condition of the antenna. The group delay of

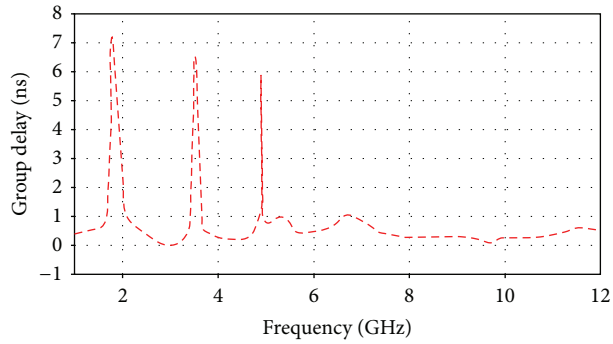

Figure 12: Group delay of the proposed triple band-notched antenna.

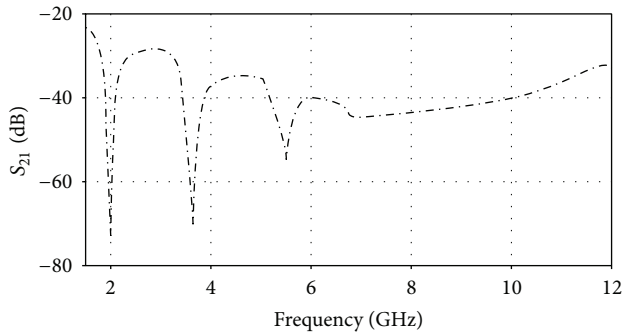

Figure 13: Transfer function of the proposed triple band-notched antenna.

the antenna system is shown in Figure 12. The group delay variation of the proposed antenna is very small, which is less than 1 ns in the pass band. However, in the notched bands, the group delay exceeds 5.5 ns. The characteristic of the group delay indicates that the phase of the antenna is linear in the far field and the pulse signal is not distorted between transmitting and receiving antennas in the pass band. The magnitude of the transfer function has also little variation over the operating band except in the notched bands, as shown in Figure 13. Apart from the notched bands, the group delay and transfer function show slightly small variations, indicating that the proposed design is suitable for UWB applications.

At last, in order to reduce potential interferences between UWB systems with WiMAX and WLAN systems, we have exploited three notched bands structures in a proposed UWB antenna for rejecting three frequency bands and adjusting of their parameters influencing only the related rejected band; the rest of the UWB frequency band remains unaffected which offers an autonomous selection and control of the rejected band and bandwidth.

5. Conclusion

To minimize the potential interferences between the UWB communication systems with the WiMAX and WLAN systems, simple, low cost, and compact printed monopole antenna with controllable triple band-notched characteristics is proposed and investigated. Two different vertical up C-shaped slots with a vertical down C-shaped slot are embedded in the radiating patch and in the ground plane, respectively, for rejecting WiMAX and WLAN frequency bands. By simply adjusting the total length and width of the corresponding band-notched structure, the rejected frequency bands can be independently controlled. Finally, a UWB antenna with controllable triple band rejected characteristics is successfully simulated, prototyped, and measured, showing a near omni-directional radiation pattern, a stable peak gain, and small group delay and transfer function variation over the whole band except in the notched frequency bands. Consequently, the advantages of simple structure, compact size, easy to fabricate, and excellent performances make this antenna a good candidate for practical UWB applications.

Conflict of Interests

The authors declare that there is no conflict of interests regarding the publication of this paper.

References

[1] Federal Communications Commission, "Revision of part 15 of the commission's rules regarding ultra-wideband transmission system from 3. 1 to 10. 6 GHz," in *Federal Communications Commission*, pp. 98–153, ET-Docket, Washington, DC, USA, 2002.

[2] R. Azim, M. T. Islam, and N. Misran, "Microstrip line-fed printed planar monopole antenna for UWB applications," *The Arabian Journal of Sciences and Engineering*, vol. 38, pp. 2415–2422, 2013.

[3] A. K. Gautam, S. Yadav, and B. K. Kanaujia, "A CPW-Fed compact UWB microstrip antenna," *IEEE Antennas and Wireless Propagation Letters*, vol. 12, pp. 151–154, 2013.

[4] A. A. Adam, S. K. A. Rahim, K. G. Tan, and A. W. Reza, "Design of 3.1-12 GHz printed elliptical disc monopole antenna with half circular modified ground plane for UWB application," *Wireless Personal Communications*, vol. 69, pp. 535–549, 2013.

[5] R. Gonçalves, P. Pinho, and N. B. Carvalho, "Compact, frequency reconfigurable, printed monopole antenna," *International Journal of Antennas and Propagation*, Article ID 602780, 2012.

[6] D.-O. Kim, N.-I. Jo, H.-A. Jang, and C.-Y. Kim, "Design of the ultrawideband antenna with a quadruple-band rejection characteristics using a combination of the complementary split ring resonators," *Progress in Electromagnetics Research*, vol. 112, pp. 93–107, 2011.

[7] X. Kang, H. Zhang, Z. Li et al., "A band-notched UWB printed half elliptical ring monopole antenna," *Progress in Electromagnetics Research C*, vol. 35, pp. 23–33, 2013.

[8] A. Karmakar, R. Ghatak, U. Banerjee, and D. R. Poddar, "An UWB antenna using modified Hilbert curve slot for dual band notch characteristics," *Journal of Electromagnetic Waves and Applications*, vol. 27, no. 13, pp. 1620–1631, 2013.

[9] L. Bing and J. S. Hong, "Design of two novel dual band-notched UWB antennas," *International Journal of Antennas AndPropagation*, vol. 2012, Article ID 303264, 7 pages, 2012.

[10] N. Ojaroudi and M. Ojaroudi, "Novel design of dual band-notched monopole antenna with bandwidth enhancement for UWB applications," *IEEE Antennas and Wireless Propagation Letters*, vol. 12, pp. 698–701, 2013.

[11] S. Soltani, M. Azarmanesh, P. Lotfi, and G. Dadashzadeh, "Two novel very small monopole antennas having frequency band notch function using DGS for UWB application," *International Journal of Electronics and Communications*, vol. 65, no. 1, pp. 87–94, 2011.

[12] T. Li, H. Q. Zhai, C. Zhu, L. Li, C. H. Liang, and Y. F. Han, "Design and analysis of compact printed dual band-notched ultrawideband (UWB) antenna," *Journal of Electromagnetic Waves and Applications*, vol. 27, no. 5, pp. 560–571, 2013.

[13] S. M. Zhang, F. S. Zhang, W. Z. Li, T. Quan, and H. Y. Wu, "A compact UWB monopole antenna with WiMAX and WLAN band rejections," *Progress in Electromagnetics Research Letters*, vol. 31, pp. 159–168, 2012.

[14] P. Gao, L. Xiong, J. Dai, S. He, and Y. Zheng, "Compact printed wide-slot UWB antenna with 3.5/5.5-GHz dual band-notched characteristics," *IEEE Antennas and Wireless Propagation Letters*, vol. 12, pp. 983–986, 2013.

[15] S. K. Mishra, R. K. Gupta, A. Vaidya, and J. Mukherjee, "Low-cost, compact printed circular monopole UWB antenna with 3.5/5.5-GHz dual band-notched characteristics," *Microwave and Optical Technology Letters*, vol. 54, no. 1, pp. 242–246, 2012.

[16] J. Kim, N. Kim, and S. Lee, "A broadband antenna using the modified ground plane with a complementary split ring resonator for 5-GHz WLAN band-notched performance," *Microwave and Optical Technology Letters*, vol. 54, no. 1, pp. 1–3, 2012.

[17] M. A. Amin, "Design of a CPW-fed band-notched UWB antenna using a feeder-embedded slotline resonator," *International Journal of Antennas and Propagation*, vol. 2008, Article ID 564317, 2008.

[18] M. Xie, Q. Guo, and Y. Wu, "Design of a miniaturized UWB antenna with band-notched and high frequency rejection capability," *Journal of Electromagnetic Waves and Applications*, vol. 25, no. 8-9, pp. 1103–1112, 2011.

[19] W. Junhui, Y. Yingzeng L Xianglong, and W. Tuo, "Trapezoid UWB antenna with dual band notched characteristics for WiMAX/WLAN bands," *Electronics Letters*, vol. 49, no. 11, 2013.

[20] S.-J. Wu and J.-H. Tarng, "Planar band-notched ultra-wideband antenna with square-looped and end-coupled resonator," *IET Microwaves, Antennas and Propagation*, vol. 5, no. 10, pp. 1227–1233, 2011.

[21] M. Almalkawi and V. Devabhaktuni, "Ultrawideband antenna with triple band-notched characteristics using closed-loop ring resonators," *IEEE Antennas and Wireless Propagation Letters*, vol. 10, pp. 959–962, 2011.

[22] Q. Q. Xing, H. C. Yang, D. K. Liu, and L. Yang, "Dual and tri-band-notched ultrawideband (UWB) antennas using compact composite resonators," *Progress in Electromagnetics Research Letters*, vol. 42, pp. 177–185, 2013.

[23] X. L. Liu, Y. Z. Yin, J. H. Wang, and J. J. Xie, "Compact dual band-notched UWB antenna with parasitic micro-strip lines and t-shape stub," *Progress in Electromagnetics Research C*, vol. 41, pp. 55–66, 2013.

[24] C.-C. Lin, P. Jin, and R. W. Ziolkowski, "Single, dual and tri-band-notched ultrawideband (UWB) antennas using capacitively loaded loop (CLL) resonators," *IEEE Transactions on Antennas and Propagation*, vol. 60, no. 1, pp. 102–109, 2012.

[25] L. Tong, Z. Huiqing, L. Guihong, L. Long, and L. Changhong, "Compact UWB band-notched antenna design using interdigital capacitance loading loop resonator," *IEEE Antennas and Wireless Propagation Letters*, vol. 11, pp. 724–727, 2012.

[26] T. Li, F. F. Huo, H. Q. Zhai, and C. H. Liang, "Compact ultra-wideband antenna with sharp band-notched characteristics for WiMax and WLAN," *Electronics Letters*, vol. 48, no. 22, 2012.

[27] S. K. Mishra and J. Mukherjee, "Compact printed dual band-notched U-shape UWB antenna," *Progress In Electromagnetics Research C*, vol. 27, pp. 169–181, 2012.

[28] X. H. Wu and Q. X. Chu, "Compact ultra-wideband antenna with dual sharp notch-bands using integrated bandstop filter," in *Proceedings of the Asia-Pacific Conference on Antennas and Propagation*, pp. 27–29, IEEE Press, Singapore, August 2012.

[29] W. Jiang and W. Che, "A novel UWB antenna with dual notched bands for WiMAX and WLAN applications," *IEEE Antennas and Wireless Propagation Letters*, vol. 11, pp. 293–296, 2012.

[30] A. Khalilzadeh, A. E. C. Tan, and K. Rambabu, "Design of an integrated UWB antenna with dual band notch characteristics," *International Journal of Electronics and Communications*, vol. 67, pp. 433–437, 2013.

[31] L. Tong, Z. Huiqing, L. Long, L. Changhong, and H. Yinfu, "Compact UWB antenna with tunable band-notched characteristic based on microstrip open-loop resonator," *IEEE Antennas and Wireless Propagation Letters*, vol. 11, pp. 1584–1587, 2012.

[32] G. Yang, Q. X. CHU, and T. G. Huang, "A compact UWB antenna with sharp dual band-notched characteristics for lower and upper WLAN band," *Progress in Electromagnetics Research C*, vol. 29, pp. 135–148, 2012.

[33] L. Xiong and P. Gao, "Dual-band planar monopole antenna for bluetooth and UWB applications with WiMAX and WLAN band-notched," *Progress in Electromagnetics Research Letters*, vol. 28, pp. 183–194, 2012.

[34] R. Azim and M. T. Islam, "Compact planar UWB antenna with band notched characteristics for WLAN and DSRC," *Progress in Electromagnetics Research Letters*, vol. 133, pp. 391–406, 2013.

[35] M. T. Islam, R. Azim, and A. T. Mobashsher, "Triple band-notched planar UWB antenna using parasitic strips," *Progress in Electromagnetics Research*, vol. 129, pp. 161–179, 2012.

[36] J. Y. Kim, B. Oh, N. Kim, and S. Lee, "Triple band-notched UWB antenna based on complementary meander line SRR," *Electronics Letters*, vol. 48, no. 15, 2012.

[37] S. Natarajamani, K. B. Santanu, and K. P. Sarat, "A triple band notched planar antenna for UWB applications," *Journal of Electromagnetic Waves and Applications*, vol. 27, no. 9, pp. 1178–1186, 2013.

[38] S. K. Mishra, R. Gupta, A. Vaidya, and J. Mukherjee, "Printed fork shaped dual band monopole antenna for bluetooth and UWB applications with 5.5GHZ WLAN band notched characteristics," *Progress In Electromagnetics Research C*, vol. 22, pp. 195–210, 2011.

[39] D. Zhou, S. Gao, F. Zhu, R. A. Abd-Alhameed, and J. D. Xu, "A simple and compact planar ultra wide-band antenna with single or dual band-notched characteristics," *Progress in Electromagnetics Research*, vol. 123, pp. 47–65, 2012.

Hindawi Publishing Corporation
International Journal of Antennas and Propagation
Volume 2014, Article ID 531959, 10 pages
http://dx.doi.org/10.1155/2014/531959

Research Article

Design and Analysis of a Novel Dual Band-Notched UWB Antenna

Ronghua Shi, Xi Xu, Jian Dong, and Qingping Luo

School of Information Science and Engineering, Central South University, Changsha 410075, China

Correspondence should be addressed to Jian Dong; dongjian@mail.csu.edu.cn

Received 17 April 2013; Revised 19 December 2013; Accepted 19 December 2013; Published 3 February 2014

Academic Editor: Alistair P. Duffy

A novel ultrawide band (UWB) antenna with dual band-notched characteristics is presented. The first band rejection is provided by an arc H-shaped slot on the radiating patch. The parametric study of the arc H-shaped slot shows that this structure enables rejectband characteristic with improved control compared to traditional H-shaped slot. Based on the single band-notched UWB antenna, the second notched band is realized by etching narrow slots on the ground plane. By tuning the parameters of these slots, the proposed UWB antenna can operate from 2.9 GHz to above 10 GHz, except for the bandwidth of 3.3–3.6 GHz for WiMAX application and 5.1–5.9 GHz for WLAN application. Simulated and measured results show that the proposed antenna provides excellent band rejection and is a good candidate for future UWB application.

1. Introduction

Since commercial ultrawide band (UWB) systems which work from 3.1 GHz to 10.6 GHz are allowed by Federal Communication Commission (FCC) [1], the technology of UWB is concerned by academia and industry due to its candidate for various applications. As an essential part of the UWB system, the UWB antenna, has drawn heavy attention from researchers. Due to broad bandwidth, low cost, and good radiation characteristic, the global approaches of UWB antenna [2–4] are increasing quickly.

In order to avoid interference of service that work in the UWB band, such as the subband 5.1–5.9 GHz for WLAN band and WiMAX operating in the 3.3–3.6 GHz, the UWB antenna with band-notched function is desirable. Various methods for designing band-notched UWB antenna have been presented and reported. Designs of using parasitic stubs as resonators to achieve band-notched function were presented in [5–8]. In [5], single band-notched and multiband-notched antennas have been implemented by integrating wideband planar monopole antennas with various types of microstrip resonator. In [6], band-notched function of the circle ring antenna was achieved by introducing a tuning stub inside the ring monopole. A monopole antenna with band-notched function using a complex resonator was presented in [7]. A printed monopole antenna with controllable band-notched performance for UWB applications was presented in [8]. Its band-notched characteristic is achieved by embedding two shorted rectangular resonators.

In the designs above, the structure of these antennas cannot be compact enough due to the use of parasitic stubs as resonators. In order to make the structure of the band-notched antenna more compact, etching slots such as C-shaped, T-shaped, E-shaped, and H-shaped slots on the radiating patch or on the ground plane were used to achieve band-notched function [9–15]. Designs of single band-notched UWB antennas were presented in [9–13]. In [9], the characteristics of the on-ground band-notched structures were analyzed in detail providing designers with useful information and flexibility for the realization of specialized band-notched antennas. In [10], characteristic modes have been used to analyze the behavior of an UWB antenna with a narrowband slot embedded in its planar geometry. It has been shown that the notched-band is caused by the slot resonance, and the intensity of the rejection depends on how much the current distribution of different antenna modes is disturbed. By using a modified shovel-shaped defected ground structure, a band-notched characteristic is achieved in [11]. A

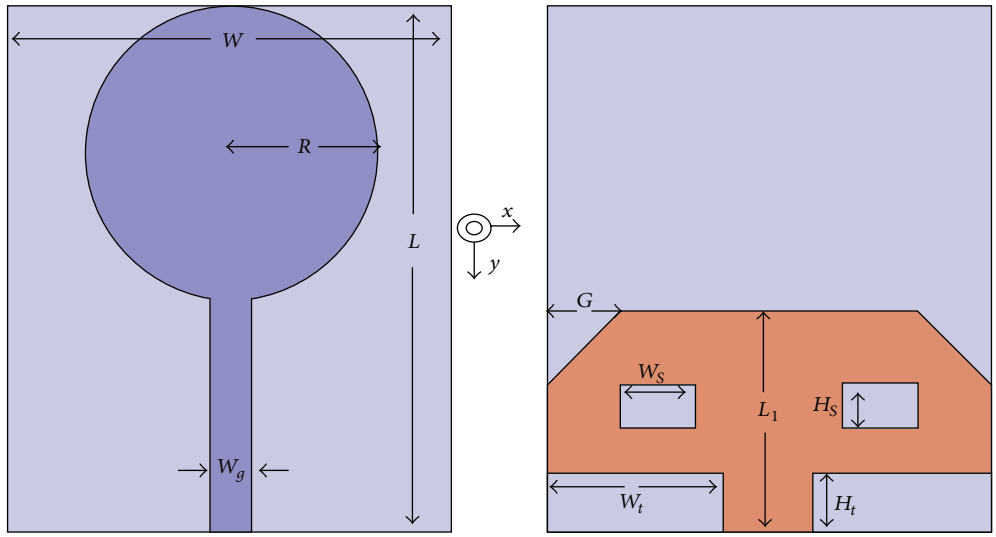

Figure 1: Geometry of the UWB antenna: (a) top view, (b) bottom view.

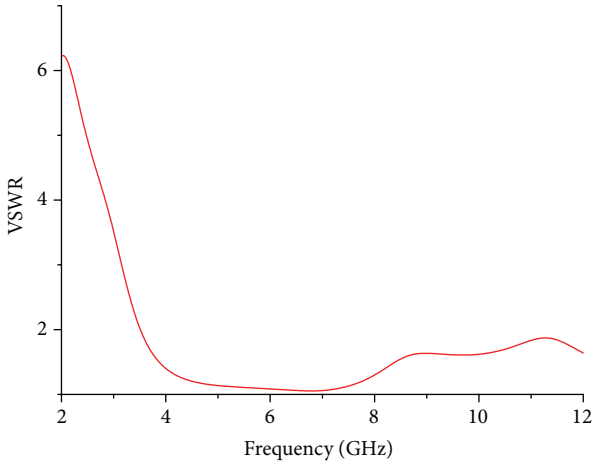

Figure 2: Simulated VSWR of the UWB antenna.

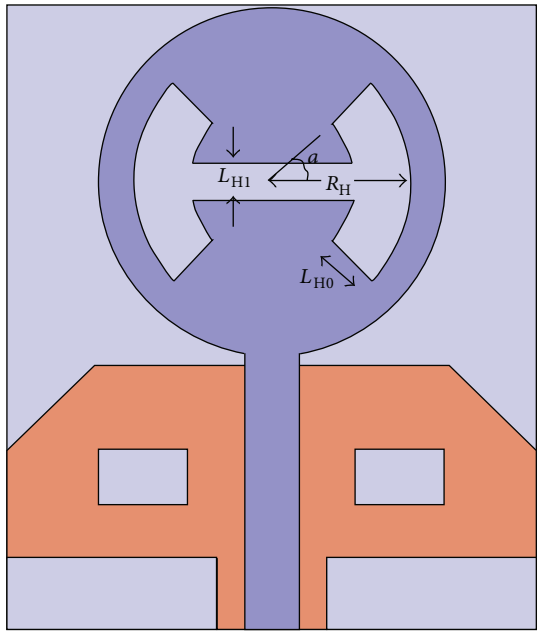

Figure 3: Geometry of the arc H-shaped slot.

frequency-reconfigurable planar antenna with two inverted S-shaped slots was presented in [12]. This antenna can be widely used in the dual-band WLAN systems and the UWB systems. In addition, a complete design method for a compact uniplanar UWB antenna with subband rejection capability is presented in [13]. In order to avoid the interference from services which work in different frequency band, dual band-notched UWB antennas were presented [14, 15]. In [14], the dual band-notched function was achieved by etching one quasi-complementary split-ring resonator in the feed line. In [15], by cutting two L-shaped slits and an E-shaped slot with variable dimensions on the radiating patch dual band-notch characteristics generated and also by inserting a V-shaped strip on the ground plane, additional resonances were excited, and hence much wider impedance bandwidth was produced, especially at the higher band.

The designed antennas above feature wide operating bandwidth and good band-notched function, but they lack powerful control of tuning the centre frequency of the notched-band. To overcome this weakness of the above designs, a novel UWB antenna with dual band-notched characteristics is proposed in this paper by employing an arc H-shaped slot on the radiating patch and etching narrow slots on the ground plane. The proposed antenna can operate within an ultrawide band from 2.9 GHz to above 10 GHz. At the same time, the antenna can avoid the interference from WiMAX and WLAN applications. The rest of the paper is organized

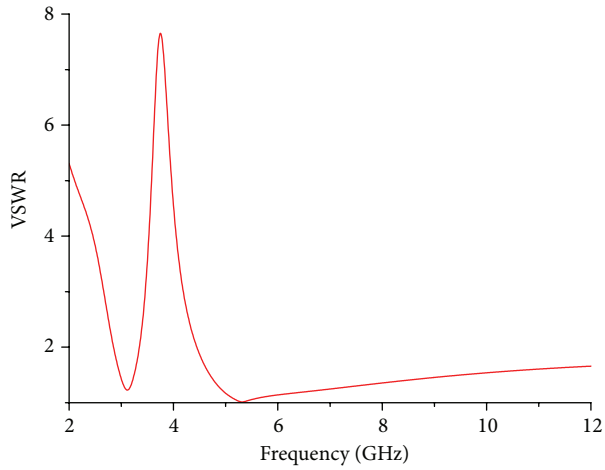

Figure 4: Simulated VSWR of the single band-notched antenna.

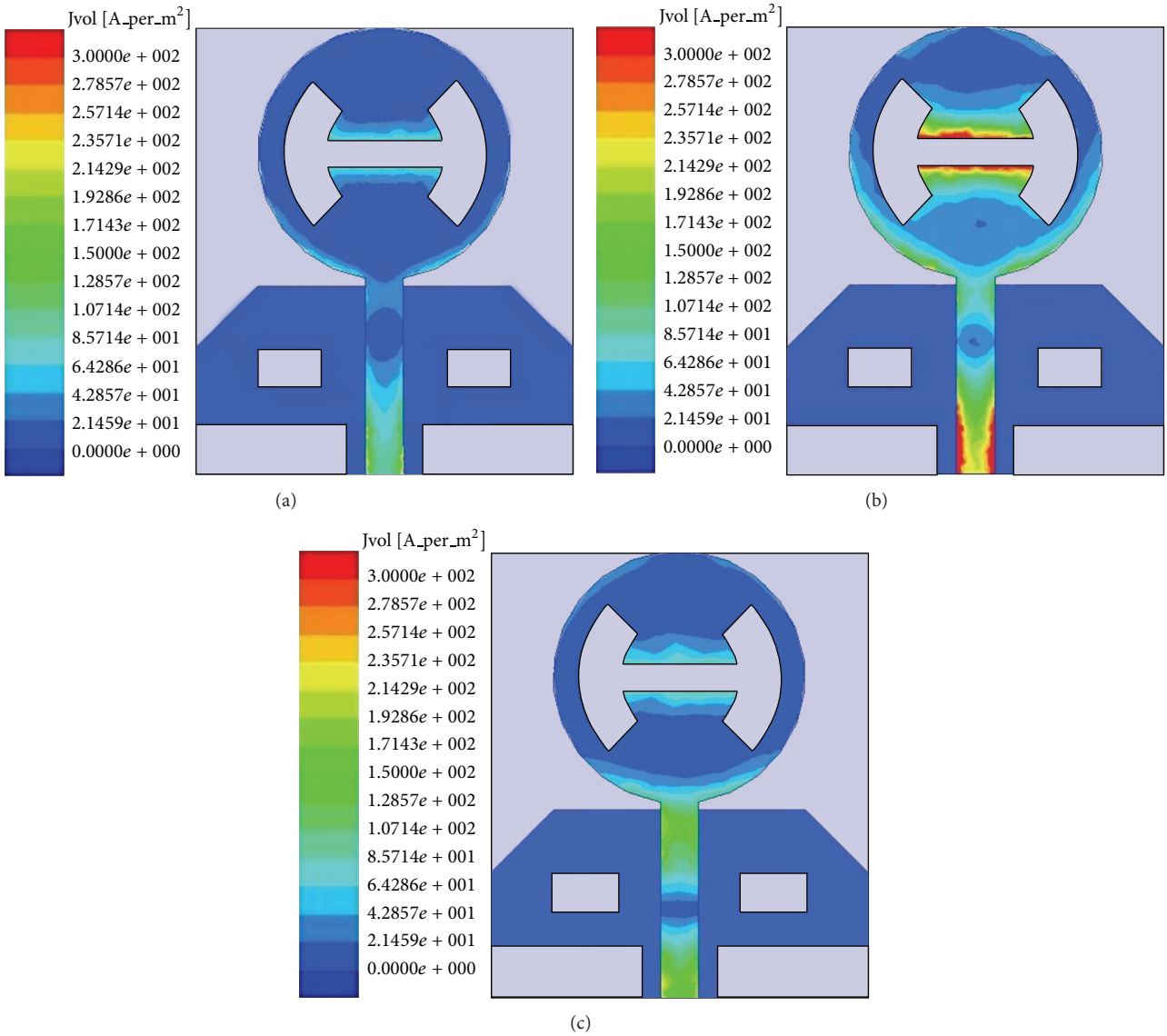

Figure 5: Surface current distribution of the antenna: (a) 3.2 GHz, (b) 3.7 GHz, and (c) 5 GHz.

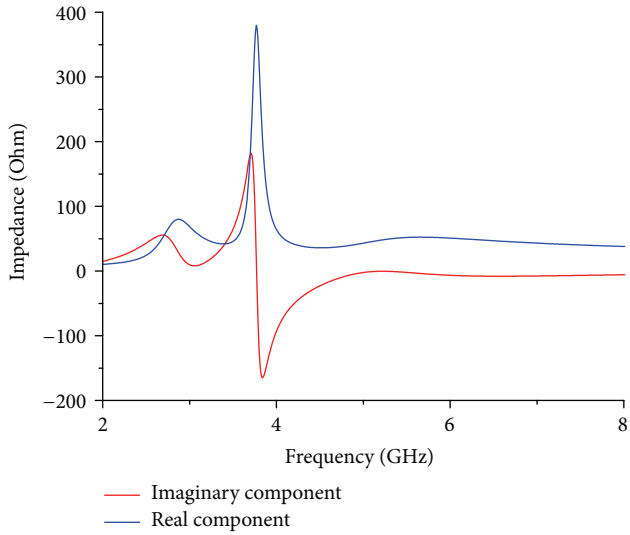

Figure 6: Impedance Z of the antenna versus frequency.

as follows. In Section 2, the antenna design is first discussed. The simulation is carried out using Ansoft High Frequency Structure Simulator (HFSS). In Section 3, advantages of the arc H-shaped slot compared with traditional H-shaped slot are presented. In Section 4, simulation and measurement results are presented to validate the performance of the proposed antenna. Finally, the conclusion is provided in Section 5.

2. Antenna Design

2.1. Single Band-Notched UWB Antenna Design

2.1.1. UWB Antenna. As shown in Figure 1. The referance antenna [4] uses FR4 substrate with the dimensions of $35.5 \times 30 \times 1.6\ \text{mm}^3$, relative permittivity $\varepsilon_r = 4.4$. The antenna is fed by a CPW line which is designed for 50 Ohm characteristic impedance. Figure 1(a) shows the top view of the antenna; the planar circular disc monopole is fabricated on the substrate. The radius of the radiating patch is R (R = 10 mm), and the width of the feed line is W_g (W_g = 3 mm). Figure 1(b) shows the rear of the antenna; the length of the ground plane is L_1 (L_1 = 15 mm). The top corners with the parameter G (G = 5 mm) are removed to improve the bandwidth of the antenna [4]. Two rectangular slots are removed to adjust the antenna impedance and reduce the return loss [4]. H_s (H_s = 3 mm) and W_s (W_s = 5 mm) denote the length and width of the rectangular slots, respectively. The ground plane is reshaped as letter "T", for W_t = 12 mm, H_t = 4 mm. The simulated VSWR result of the UWB antenna is shown in Figure 2; it can be seen that the antenna could operate from 3.5 GHz to above 12 GHz with VSWR less than 2.

2.1.2. Single Band-Notched UWB Antenna. Before developing the dual band-notched UWB antennas, we need to investigate the method generating the single notched band. In order to achieve band-notched function, we employ an arc H-shaped slot on the circular radiating patch. The arc H-shaped slot is removed from the centre of the radiating patch. As shown in Figure 3, the shape of the slot is designed as an arc letter "H." R_{H} denotes the radius of the outer circular arc. L_{H0} denotes the distance between outer arc and inner arc. The simulation is carried out using HFSS. The optimized slot dimensions are as follows: $R_{\text{H}} = 8$ mm, $L_{\text{H0}} = 3.2$ mm, $L_{\text{H1}} = 2$ mm, and $\alpha = \pi/4$. It can be seen in Figure 4 that the simulated VSWR of the antenna is larger than 2 from 3.2 GHz to 4.2 GHz acting as a stopband, meaning that this antenna can avoid the interference from IEEE 802.16 WiMAX application.

The simulated results of surface current distribution for the antenna at the passband (3.2 GHz, 5 GHz) and at the rejectband (3.7 GHz) are given in Figure 5. It can be seen that the surface current distribution is very strong at the feed line and the surface current is highly concentrated at the arc H-shaped slot in Figure 5(b), but the situations are different in Figures 5(a) and 5(c). These clearly show the positive effects of the slot upon obtaining the band-notched characteristics. It is noted that the UWB antenna cannot work at the stopband (3.7 GHz) because of the effect of the arc H-shaped slot resonator. The impedance Z of the antenna versus frequency is given in Figure 6 to show the band-notched function of this antenna. The input resistance should be around 50 Ohm and the input reactance should be around 0 Ohm when the antenna is operating at the passband. At the stopband, their values largely deviate from the nominal values.

2.2. Dual Band-Notched UWB Antenna Design. The high frequency band-notched function is designed to avoid the other band such as WLAN operating from 5.1 to 5.9 GHz. To achieve this function, we etch a couple of narrow slots on the ground plane. Figure 7 shows the geometry of the antenna; the top view of this antenna and the slots on the ground plane are given in Figures 7(a) and 7(b), respectively. The simulated results show that the optimized slot dimensions are as follows: $W_d = 0.5$ mm, $L_d = 7.5$ mm, and $S = 0.2$ mm. The VSWR result is shown in Figure 8; it can be seen that the antenna could not operate from 5.1 GHz to 6 GHz as a stopband. The centre frequency of the stopband, given the dimensions of the band-notched feature, can be postulated as [16]

$$f_{\text{notch}} = \frac{c}{4L'\sqrt{(\varepsilon_r + 1)/2}}. \quad (1)$$

Let $L' = L_d + W_d$; ε_r is the effective dielectric constant, and c is the speed of light. The lengths of the slot have great effects on the band rejection performance and should be tuned carefully. By varying the length of parameter L_d, we could control the length of L' to tune the centre frequency of the stopband.

Based on the single band-notched UWB antenna, the dual band-notched function is investigated, and the geometry of the antenna is given in Figure 9. Figure 10 shows the simulated VSWR result of the dual band-notched UWB antennap; it can be observed that the proposed antenna bandwidth with good stopband rejection, the band-notched characteristic of low frequency formed by the arc H-shaped slot on the radiating patch, and the band-notched characteristic of high

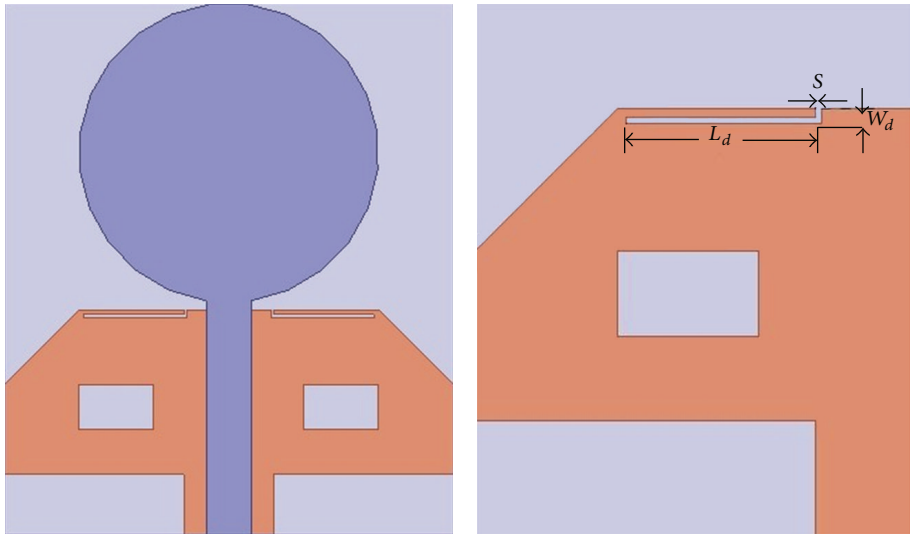

Figure 7: Geometry of the high frequency band-notched antenna: (a) top view, (b) narrow slot on the ground plane.

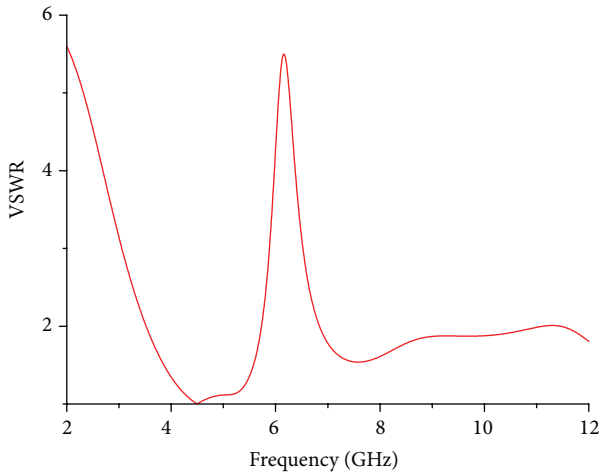

Figure 8: Simulated VSWR of the high frequency band-notched UWB antenna.

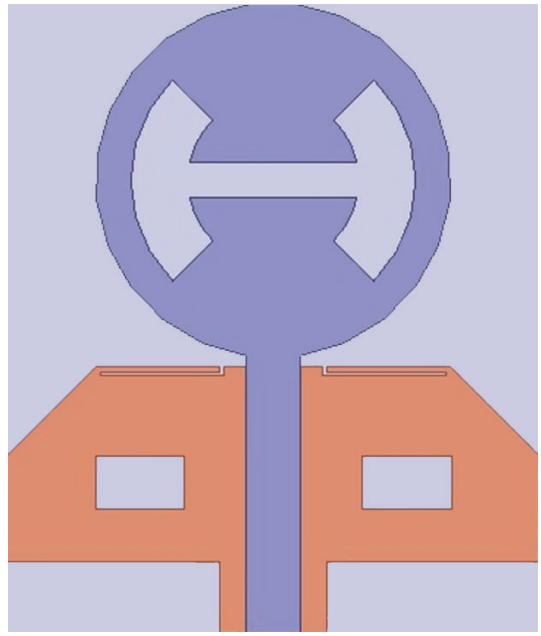

Figure 9: Geometry of the proposed antenna.

frequency formed by the narrow slots on the ground plane hardly interfere with each other. Figure 11 shows that the centre frequency of the stopband shifts down as L_d increases. The impedance Z of the dual band-notched UWB antenna is displayed in Figure 12, which shows that the input resistance and the input reactance keep the nominal value when the antenna working on the passband. It shows that the proposed antenna is suitable for UWB applications.

According to the impedance Z of the dual band-notched UWB antenna shown in Figure 12, the approximate equivalent circuit of the proposed antenna is presented in Figure 13. The arc H-shaped slot on the radiating patch and narrow slots on the ground plane can be modeled by two circuit-resonance stubs at different positions in a transmission line model. At the passband, neither of the stubs has any effect in generating notched bands. On the 3.7 GHz band-notched characteristic, stub 1 makes the circuit resonate. Therefore, stub 1 behaves as a parallel resonator with an unusual input impedance Z (i.e., the input resistance is much larger than 50 Ohm, and the input reactance is not equal to 0 Ohm), causing a total impedance mismatch between the feed line and the radiating patch. As a result, VSWR of the antenna in this frequency band becomes greater, and the first notched band is created. On the 5.7 GHz band-notched characteristic, stub 2 works similarly as stub 1. The input impedance Z becomes unusual; stub 2 operates as a parallel resonator in

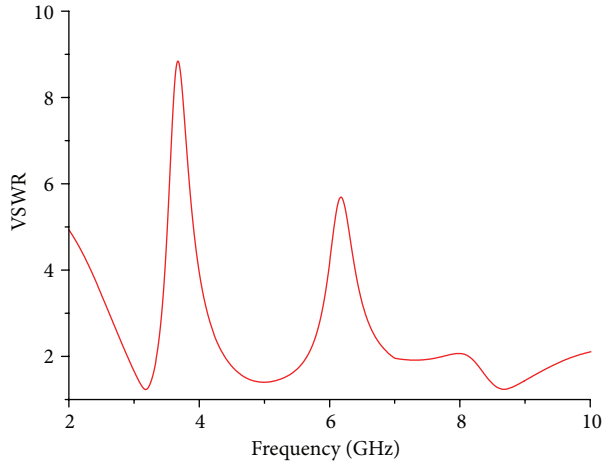

Figure 10: Simulated VSWR result of the proposed antenna.

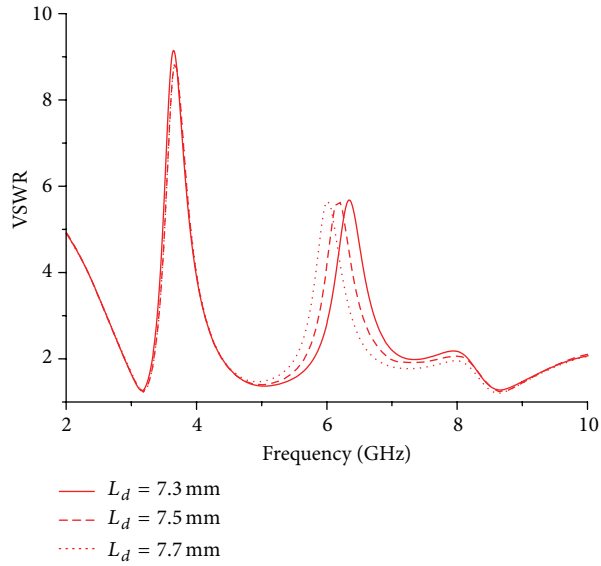

Figure 11: Effect of length of the narrow slot.

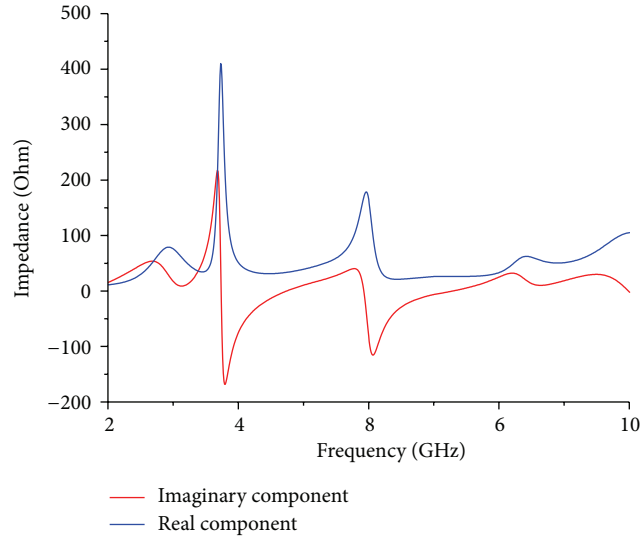

Figure 12: Impedance Z of the proposed antenna versus frequency.

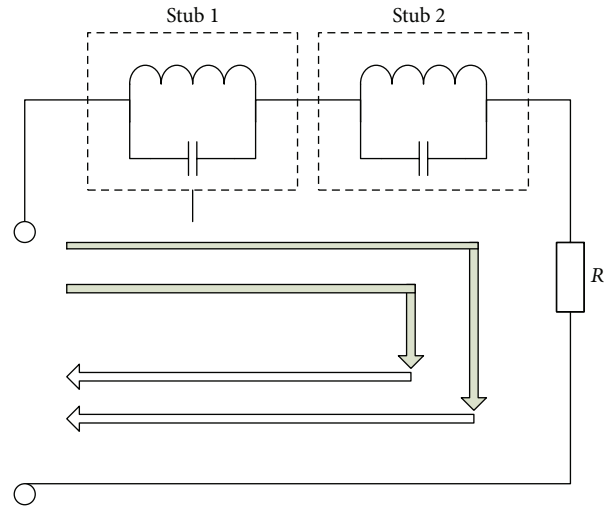

Figure 13: Approximate equivalent circuit of the proposed antenna.

the circuit. Essentially, the dual band-notched function is achieved by these resonators.

3. Advantages of the Arc H-Shaped Slot

Traditional H-shaped slot is designed as follows. The geometry and parameters of the H-shaped slot are shown in Figure 14. Through the parametric study [17], the effects of H-shaped slot parametric variation on stopband centre frequency are presented in Table 1 [17]. It can be seen that stopband centre frequency can be tuned effectively only by varying parameter W_{S1}.

In the proposed antenna, the first rejectband centre frequency is mainly determined by the dimensions of the parameters of the arc H-shaped slot. In order to show the advantages of the arc H-shaped slot, the parametric effects

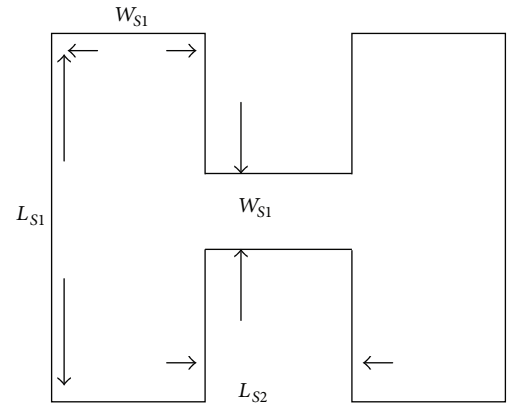

Figure 14: geometry and parameters of the H-shaped slot.

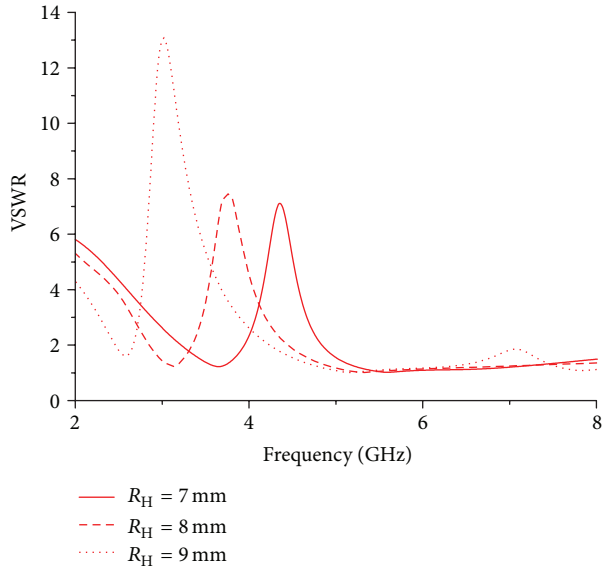

Figure 15: Effect of parameter R_H.

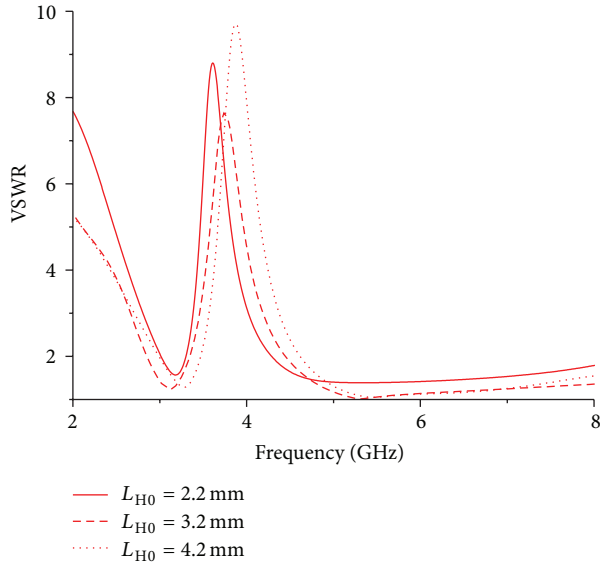

Figure 16: Effect of parameter L_{H0}.

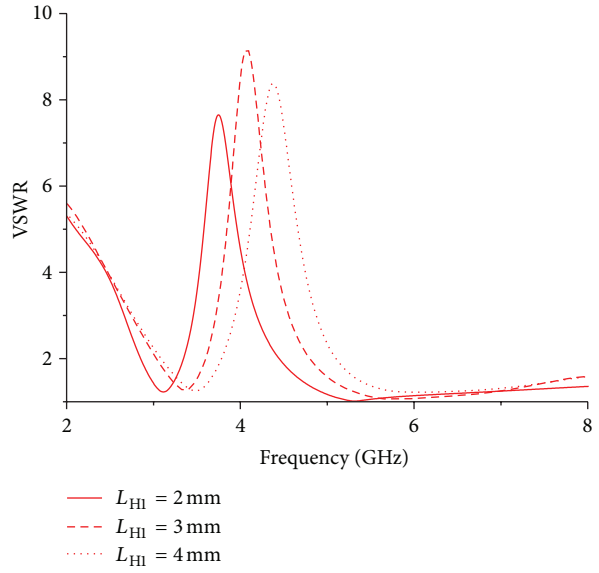

Figure 17: Effect of parameter L_{H1}.

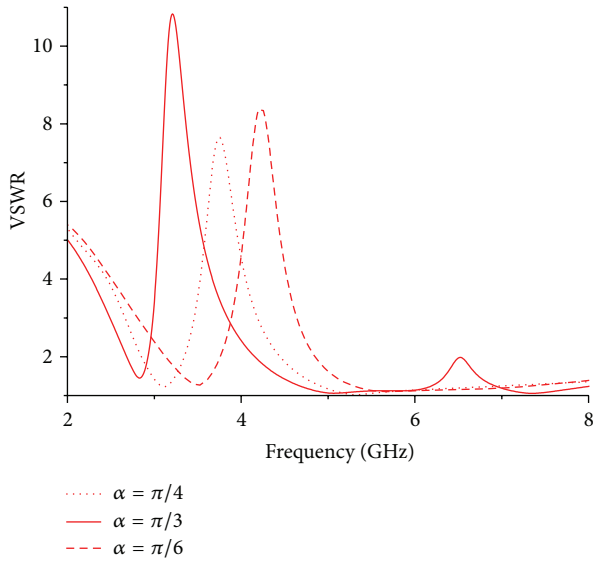

Figure 18: Effect of parameter angle α.

(R_H, L_{H0}, L_{H1}, and α) of the slot are analyzed to show the advantages of the novel design.

On the 3.7 GHz band-notched characteristic, the effect of parameter R_H is simulated and shown in Figure 15. The dimensions of the arc H-shaped slot are L_{H0} = 3.2 mm, L_{H1} = 2 mm, and $\alpha = \pi/4$; we can be informed that centre frequency of the band changes from 3.2 GHz to 4.4 GHz when parameter R_H varies from 7 mm to 9 mm. It can be seen that the centre frequency of the stopband shifts down as R_H increases. The notch frequency is heavily dependent on this parameter.

The slot dimension L_{H0}, varies, for R_H = 8 mm, L_{H1} = 2 mm, and $\alpha = \pi/4$. The simulated VSWR of Figure 16 shows that frequency band notch varied from 3.7 GHz to 4 GHz as L_{H0} increases. Relatively, the notch frequency shows light dependence on L_{H0}.

Figure 17 shows the simulated VSWR of the effect of parameter L_{H1}. It can be seen that the centre frequency varies from 3.6 GHz to 4.6 GHz as L_{H1} varies from 2 mm to 4 mm. The simulated VSWR in Figures 16 and 17 illustrate that the slot dimension L_{H0} has a smaller effect on notch frequency than the parameter L_{H1}. It can be informed that the centre frequency is heavily dependent on parameter L_{H1} (R_H = 8 mm, L_{H0} = 3.2 mm, and $\alpha = \pi/4$).

In addition, another important parameter α is analyzed below. The effect of angle α is simulated and shown in Figure 18. The slot dimension α, varies, for R_H = 8 mm, L_{H0} = 3.2 mm, and L_{H1} = 2 mm. It can be seen that the centre

Figure 19: Photograph of the proposed antenna.

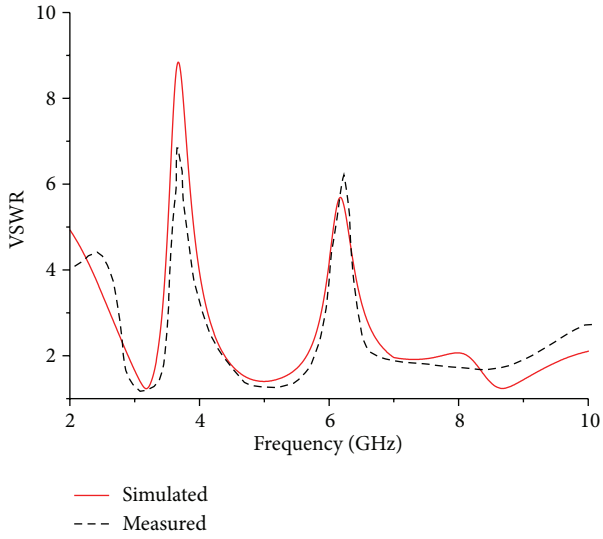

Figure 20: Simulated and measured VSWR results of the proposed antenna.

frequency of the stopband changes from 3.2 GHz to 4.5 GHz as angle α varies from $\pi/6$ to $\pi/3$. The simulated results show that a large shift in notch frequency took place with no other significant changes, so angle α is also one of the most important factors of tuning the centre frequency.

In conclusion, the effects of arc H-slot parametric variation on stopband centre frequency are presented in Table 2. It can be seen that the band-notched frequency is heavily dependent on parameters R_H, L_{H1}, and angle α and is lightly dependent on parameter L_{H0}. It can be easy to observe that the notch frequency can be tuned efficiently by changing any parameter except L_{H0}. Relative to the conventional H-shaped slot which can only change the length of the parameter W_{S1} [17], the desirable notch frequency can be achieved by varying one or more parameters of the arc H-shaped slot. Due to the characteristics of the arc H-shaped slot, the antenna provides easier tuning of the band-notched function. Through the analysis of the parameters of the arc H-shaped slot, advantages of the proposed antenna are presented.

Table 1: The effects of H-shaped slot parametric variation on stopband centre frequency [17].

Parameters	Stopband centre frequency
L_{S1}	Light dependence
L_{S2}	Light dependence
W_{S1}	Heavy dependence
W_{S2}	No dependence

Table 2: The effects of Arc H-shaped slot parametric variation on stopband centre frequency.

Parameters	Centre frequency changes per 2 mm	Stopband centre frequency
R_H	1.2 GHz	Heavy dependence
L_{H0}	0.3 GHz	Light dependence
L_{H1}	1 GHz	Heavy dependence
α	1.3 GHz (α varied from $\pi/6$ to $\pi/3$)	Heavy dependence

4. Results and Discussion

The photograph of fabricated dual band-notched UWB antenna is shown in Figure 19. A rectangular finite FR4 board is used for manufacture. The circular radiating patch is supported by an SMA connector. Figure 20 shows the simulated and measured VSWR results of the dual band-notched UWB antenna, it can be seen that the measured VSWR agrees well with the simulated result. The fabricated antenna covers the frequency range for UWB systems from 2.9 GHz to above 10 GHz with rejection bands around 3.3–4.2 GHz and 5.2–5.9 GHz. The discrepancy between the simulated and measured results could be mainly due to errors in processing and effect of the SMA connector. In order to confirm the accurate VSWR for the designed antenna, it is recommended that the manufacturing and measuring process should be performed carefully.

The antenna is usually required to have an omnidirectional radiation concerning the UWB applications. The simulated and measured radiation patterns at 3.2 GHz, 5 GHz, and 8 GHz are illustrated in Figures 21(a), 21(b), and 21(c); we can see that the measurements and the simulations show good agreement. The main purpose of these radiation patterns is to demonstrate that the antenna actually radiates over a wide frequency band. At the passband frequencies out of the notched bands, the antenna needs to have good omnidirectional radiation patterns. As shown in the figure, the radiation patterns in the yz-plane look like an "8" shape and in the xz-plane they are nearly round-shaped. It is noted that the proposed antenna gives nearly omnidirectional radiation patterns in the H-plane (xz-plane) and E-plane (yz-plane) at the passband.

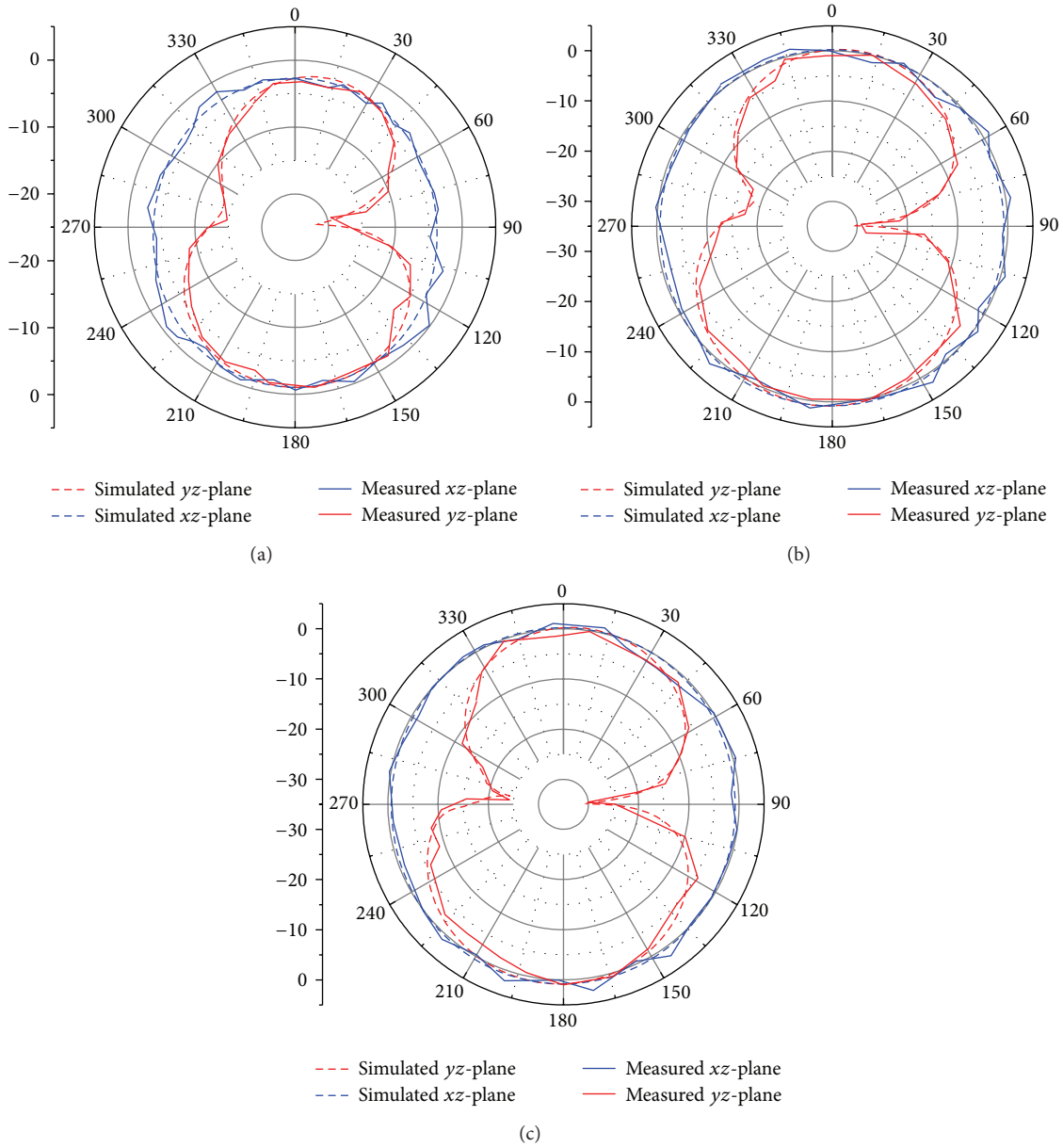

Figure 21: Measured and simulated radiation patterns of the proposed antenna: (a) 3.2 GHz, (b) 5 GHz, and (c) 8 GHz.

In addition, the total efficiency versus frequency of the proposed antenna is given in Figure 22. The proposed antenna should exhibit two sharp efficiency decreases at 3.7 GHz and 5.6 GHz. According to the figure, the range of the measurements is from 3 GHz to 10 GHz; the efficiency decreases sharply at the notched frequency band because of the resonators of the proposed antenna. At the passband, the efficiency remains at high level. It is clear from the results that the antenna cannot operate at the rejectband and can work efficiently at the passband.

5. Conclusions

A novel UWB antenna with dual band-notched function has been proposed and analyzed in this paper. The primitive UWB antenna is fabricated on a FR4 substrate. An arc H-shaped slot etched on the radiating patch and narrow slots etched on the ground plane are used to achieve the dual band-notched function. The parameters of the arc H-shaped slot are analyzed to show the advantages of the proposed antenna which provides improved control of tuning the centre frequency of the rejectband. The bandwidth of the low frequency band-notched antenna formed by the arc H-shaped slot and the bandwidth of the high frequency band-notched antenna formed by the narrow slots do not interfere with each other. The results of surface current distributions and the input impedance show that the designed antenna bandwidth with good band rejection is presented. Nearly omnidirectional radiation patterns and desirable efficiency of the antenna which could be observed by the simulated and

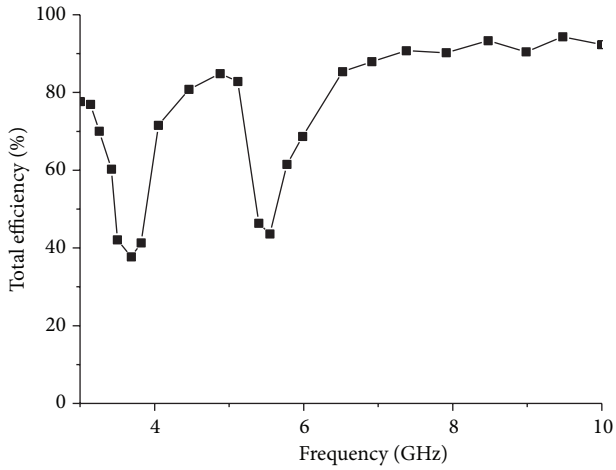

Figure 22: Total efficiency versus frequency.

measured results are also presented to verify the satisfactory performance of the proposed antenna.

Conflict of Interests

The authors declare that there is no conflict of interests regarding the publication of this paper.

Acknowledgments

This work was supported in part by the National Science Foundation of China under Grant NSFC61201086 and Grant NSFC61101235, the Doctoral Fund of Ministry of Education of China under Grant 20110162120044, and China Postdoctoral Science Foundation under Grant no. 2012T50660.

References

[1] Federal Communications Commission, *First Report and Order in the Matter of Revision of Part 1-5 of the Commission Rules Regarding Ultra-Wideband Transmission Systems*, 2002.

[2] T. Aboufoul and A. Alomainy, "Reconfigurable printed UWB circular disc monopole antenna," in *Proceedings of the 7th Loughborough Antennas and Propagation Conference (LAPC '11)*, Loughborough, November 2011.

[3] T. Aboufoul and A. Alomainy, "Single-element reconfigurable planar ultra wideband antenna for cognitive radio front end," in *Proceedings of the 4th International Conference on Cognitive Radio and Advanced Spectrum Management (CogART '11)*, Barcelona, Spain, October 2011.

[4] N. Prombutr, P. Kirawanich, and P. Akkaraekthalin, "Bandwidth enhancement of UWB microstrip antenna with a modified ground plane," *International Journal of Microwave Science and Technology*, vol. 2009, Article ID 821515, 7 pages, 2009.

[5] D.-Z. Kim, W.-I. Son, W.-G. Lim, H.-L. Lee, and J.-W. Yu, "Integrated planar monopole antenna with microstrip resonators having band-notched characteristics," *IEEE Transactions on Antennas and Propagation*, vol. 58, no. 9, pp. 2837–2842, 2010.

[6] S. Ghosh, "Band-notched modified circular ring monopole antenna for ultrawideband applications," *IEEE Antennas and Wireless Propagation Letters*, vol. 9, pp. 276–279, 2010.

[7] S.-J. Wu, C.-H. Kang, K.-H. Chen, and J.-H. Tarng, "Study of an ultrawideband monopole antenna with a band-notched open-looped resonator," *IEEE Transactions on Antennas and Propagation*, vol. 58, no. 6, pp. 1890–1897, 2010.

[8] A. Ghobadi, C. Ghobadi, and J. Nourinia, "A novel band-notched planar monopole antenna for ultrawideband applications," *IEEE Antennas and Wireless Propagation Letters*, vol. 9, pp. 608–611, 2010.

[9] Y. D. Dong, W. Hong, Z. Q. Kuai, and J. X. Chen, "Analysis of planar ultrawideband antennas with on-ground slot band-notched structures," *IEEE Transactions on Antennas and Propagation*, vol. 57, no. 7, pp. 1886–1893, 2009.

[10] E. Antonino-Daviu, M. Cabedo-Fabrés, M. Ferrando-Bataller, and V. M. R. Peñarrocha, "Modal analysis and design of band-notched UWB planar monopole antennas," *IEEE Transactions on Antennas and Propagation*, vol. 58, no. 5, pp. 1457–1467, 2010.

[11] A. Nouri and G. R. Dadashzadeh, "A compact UWB band-notched printed monopole antenna with defected ground structure," *IEEE Antennas and Wireless Propagation Letters*, vol. 10, pp. 1178–1181, 2011.

[12] B. Li, J. S. Hong, and B. Z. Wang, "Switched band-notched UWB/dual-band WLAN slot antenna with inverted S-shaped slots," *IEEE Antennas and Wireless Propagation Letters*, vol. 11, pp. 572–575, 2012.

[13] A. M. Abbosh, "Design of a CPW-fed band-notched UWB antenna using a feeder-embedded slotline resonator," *International Journal of Antennas and Propagation*, vol. 2008, Article ID 564317, 5 pages, 2008.

[14] W. T. Li, Y. Q. Hei, W. Feng, and X. W. Shi, "Planar antenna for 3G/Bluetooth/WiMAX and UWB applications with dual band-notched characteristics," *IEEE Antennas and Wireless Propagation Letters*, vol. 11, pp. 61–64, 2012.

[15] M. Mehranpour, J. Nourinia, C. Ghobadi, and M. Ojaroudi, "Dual band-notched square monopole antenna for ultrawideband applications," *IEEE Antennas and Wireless Propagation Letters*, vol. 11, pp. 172–175, 2012.

[16] L.-H. Ye and Q.-X. Chu, "3.5/5.5GHz dual band-notch ultrawideband slot antenna with compact size," *Electronics Letters*, vol. 46, no. 5, pp. 325–327, 2010.

[17] X. L. Bao and M. J. Ammann, "Printed UWB antenna with coupled slotted element for notch-frequency function," *International Journal of Antennas and Propagation*, vol. 2008, Article ID 713921, 8 pages, 2008.

Hindawi Publishing Corporation
International Journal of Antennas and Propagation
Volume 2014, Article ID 937423, 10 pages
http://dx.doi.org/10.1155/2014/937423

Research Article

Compact Dual-Band Planar Inverted-e-Shaped Antenna Using Defected Ground Structure

Wen Piao Lin, Dong-Hua Yang, and Zong-De Lin

Department of Electrical Engineering, Chang Gung University, 259 Wen-Hwa 1st Road, Kwei-Shan, Taoyuan 333, Taiwan

Correspondence should be addressed to Dong-Hua Yang; belldandy1p@yahoo.com.tw

Received 11 April 2013; Revised 5 December 2013; Accepted 5 December 2013; Published 23 January 2014

Academic Editor: Alistair P. Duffy

This paper presents a novel dual-band planar inverted-e-shaped antenna (PIEA) using defected ground structure (DGS) for Bluetooth and wireless local area network (WLAN) applications. The PIEA can reduce electromagnetic interferences (EMIs) and it is constructed on a compact printed circuit board (PCB) size of $10 \times 5 \times 4\ mm^3$. Experimental results indicate that the antenna with a compact meandered slit can improve the operating impedance matching and bandwidths at 2.4 and 5.5 GHz. The measured power gains at 2.4 and 5.5 GHz band are 1.99 and 3.71 dBi; antenna efficiencies are about 49.33% and 55.23%, respectively. Finally, the good performances of the proposed antenna can highly promote for mobile device applications.

1. Introduction

In recent years, wireless local area networks (WLANs) have tremendously advanced. The WLAN facilitates the wireless connection between laptop computers, mobile devices, and other equipment within a local area. Small volume antennas are highly attractive for Bluetooth and wireless local area network (WLAN)/worldwide interoperability mobile access (WiMAX) applications [1–4]. Additionally, the frequency bands located around 2.4 GHz and 5 GHz have been widely used in Bluetooth and WLAN/WiMAX simultaneously. A multiband antenna is thus more efficient than multiple antennas specifically designed to operate on each frequency band.

Dual-band antennas, composed of a pair of dipoles or of a T-shaped monopole, have been presented to cover the frequency band of 2.4 and 5 GHz in [5, 6]. According to [7–15], the meander slit antenna includes many basic folded elements in various patterns and it can produce various resonant frequencies markedly lower than resonances frequency of a single-element antenna under the same length. Apparently, owing to the various current cancellation and reinforcements, a larger number of higher resonances frequencies can occur on a meander monopole antenna than on a simple monopole of the same length [7–11]. The antenna with a meandered slit can reduce the tag sizes. Moreover, meandered slit can use open-end slots in the ground plane, generally located under the radiating patch. The size reduction method is highly promising for implementing practical antenna. Previous work [12–15] described the feasibility of using a slotted ground plane for broadening the operational bandwidth of a small terminal antenna.

Additionally, due to their small size, the planar inverted-F antennas (PIFAs) or monopole antennas have a narrow bandwidth, especially at 5 GHz band. Numerous dual-band designs have been developed for WLAN and Bluetooth applications [16, 17]. Our previous studies have established that dual-band F-shaped monopole antennas are characterized by a simple geometrical structure that assures a small volume, a low cost, and a simple integration on a circuit board, as required by the modern handset terminals [18, 19]. Recent studies have also demonstrated the effectiveness of the WLAN antennas using an inverted-F strip integrated on the circuit board of a communication device in further reducing the antenna volume and decreasing the fabrication cost. Therefore, owing to its sufficient bandwidth, radiation efficiency, power gain, and electrostatic discharge (ESD) protection, the PIFA is highly attractive for WLAN applications [20].

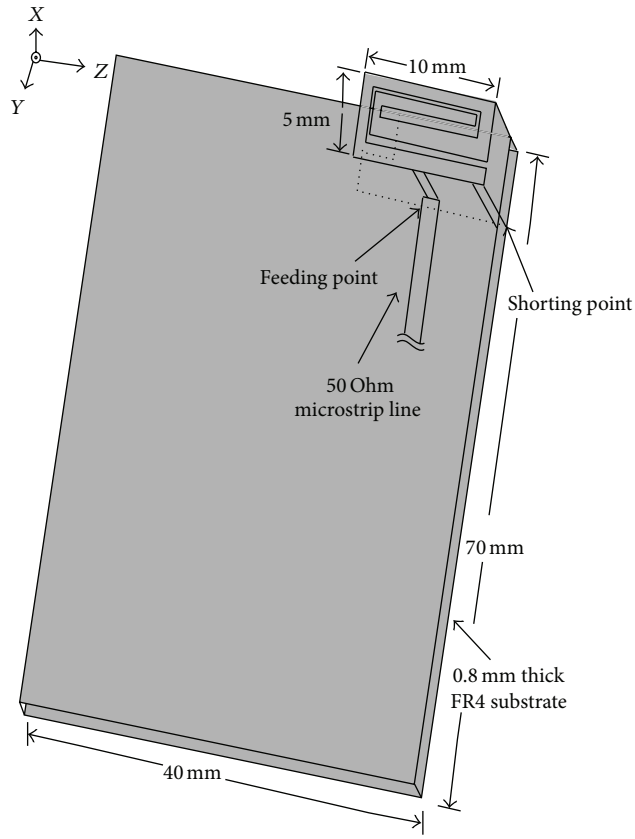

Figure 1: Proposed dual-band meander inverted-e-shaped antenna.

This work presents a planar inverted-e-shaped antenna (PIEA) based on a flaw earth structure to increase the bandwidth of PIFA. The shape of the antenna resembles that of the inverted alphabet e, explaining why the antenna is referred to as an e antenna. The radiating part is shorted with the ground plane to reduce the antenna size. Moreover, with its satisfactory gain, the proposed PIEA can be accommodated in small card shaped areas for different compact wireless systems. The proposed antenna can also be considered as a miniaturized and low-cost antenna model, applicable for many small wireless systems requiring an omnidirectional radiation pattern.

2. Antenna Design

Figure 1 shows the configuration of proposed dual-band inverted-e-shaped antenna. All of the electromagnetic analyses have been performed using a software package of Ansoft high frequency structure simulator (HFSS), based on the three-dimensional finite element method (3D FEM). The size of a ground plane is $70 \times 40\,\text{mm}^2$ considered as the printed circuit board (PCB) of a practical handset, and the metal is only printed on the front surface of an FR-4 substrate with relative permittivity 4.6 and height of 0.8 mm. The antenna has a compact size of $10 \times 5 \times 4\,\text{mm}^3$. Figure 2 shows the geometrical configuration with the designed shapes of L, U, and e. Figures 2(a), 2(b), and 2(c) show the top view of the designed antenna size, where $W_1 = 10$ mm, $W_2 = 9$ mm, $W_3 = 7.75$ mm, $W_4 = 7.15$ mm, $L_1 = 5$ mm, $L_2 = 3.5$ mm, $L_3 = 2.5$ mm, $L_4 = 0.65$ mm, $S_1 = 0.5$ mm, $S_2 = 0.25$ mm, $S_3 = 0.25$ mm, $S_4 = 0.25$ mm, and $S_5 = 0.7$ mm. In addition, the meander slit e-shaped structure can obtain the resonance at 2.4 and 5.8 GHz in the small area. The structure causes the cancellation of the current due to the length of the proposed antenna longer than the quarter free-space wavelengths (31.25 mm) at 2.4 GHz, which results the total length is 41 mm. According to the side view of the designed antenna shown in Figure 2(d), the distance of D between the feeding point and the shorting point is 4.5 mm, while the distance between the ground plane and the radiating structure is 4 mm.

The conventional meandered slit antenna produces a wire configuration presenting capacitive and inductive reactance effects, which mutually cancel out each other. Resonance frequencies are therefore produced at markedly lower frequencies than those in the case of straight wire antenna of the same height at the expense of a narrow bandwidth and low gain, especially when the antenna must be arranged in a surface of few square centimeters. The proposed planar inverted-e-shaped antenna (PIEA) uses a meander slit with a DGS, in which an "e" folding of the meandered slit confers to the radiating structure which differs from that of a conventional straight dipole of the same length. Moreover, the lowest resonant frequency can be tuned using the same tuning elements.

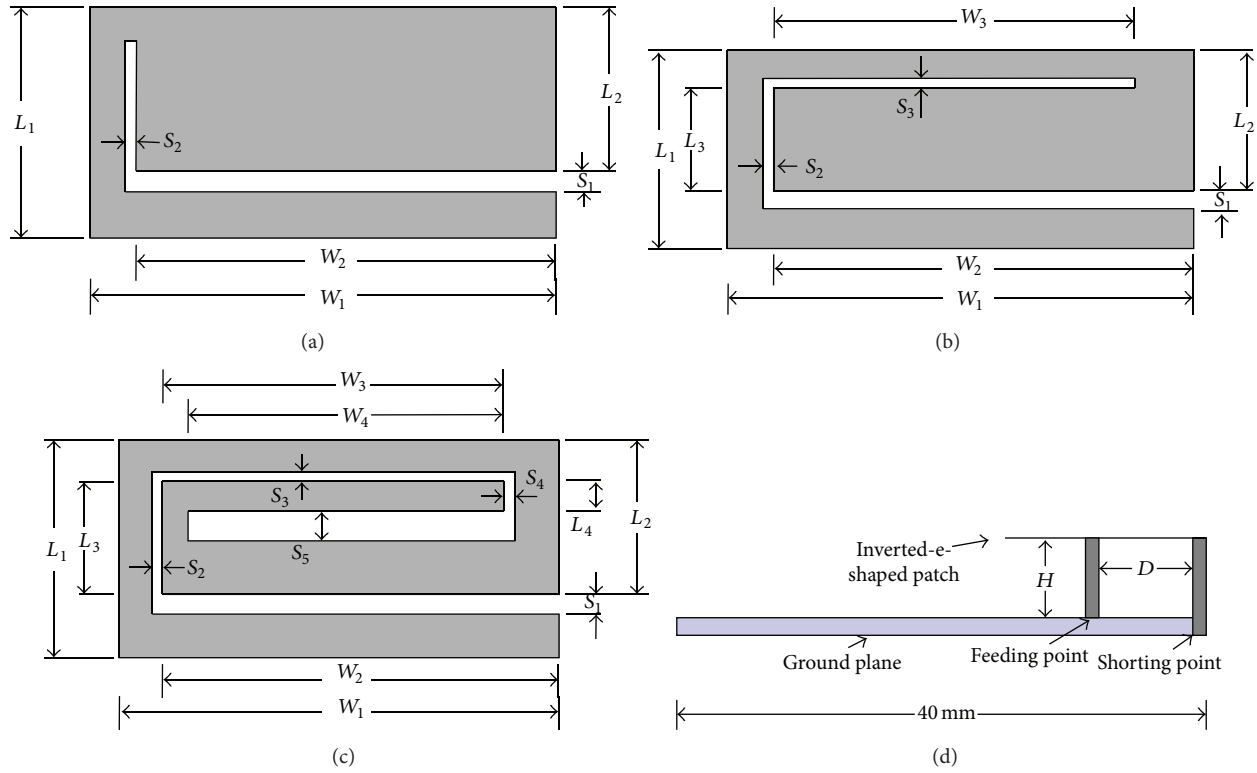

Figure 2: The geometry of designed ((a), (b), and (c)) top view and (b) side view of planar inverted-e antenna.

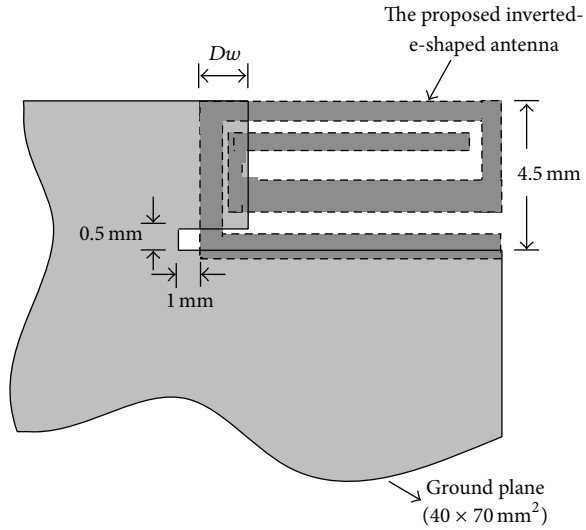

Figure 3: The geometry of the designed top view of proposed DGS.

As mentioned earlier, the proposed antenna consists of an inverted-e-shaped meander slit with a rectangular DGS. Figure 3 schematically depicts the proposed DGS. A previous work [12–15] has shown that the size and shape of the chassis could play a significant role in broadening the bandwidth of a terminal antenna. This means that slits in a ground plane could facilitate efforts to optimize the bandwidth of the antenna.

Figure 4 shows the simulation S-parameters for the various antenna shapes of L, U, and e. It is clearly observable that the return loss is changed for three designs. In the U-shaped structure, slit is added to lengthen the path of the average current for the resonance frequency at 3 and 7.4 GHz. In the e-shaped structure, the small area can obtain the resonance at 2.4 and 5.99 GHz.

The simulated real and imaginary impedance of proposed PIEA without DGS in the ground plane are shown in Figures 5(a) and 5(b). In order to change the resonant frequencies, we adjust the capacitor and inductor parameters, in the antenna circuit. Moreover, the real and imaginary

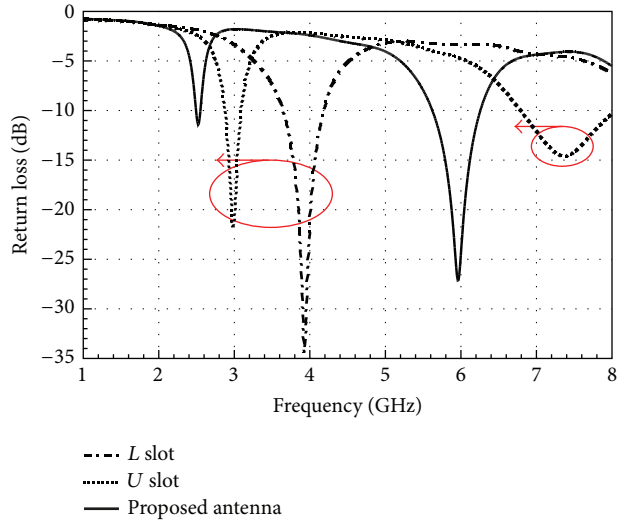

Figure 4: The simulation return losses results for the proposed L, U, and e-shaped slit S-parameter.

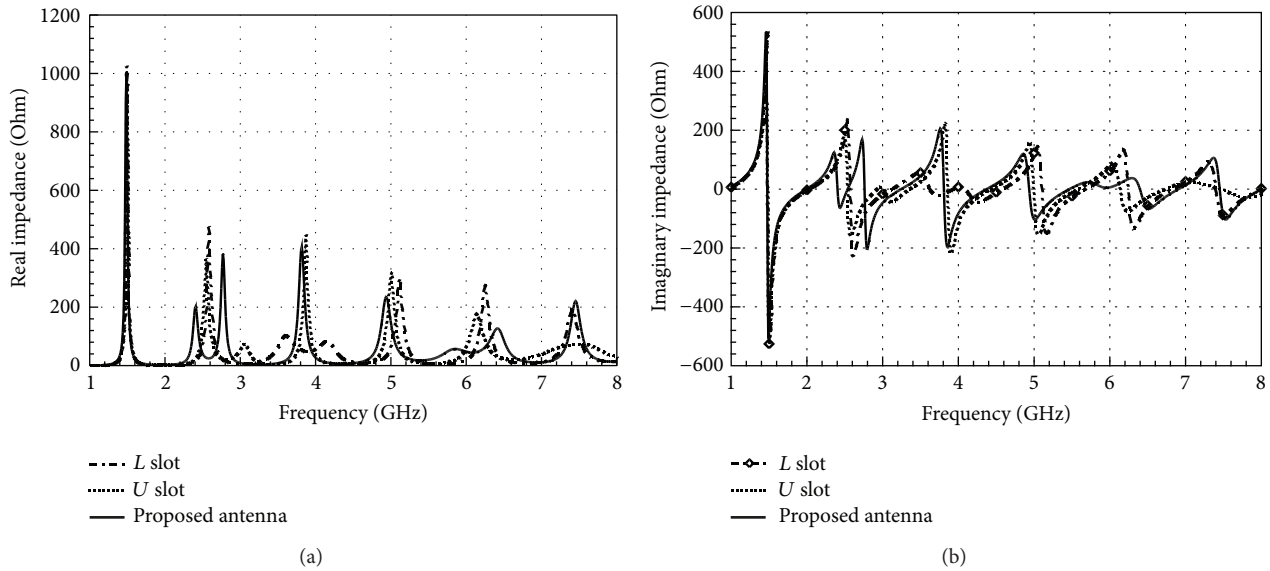

Figure 5: Simulation results of proposed slit shaped (a) real and (b) imaginary impedance.

impedance part of its admittance are approximately 50 and 0 Ohm, respectively, according to simulation results.

The simulated results of the antenna are shown in Figure 6 by the tuned parameters of D in Figure 2(d) and Dw in Figure 3, respectively. From Figure 6(a), we can see that the optimal distance of D is 4.5 mm to obtain the better impedance matching. Moreover, the better bandwidth can be achieved to adjust the distance of Dw at 1.5 mm as shown in Figure 6(b).

Figure 7 shows the simulated reflection coefficient S_{11} of proposed PIEA without DGS and with DGS in the ground plane. According to this figure, the proposed antenna without DGS presents two resonant peaks (see dotted line in Figure 7). In particular, the first peak appears at about 2.45 GHz with a return loss of −11 dB, while the second peak appears at 5.99 GHz where a return loss of about −27 dB is found. From Figure 7 it appears that a bandwidth of 0.63 GHz (5.6–6.23 GHz) is obtained only in the neighborhood of 5.99 GHz. A different frequency behavior is observed for the radiating structure equipped with DGS. In fact, in this case the two peaks in the curve of the return loss (solid line in Figure 7) are equal to about −14.9 dB at 2.4 GHz and about −18.2 dB at 5.62 GHz, respectively. The bandwidths of these frequencies are approximately 0.06 (2.39–2.45) and 0.9 (5.22–6.12) GHz, respectively. Numerical results indicate a fairly good impedance matching of the proposed PIEA with DGS, excellent broadband characteristics, and enhanced resonant performances.

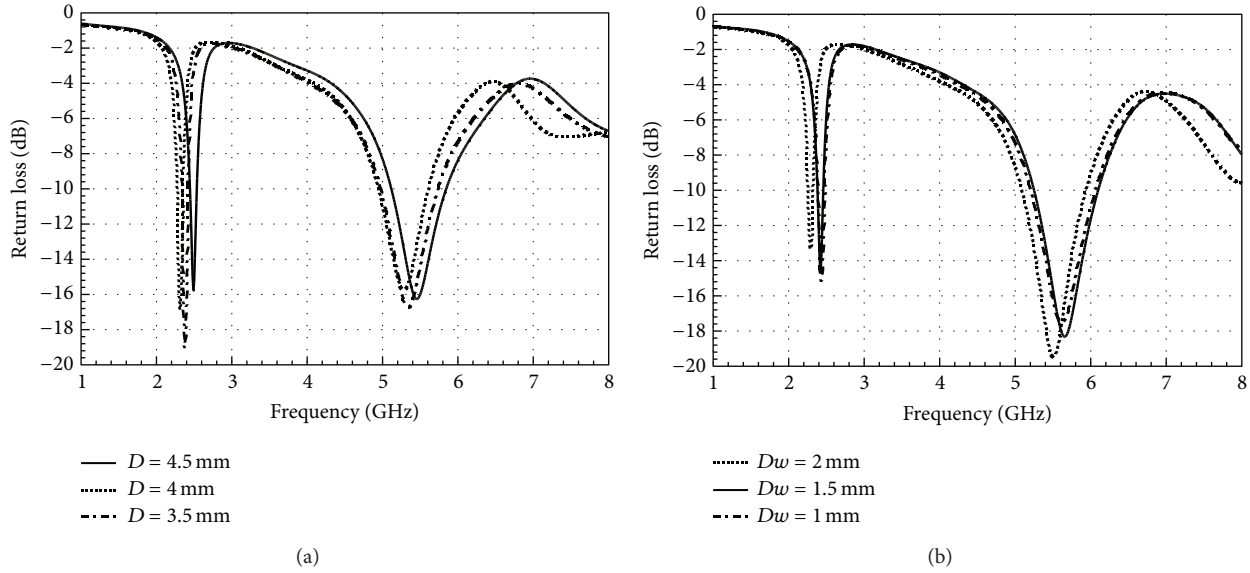

Figure 6: Simulation results by tuned parameters to the distance between (a) feeding and shorting plate. (b) DGS and inverted-e-shaped edge.

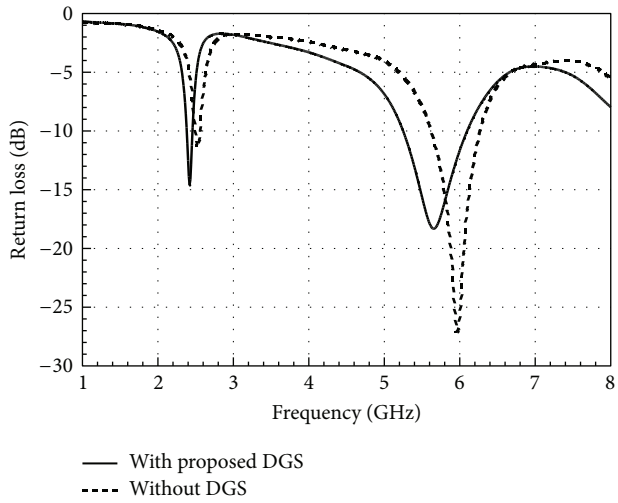

Figure 7: The simulated return losses S_{11} for the proposed PIEA with DGS and without DGS in the ground plane.

3. Results and Discussion

To demonstrate the performances of the proposed PIEA, a prototype antenna which is performed by numerical simulation has been realized as shown in Figure 8. Constructed on a FR4 substrate having $\varepsilon = 4.6$ and height = 0.8 mm, the fabricated antenna was measured in 3D anechoic chamber using the Agilent E5071C Network Analyzer. Figure 9 shows the simulated and measured reflection coefficients S_{11}. The measured bandwidths at return loss of −10 dB are 83 and 675 MHz at the center frequency of 2.44 and 5.5 GHz, respectively. This figure reveals that the measured reflection coefficient of S_{11} is rather close to the simulation results of S_{11}. Above results indicate that the antenna is well matched to 50 Ω presenting bandwidths that are adequate for applications working at 2.4 and 5.5 GHz.

Figures 10(a) and 10(b) display the surface current distributions of the proposed antenna at the working frequency of 2.4 and 5.5 GHz, respectively. Figure 10 indicates that a stronger current distribution in an inverted-e-shaped stub than any other area implies, for the antenna impedance matching, a closer relation of the voltage to the current at the input to the antenna.

Figure 11 shows the measured 2D radiation power patterns in the X-Z and X-Y plane at 2.402, 2.441, 2.45, 2.48, and 5.5 GHz band. The proposed antenna has an almost monopole-like of radiation pattern in the X-Z (cross-polarization) and X-Y (co- and cross-polarization) plane

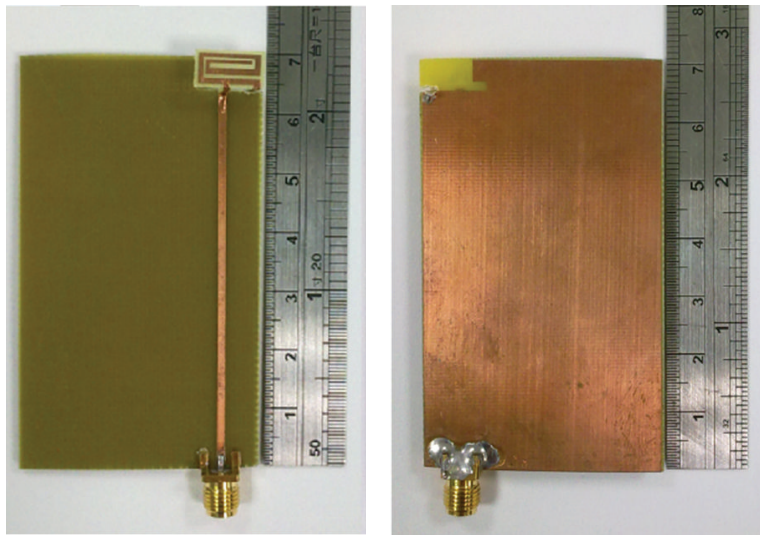

(a) (b)

Figure 8: Numerical simulation and experimental measurement return losses for the proposed PIEA with DGS.

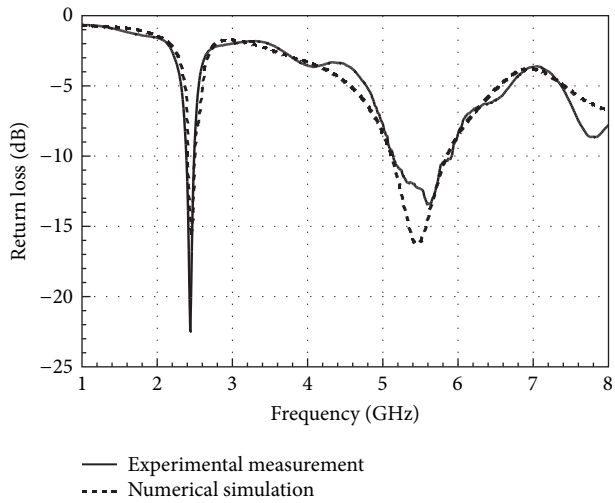

Figure 9: Photograph of the fabricated planar inverted-e-shaped antenna with DGS.

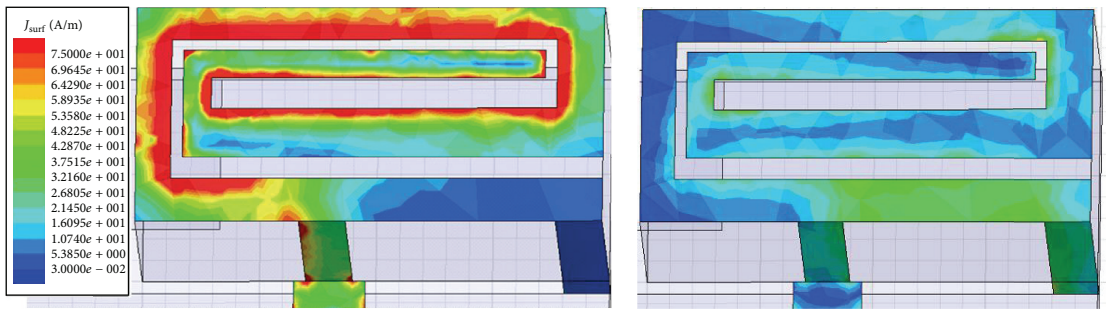

(a) (b)

Figure 10: Current distributions at (a) 2.4 GHz and (b) 5.5 GHz.

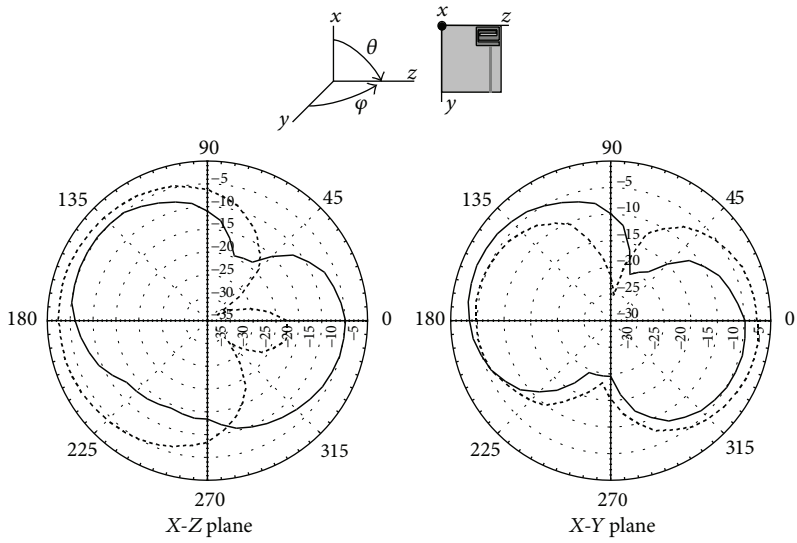

(a) At 2.402 GHz

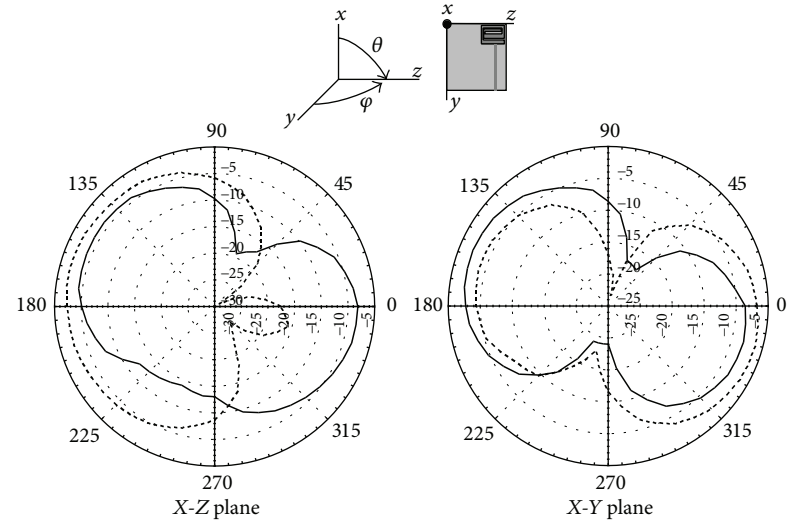

(b) At 2.441 GHz

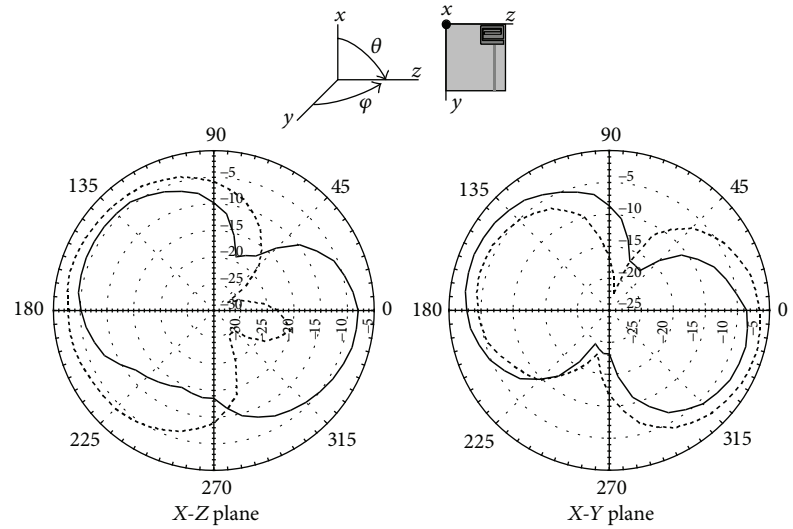

(c) At 2.45 GHz

Figure 11: Continued.

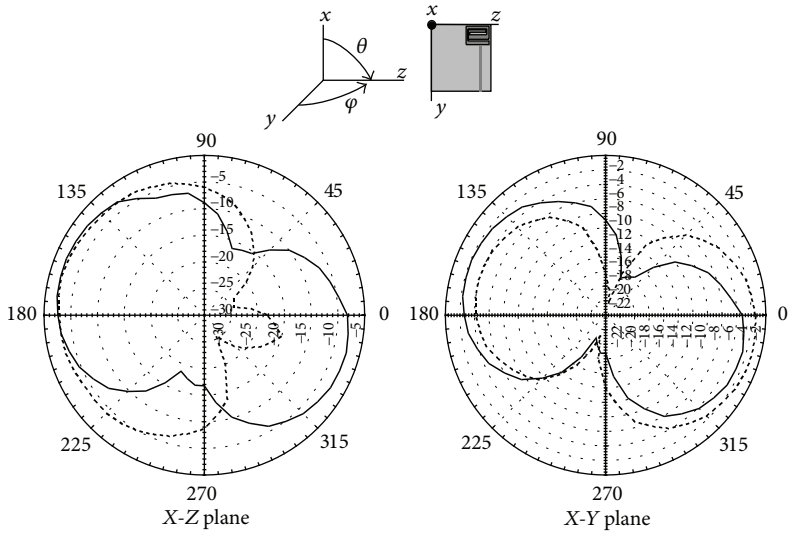

(d) At 2.48 GHz

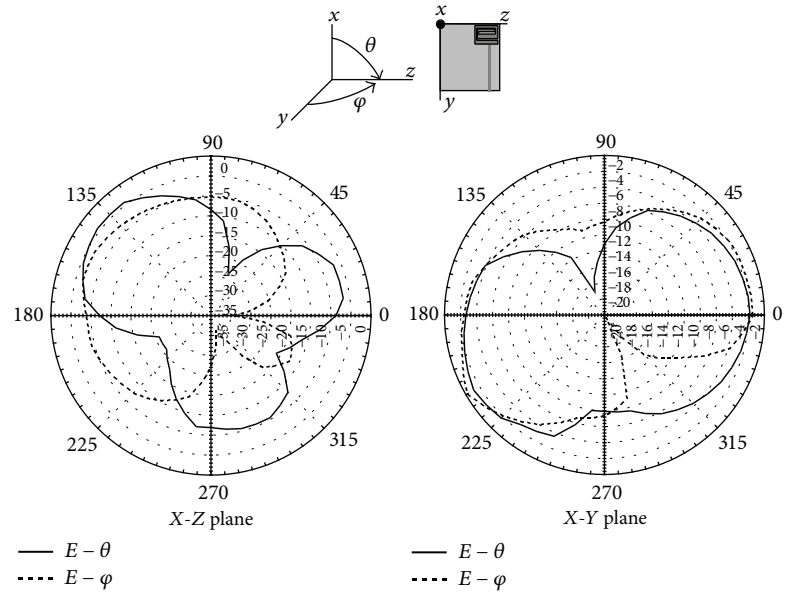

(e) At 5.5 GHz

Figure 11: The measured 2D radiation patterns of the proposed antenna.

due to the meander slit of a full-wavelength radiator. The antenna also exhibits a better directivity radiation power gain pattern at X-Z (copolarization) plane. Our proposed antenna is an asymmetric architecture from the current distributions shown in Figure 10(a). The reference direction is along the direction of maximum current in the radiating structure and a stronger radiation pattern can produce on the copolarization. The obtained radiation patterns are near omnidirectional in X-Z plane, and the radiation patterns exhibit monopole-like patterns in the X-Y plane. Above experimental results indicate that the maximum antenna power gains at 2.4 and 5.5 GHz band are 1.99 and 3.71 dBi; in addition, antenna efficiencies are 49.33 and 55.23%, respectively. Measurement results demonstrate that the radiation characteristics of the proposed antenna at the operating frequencies of 2.4 and 5.5 GHz are quite stable. The measured peak gain and antenna efficiency for the e-shaped antenna are plotted in Figure 12. The peak gain is about 2~2.2 dBi for the lower band and 0.9~3.7 dBi for the upper band. The antenna efficiency is about 40% for the lower band and 40~55% for the upper band. In general, the measured radiation patterns of horizontally polarized omnidirectional cover complementary space regions. Therefore, the proposed antenna can provide pattern diversity in a wireless communication system. The proposed antenna can satisfy the required specifications of fixed and mobile devices.

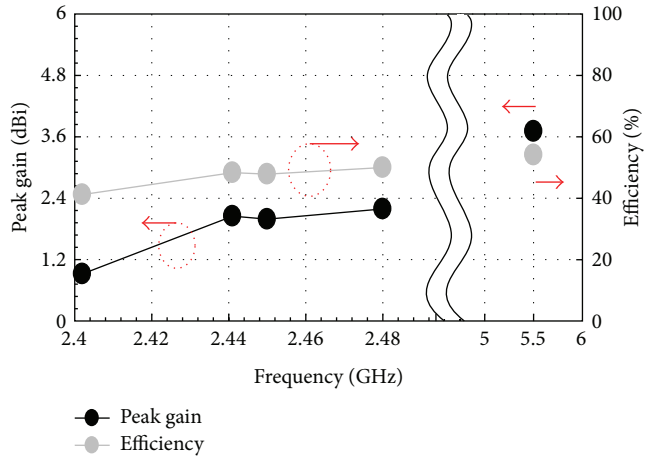

FIGURE 12: The simulated peak gain and efficiency for proposed antenna.

4. Conclusion

A novel planar compact meander inverted-e-shaped antenna with a DGS size of $10 \times 5 \times 4\,\text{mm}^3$ in the ground plane has been presented. The proposed antenna with DGS can enhance the antenna performance in terms of its suppressed broadened impedance bandwidth. The measured antenna efficiencies at 2.4 and 5.5 GHz are about 49.33 and 55.23%, respectively. Additionally, experimental results correlate well with the simulation results. Moreover, desired characteristics such as excellent radiation patterns, moderate antenna gain, and low cost make the proposed antenna highly promising for Bluetooth and WLAN/WiMAX applications.

Conflict of Interests

The authors declare that there is no conflict of interests regarding the publication of this paper.

Acknowledgments

The authors wish to thank the Arima Communications Corp. for providing the test equipments and anechoic chamber and the technicians of the company for their valued suggestions useful to complete this study. The authors wish also to thank the support of the National Science Council under Contract no. NSC 99-2632-E-182-001-MY3 and the partial support received by the Chiang Education Foundation of Taipei, Taiwan. The support of the High Speed Intelligent Communication (HSIC) Research Center of the Chang Gung University, Taoyuan, Taiwan, has been also appreciated.

References

[1] X. Cai, A. Wang, and S. Gao, "A compact gourd-shaped dual-band antenna for WiMAX/WLAN applications," in *Proceedings of the 9th International Symposium on Antennas Propagation and EM Theory (ISAPE '10)*, pp. 75–78, Guangzhou, China, December 2010.

[2] P. Ciais, R. Staraj, G. Kossiavas, and C. Luxey, "Compact internal multiband antenna for mobile phone and WLAN standards," *Electronics Letters*, vol. 40, no. 15, pp. 920–921, 2004.

[3] H.-W. Hsieh, Y.-C. Lee, K.-K. Tiong, and J.-S. Sun, "Design of a multiband antenna for mobile handset operations," *IEEE Antennas and Wireless Propagation Letters*, vol. 8, pp. 200–203, 2009.

[4] Y.-S. Shin and S.-O. Park, "A compact loop type antenna for Bluetooth, S-DMB, Wibro, WiMax, and WLAN applications," *IEEE Antennas and Wireless Propagation Letters*, vol. 6, pp. 320–323, 2007.

[5] X. -L. Quan, R. Li, Y. -H. Cui, and M. M. Tentzeris, "Analysis and design of a compact dual-band directional antenna," *IEEE Antennas and Wireless Propagation Letters*, vol. 11, pp. 547–5550, 2012.

[6] T. N. Chang and J.-H. Jiang, "Meandered T-shaped monopole antenna," *IEEE Transactions on Antennas and Propagation*, vol. 57, no. 12, pp. 3976–3978, 2009.

[7] H.-D. Chen, J.-S. Chen, and Y.-T. Cheng, "Modified inverted-L monopole antenna for 2.4/5 GHZ dual-band operations," *Electronics Letters*, vol. 39, no. 22, pp. 1567–1569, 2003.

[8] Y. -F. Weng, S. -W. Cheung, and T. -I. Yuk, "Design of multiple band-notch using meander lines for compact ultra-wide band antennas," *IET Microwaves Antennas and Propagation*, vol. 6, no. 8, pp. 908–9914, 2012.

[9] F. Shen, Y. Wei, X. Xu et al., "Symmetric double V-shaped microstrip meander-line slow-wave structure for W-band traveling-wave tube," *IEEE Transactions on Electron Devices*, vol. 59, no. 5, pp. 1551–1557, 2012.

[10] C. Di Nallo and A. Faraone, "Multiband internal antenna for mobile phones," *Electronics Letters*, vol. 41, no. 9, pp. 514–515, 2005.

[11] M. Ali, G. J. Hayes, H.-S. Hwang, and R. A. Sadler, "Design of a multiband internal antenna for third generation mobile phone handsets," *IEEE Transactions on Antennas and Propagation*, vol. 51, no. 7, pp. 1452–1461, 2003.

[12] Y. X. Guo, K. M. Luk, K. F. Lee, and Y. L. Chow, "Double U-slot rectangular patch antenna," *Electronics Letters*, vol. 34, no. 19, pp. 1805–1806, 1998.

[13] T.-H. Kim and D.-C. Park, "Compact dual-band antenna with double L-slits for WLAN operations," *IEEE Antennas and Wireless Propagation Letters*, vol. 4, no. 1, pp. 249–252, 2005.

[14] O. O. Olaode, W. D. Palmer, and W. T. Joines, "Effects of meandering on dipole antenna resonant frequency," *IEEE Antennas and Wireless Propagation Letters*, vol. 11, pp. 122–125, 2012.

[15] C.-I. Lin and K.-L. Wong, "Printed monopole slot antenna for internal multiband mobile phone antenna," *IEEE Transactions on Antennas and Propagation*, vol. 55, no. 12, pp. 3690–3697, 2007.

[16] Y.-M. Chen, S.-F. Chang, C.-L. Wei, Y.-T. Wang, and C.-H. Huang, "Packaged ultra-wide-band bandpass filter based on inverted-T multiple-mode resonators and inverted-F impedance transformers: TC contests," *IEEE Microwave Magazine*, vol. 11, no. 1, pp. 126–129, 2010.

[17] G. H. Huff and J. J. McDonald, "A spherical inverted-F antenna (SIFA)," *IEEE Antennas and Wireless Propagation Letters*, vol. 8, pp. 649–652, 2009.

[18] D.-B. Lin, I.-T. Tang, M.-Z. Hong, and H.-P. Lin, "A compact quad-band PIFA by using defected ground structure," in *Proceedings of the IEEE Antennas and Propagation Society International Symposium (AP-S '07)*, pp. 4677–4680, Honolulu, Hawaii, USA, June 2007.

[19] C.-S. Kim, J.-S. Park, D. Ahn, and J.-B. Lim, "A novel 1-D periodic defected ground structure for planar circuits," *IEEE Microwave and Wireless Components Letters*, vol. 10, no. 4, pp. 131–133, 2000.

[20] A. Babar, L. Ukkonen, M. Soini, and L. Sydanheimo, "Planar inverted miniaturized E antenna, for compact wireless systems," in *Proceedings of the IEEE International Symposium on Antennas and Propagation and USNC/URSI National Radio Science Meeting (APSURSI '09)*, pp. 1–4, Charleston, SC, USA, June 2009.

Hindawi Publishing Corporation
International Journal of Antennas and Propagation
Volume 2014, Article ID 805853, 6 pages
http://dx.doi.org/10.1155/2014/805853

Research Article

A Compact UWB Diversity Antenna

Hui Zhao,[1,2] Fushun Zhang,[1] Chunyang Wang,[2] and Jiangang Liang[2]

[1] *National Key Laboratory of Antennas and Microwave Technology, Xidian University, Xi'an, Shaanxi 710071, China*
[2] *Missile Institute of Air Force Engineering University, Sanyuan, Shaanxi 713800, China*

Correspondence should be addressed to Hui Zhao; microwave_zhao@163.com

Received 5 May 2013; Accepted 16 December 2013; Published 9 January 2014

Academic Editor: Alistair P. Duffy

A compact printed ultrawideband (UWB) diversity antenna with a size of 30 mm × 36 mm operating at a frequency range of 3.1–10.6 GHz is proposed. The antenna is composed of two semielliptical monopoles fed by two microstrip lines. Two semicircular slots, two rectangular slots, and one stub are introduced in the ground plane to adjust the impedance bandwidth of the antenna and improve the isolation between two feeding ports. The simulated and measured results show that impedance bandwidth of the proposed antenna can cover the whole UWB band with a good isolation of < −15 dB. The radiation patterns, peak antenna gain, and envelope correlation coefficient are also measured and discussed. The measured results show that the proposed antenna can be a good candidate for some portable MIMO/diversity UWB applications.

1. Introduction

Ultrawideband (UWB) communication systems attract great attention in the wireless world because of their advantages, including high speed data rate, extremely low spectral power density, high precision ranging, low cost, and low complexity, since the Federal Communication Commission (FCC) allowed 3.1–10.6 GHz unlicensed band for UWB communication [1]. Multiple input and output (MIMO) antennas used in UWB systems can improve systems' performance such as providing increased data rates and making increased range available through beam forming [2]. Antenna diversity is a well-known technique to enhance the performance of MIMO systems by mitigating the multipath fading and cochannel interference [3–5]. Thus, a MIMO/diversity antenna covering UWB band and having good radiation patterns and diversity performance has become the focus of wireless communications [6–10]. However, the operating frequency of the antennas in [6–10] cannot cover the whole band of 3.1–10.6 GHz and the size of the antenna in [6–8] is relatively large. Recently, an UWB diversity antenna covering the whole UWB and having a small size has been presented in [11]. The proposed antenna has a size of 35 mm × 40 mm, and a good isolation better than −16 dB has been achieved through a tree-like structure introduced in the ground plane. However, the size of the antenna in [11] is still relatively large and a complicate tree-like structure should be designed to weaken the mutual coupling between two monopoles due to the close distance between them.

In this paper, we propose a simple MIMO/diversity antenna covering the whole UWB band and having a small size of 30 mm×36 mm which is only 75 percent of the antenna in [11]. The proposed antenna is designed by using two semielliptical monopoles. By properly adjusting the distance between two monopoles and introducing two semicircular slots, two rectangular slots, and one stub in the ground plane, the antenna can achieve a broad impedance bandwidth covering the whole UWB with good isolation of < −15 dB.

2. Antenna Configuration and Analysis

2.1. Antenna Configuration. The specific geometry with detailed dimensions of the proposed antenna is illustrated in Figure 1(a), and the photograph of the proposed antenna is shown in Figure 1(b). The antenna consists of dual semielliptical monopoles which are aligned along y-axis with an optimized distance of 15.3 mm which is about a quarter

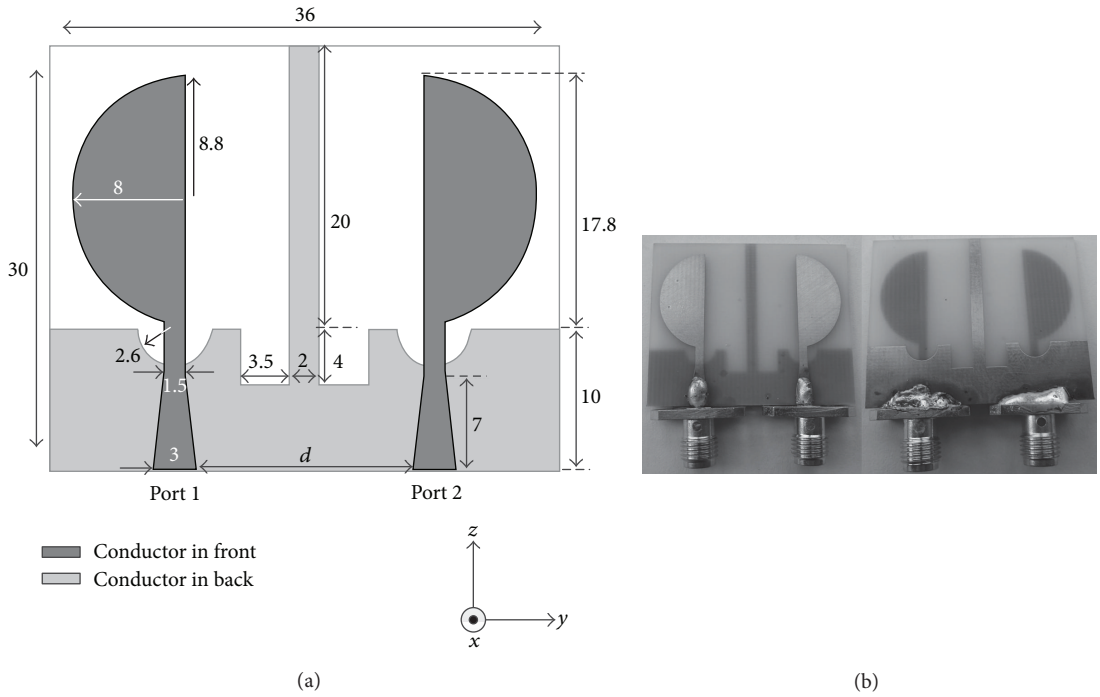

Figure 1: Geometry and photograph of the proposed antenna (d = 15.3, dimensions, mm).

guided wavelengths at 3 GHz. The guided wavelengths λ_g can be calculated by using

$$\lambda_g = \frac{c}{f\sqrt{(\varepsilon_r + 1)/2}}, \quad (1)$$

where f is the frequency, ε_r and $\sqrt{(\varepsilon_r + 1)/2}$ are the relative permittivity and effective permittivity of the substrate, respectively, and c is the speed of light. The major radius and the radius ratio of the semielliptical monopole are 8 mm and 1.1, respectively. Each monopole is fed by a 50 Ω tapered microstrip line with an upper width of 1.5 mm, lower width of 3 mm, and height of 7 mm. The monopoles are printed on the upper part of a partially grounded FR4 substrate with dimensions 30 mm × 36 mm × 1.6 mm and relative permittivity 4.6. On the back surface of the substrate, the main rectangular ground plane of 36 mm in width and 10 mm in length is printed. Note that two semicircular slots with same radius of 2.6 mm, one stub of 2 mm in width, and 20 mm in length in the middle of the ground plane and two rectangular slots of 3.5 mm in width and 4 mm in length at the bottom of the stub are introduced in the ground plane to adjust the impedance bandwidth of the antenna and improve the isolation between two feeding ports.

2.2. Antenna Analysis. By aligning two semielliptical monopoles along y-axis with a proper distance between them and introducing two semicircular slots, one stub, and two rectangular slots in the ground plane in turn, the proposed antenna can be designed conventionally.

To well understand the design mechanisms of the proposed antenna, the scattering parameters of the proposed antenna with or without the slots and stub are simulated by using High-Frequency Structure Simulation (HFSS), Version-12, software. Due to the symmetrical structure of the proposed antenna, only the reflection coefficient $|S_{11}|$ at port 1 and isolation $|S_{21}|$ between two feeding ports are simulated. The simulated results are shown in Figure 2.

As shown in Figure 2(a), one can observe that the impedance bandwidth of the proposed antenna without all slots and stub tends to cover the whole UWB band, and the isolation between two feeding ports is very poor. In order to enhance or adjust the impedance bandwidth of the antenna, dual semicircular slots with a radius of 2.6 mm are introduced in the ground plane and the simulation results are shown in Figure 2(b). The slots in the ground plane are achieved to obtain the necessary interaction between this plane and the radiator so that the proper matching impedance is received. It can be observed from Figure 2(b) that the impedance bandwidth of the antenna is enhanced and can cover the whole UWB but a poor isolation is still achieved especially in the upper band. To improve the isolation between two feeding ports, a stub of 2 mm in width and 20 mm in length in the middle of the ground plane is introduced and the simulation results are shown in Figure 2(c). The stub can be viewed as a reflector to reduce the mutual coupling through separating the radiation patterns of two radiators. As shown in Figure 2(c), it can be observed that a high isolation is achieved by introducing the stub in the ground plane. However, the impedance bandwidth of the antenna around the 7 to 9 GHz region is mismatched, and the isolation around the 9 to 10.6 GHz region is still a little poor. Thus, two rectangular slots of 3.5 mm in width and 4 mm in length at the bottom of the stub are introduced in the ground plane.

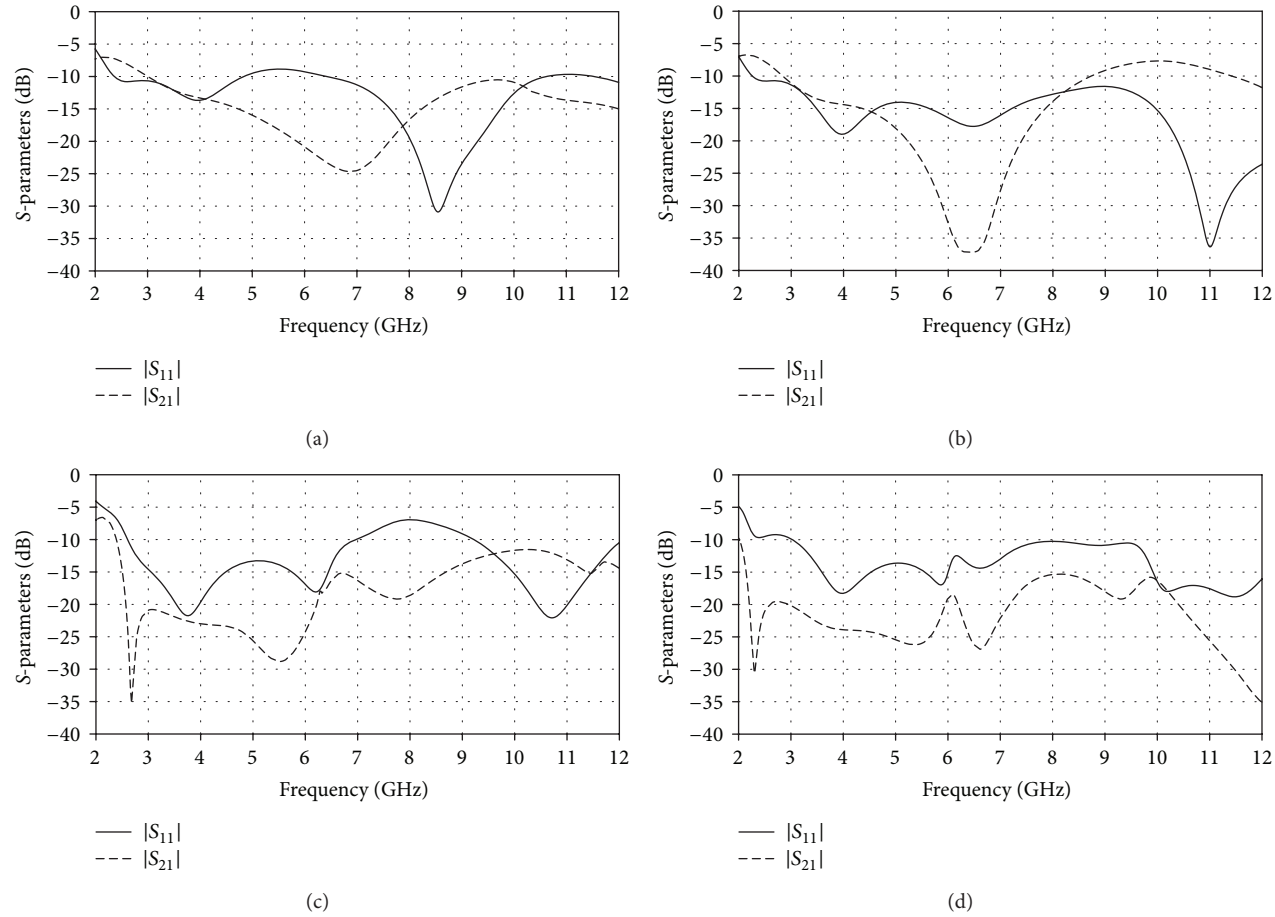

Figure 2: Simulated reflection coefficient $|S_{11}|$ and isolation $|S_{21}|$ against frequency of the proposed antenna: (a) without all of the slots and the stub in the ground plane, (b) without two rectangular slots and the stub in the ground plane, (c) without the stub in the ground plane, and (d) with all of the slots and the stub in the ground plane, that is, the proposed antenna.

The rectangular slots in the ground plane are achieved to not only obtain the necessary interaction between ground plane and the radiators but also adjust the length of the stub so that the proper matching impedance and a good isolation are received. The simulation results of the proposed antenna are shown in Figure 2(d); one can observe that a broad impedance bandwidth covering the whole UWB with good isolation of < -15 dB is achieved.

Additionally, the influence of the distance between two feeding lines on the performance of the proposed antenna is also simulated and the simulated results are shown in Figure 3. It can be seen that by increasing or decreasing the distance between feeding lines the isolation can be improved or weakened as shown in Figure 3(b), and the impedance bandwidth cannot cover the whole UWB with too far or too close distance between the monopoles as shown in Figure 3(a). Therefore, the distance between the monopoles should be optimized with attention to the impedance bandwidth and isolation.

Furthermore, unlike the antenna in [11], in our design two semielliptical monopoles are aligned along y-axis back-to-back as shown in Figure 1; the advantage of this configuration is that the minimum distance between the monopoles is almost equal to the distance between two feeding lines, therefore, a more complicate structure such as a tree-like one [11] to improve the isolation is not necessary in the design; that is, fewer parameters need to be optimized and the antenna can be designed simply.

3. Experimental Results and Discussion

Based upon the design dimensions shown in Figure 1, the proposed UWB MIMO/diversity antenna was constructed, measured, and analysed as follows.

3.1. Input Characteristic. Figure 4 shows the measured reflection coefficient $|S_{11}|$ and isolation $|S_{21}|$ against frequency of the proposed antenna. Note that, due to the symmetric structures of the proposed antenna, the measured $|S_{22}|$ is almost the same as $|S_{11}|$ and is thus not shown in the figure for the sake of brevity. It can be observed from Figure 4 that the obtained impedance bandwidth defined by $|S_{11}| < -10$ dB can cover the whole UWB of 3.1–10.6 GHz. In addition, across the whole UWB, a good isolation between two feeding ports is obtained ($|S_{21}| < -15$ dB).

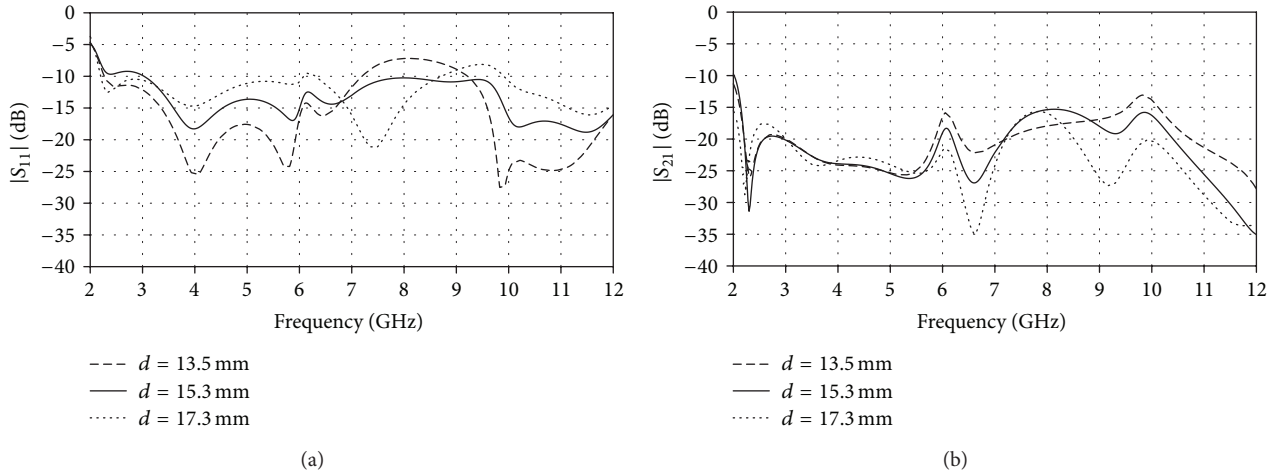

FIGURE 3: Simulated S-parameters against frequency of the proposed antenna with different d: (a) reflection coefficient $|S_{11}|$ and (b) isolation $|S_{21}|$.

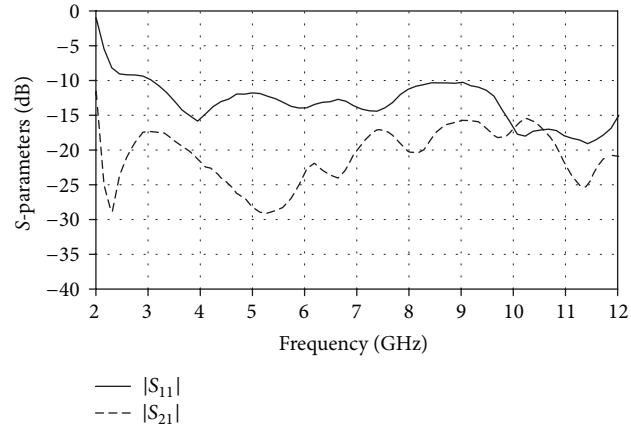

FIGURE 4: Measured reflection coefficient $|S_{11}|$ and isolation $|S_{21}|$ against frequency of the proposed antenna.

3.2. Radiation Patterns. The radiation patterns at 4, 7, and 10 GHz of the proposed antenna were measured in an anechoic chamber. Figure 5 plots the radiation patterns for the proposed antenna on the x-z (E-plane), x-y (H-plane) plane, and y-z plane with port 1 excited and port 2 connected to a 50 Ω load. As shown in Figure 5, the radiation patterns of the proposed antenna are relatively stable across the UWB. In addition, due to the symmetric structures of two monopoles, when port 2 is excited, with port 1 terminated, the patterns in the x-z plane are similar to those in Figure 5, but the patterns in the x-y and y-z planes are mirror transformations about x-z plane of those in Figure 5. In other words, the radiation patterns tend to cover complementary space regions, which provide spatial diversity for the system operation to overcome the multipath fading problem and enhance the system's performance.

The measured peak antenna gain for port 1 excitation is shown in Figure 6. Due to the symmetric structures of two monopoles, the measured peak antenna gain for port 2 excitation is about the same and not shown in the figure. The result shows a gain level of about 6.9 dBi, with gain variations less than 3.9 dBi across the operating band.

3.3. Diversity Performance. A diversity antenna is characterised by the individual antenna gain and the overall diversity gain. Diversity gain could be calculated using the analysis in [12–14]. The measured far field radiation pattern can be used for calculating the envelope correlations of the proposed antenna using [15]

$$\rho_e = \frac{A}{BC}, \tag{2}$$

where

$$A = \left(\oint \left(\mathrm{XPR} E_{\theta 1}(\Omega) E^*_{\theta 2}(\Omega) P_\theta(\Omega) + E_{\varphi 1}(\Omega) E^*_{\varphi 2}(\Omega) P_\varphi(\Omega) \right) d(\Omega) \right)^2,$$

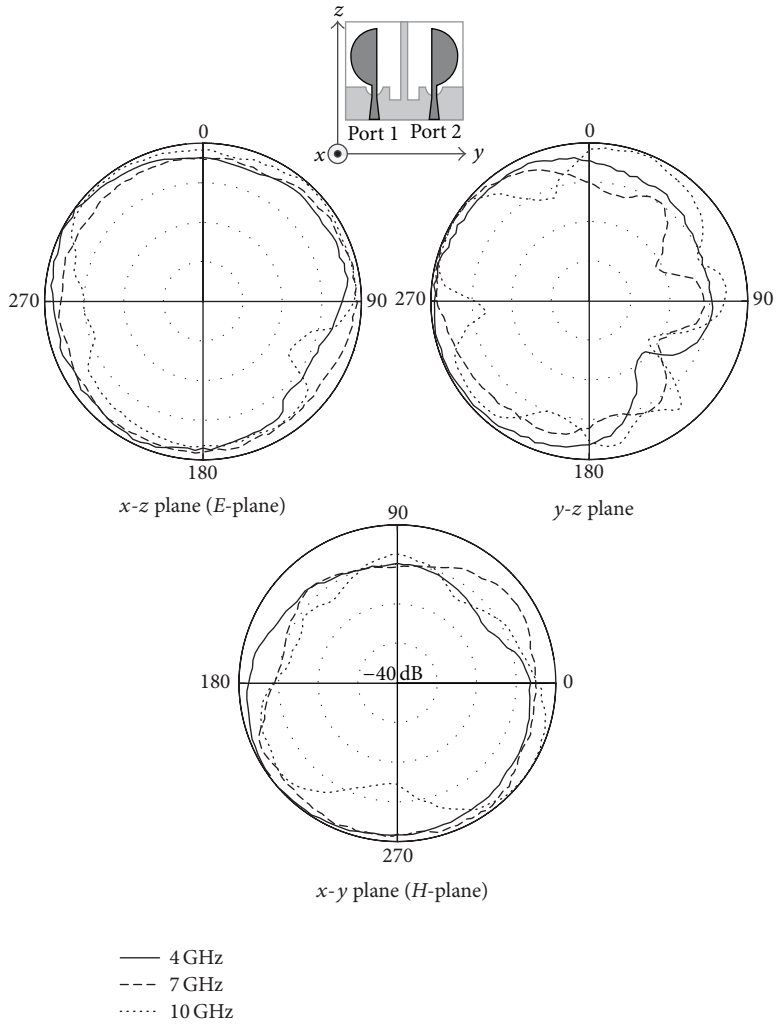

Figure 5: Measured radiation patterns of the proposed antenna.

$$B = \oint \left(\mathrm{XPR} G_{\theta 1}(\Omega) P_{\theta}(\Omega) + G_{\varphi 1}(\Omega) P_{\varphi}(\Omega)\right) d(\Omega),$$

$$C = \oint \left(\mathrm{XPR} G_{\theta 2}(\Omega) P_{\theta}(\Omega) + G_{\varphi 2}(\Omega) P_{\varphi}(\Omega)\right) d(\Omega),$$

$$G_{\theta} = E_{\theta}(\Omega) * E_{\theta}^{*}(\Omega),$$

$$\Omega = (\theta, \varphi). \tag{3}$$

$E_{\theta 1}(\Omega)$, $E_{\theta 2}(\Omega)$, $E_{\varphi 1}(\Omega)$, $E_{\varphi 2}$, (Ω), and $P_{\theta,\varphi}(\Omega)$ are, respectively, the vertical (θ) and horizontal (φ) polarized complex patterns of the two semielliptical monopoles and the incident power spectrum of the different polarizations. Cross-polar discrimination (XPR) is the time-averaged vertical-to-horizontal power ratio.

The diversity gain at 1% of the cumulative distribution functions and envelope correlation coefficient for the proposed UWB MIMO/diversity antenna is larger than 9.6 dB and below −17 dB, respectively, across the whole UWB of 3.1–10.6 GHz. These results indicate that the proposed antenna has a good diversity performance and can be a good candidate for an UWB system.

4. Conclusions

An UWB MIMO/diversity monopole antenna has been presented. The antenna has a more compact size than the antennas presented in the existing literature. The obtained operating bandwidth of the proposed antenna can cover the whole UWB of 3.1 to 10.6 GHz. Across the UWB, the antenna also shows good port isolation and stable radiation pattern, and can provide spatial diversity to combat the multipath fading problem. Thus, the proposed antenna is suitable for some portable UWB MIMO/diversity applications.

Conflict of Interests

The authors declare that there is no conflict of interests regarding the publication of the paper.

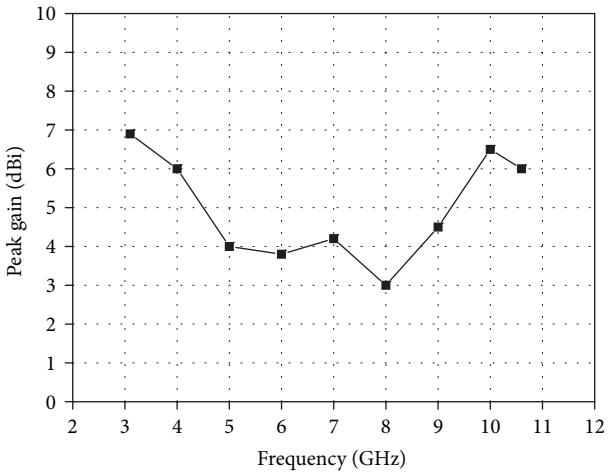

Figure 6: Measured peak antenna gain across the UWB for port 1 excitation.

Acknowledgment

The authors should deliver their sincere gratitude to the anonymous reviewers for their constructive comments which have made the authors' much better than before.

References

[1] "First report and order in the matter of Revision of Part 15 of the commission's rules regarding ultra-wideband transmission systems," Federal Communications Commission, ET-Docket 98-153, 2002.

[2] T. Kaiser, F. Zheng, and E. Dimitrov, "An overview of ultra-wideband systems with MIMO," *Proceedings of the IEEE*, vol. 97, no. 2, pp. 285–312, 2009.

[3] B. Yu, C. W. Jung, H. Lee et al., "Closely mounted compact wideband diversity antenna for mobile phone applications," *International Journal of Antennas and Propagation*, vol. 2012, Article ID 798046, 6 pages, 2012.

[4] J. F. Zheng, Y. Li, and Z. H. Feng, "Impact of mutual coupling and polarization of antennas on BER performances of spatial multiplexing MIMO systems," *International Journal of Antennas and Propagation*, vol. 2012, Article ID 795205, 12 pages, 2012.

[5] R. G. Vaughan and J. B. Andersen, "Antenna diversity in mobile communications," *IEEE Transactions on Vehicular Technology*, vol. 36, no. 4, pp. 149–172, 1987.

[6] K.-L. Wong, S.-W. Su, and Y.-L. Kuo, "A printed ultra-wideband diversity monopole antenna," *Microwave and Optical Technology Letters*, vol. 38, no. 4, pp. 257–259, 2003.

[7] L. Liu, H. Zhao, T. S. P. See, and Z. N. Chen, "A printed ultra-wideband diversity antenna," in *Proceedings of the IEEE International Conference on Ultra-Wideband (ICUWB '06)*, pp. 351–356, Waltham, Mass, USA, September 2006.

[8] S. Hong, K. Chung, J. Lee, S. Jung, S.-S. Lee, and J. Choi, "Design of a diversity antenna with stubs for UWB applications," *Microwave and Optical Technology Letters*, vol. 50, no. 5, pp. 1352–1356, 2008.

[9] T. S. P. See and Z. N. Chen, "An ultrawideband diversity antenna," *IEEE Transactions on Antennas and Propagation*, vol. 57, no. 6, pp. 1597–1605, 2009.

[10] W. K. Toh, Z. N. Chen, X. Qing, and T. S. P. See, "A planar UWB diversity antenna," *IEEE Transactions on Antennas and Propagation*, vol. 57, no. 11, pp. 3467–3473, 2009.

[11] S. Zhang, Z. Ying, J. Xiong, and S. He, "Ultrawideband MIMO/diversity antennas with a tree-like structure to enhance wideband isolation," *IEEE Antennas and Wireless Propagation Letters*, vol. 8, pp. 1279–1282, 2009.

[12] M. Karaboikis, V. Papamichael, C. Soras, and V. Makios, "A multiband diversity antenna system for compact mobile/wireless devices: modeling and performance evaluation," *International Journal of Antennas and Propagation*, vol. 2008, Article ID 782153, 7 pages, 2008.

[13] P.-S. Kildal and K. Rosengren, "Electromagnetic analysis of effective and apparent diversity gain of two parallel dipoles," *IEEE Antennas and Wireless Propagation Letters*, vol. 2, pp. 9–13, 2003.

[14] S. Blanch, J. Romeu, and I. Corbella, "Exact representation of antenna system diversity performance from input parameter description," *Electronics Letters*, vol. 39, no. 9, pp. 705–707, 2003.

[15] R. Addaci, A. Diallo, C. Luxey, P. le Thuc, and R. Staraj, "Dual-band WLAN diversity antenna system with high port-to-port isolation," *IEEE Antennas and Wireless Propagation Letters*, vol. 11, pp. 244–247, 2012.

Hindawi Publishing Corporation
International Journal of Antennas and Propagation
Volume 2013, Article ID 757061, 10 pages
http://dx.doi.org/10.1155/2013/757061

Research Article

Design of Arbitrarily Shaped Planar Microstrip Antenna Arrays with Improved Efficiency

Sheng Ye,[1] Xianling Liang,[1] Wenzhi Wang,[1] Junping Geng,[1] Ronghong Jin,[1] Y. Jay Guo,[2] and Trevor S. Bird[2]

[1] *Department of Electronic Engineering, Shanghai Jiao Tong University, Shanghai 200030, China*
[2] *Commonwealth Scientific and Industrial Research Organisation (CSIRO), Computational Informatics, P.O. Box 76, Epping, NSW 1710, Australia*

Correspondence should be addressed to Sheng Ye; zqntoys@sjtu.edu.cn

Received 24 March 2013; Revised 28 November 2013; Accepted 28 November 2013

Academic Editor: Bal Singh Virdee

A design technique is described for an arbitrarily shaped planar microstrip antenna array with improved radiation efficiency. In order to fully utilize the limited antenna aperture, several basic modules are proposed from which we construct the array. A consideration of the aperture shape shows that with several practical examples a proper combination of these basic modules not only allows the convenient design of arbitrarily-shaped microstrip array, but also helps to improve the aperture radiation efficiency. To confirm the feasibility of the approach, a circular array with 256 elements was constructed and fabricated. Both computed and measured aperture radiation results are compared and these demonstrate that the design technique is effective for arbitrarily-shaped planar microstrip arrays.

1. Introduction

With the rapid deployment of wireless communications systems during recent years, it is becoming imperative for the radiofrequency subsystem to be multifunctional as well as have smaller size. This is especially true for satellite communications applications where weight and functionality are at a premium. As one of main parts in the wireless system, the antenna is required to perform at a high performance level, whilst maintaining conformability with the remainder of the system. Accordingly, making full use of the available system space is very important in future antenna design for on-board space communications due to space limitations.

Traditional parabolic or reflector antennas have a high radiation efficiency, and they have been employed successfully in current satellite communication systems [1, 2]. However, they have a large profile and high volume due to their support structures. To utilize the system space more effectively, a planar array antenna with a low profile has significant potential for space saving: such antennas include the radial line slot antenna (RLSA) array, the waveguide slot antenna array [3–8], and planar microstrip antenna array [9]. However, the RLSA is commonly suitable for a circular space design, where the waveguide slot array antenna needs an additional power divider, which may not be suitable for the arbitrarily shaped array designs. By contrast, the planar microstrip antenna array is more adaptable and more easily made conformal with the system. For example, several special shaped microstrip arrays have been proposed and designed to be conformal in [10–14]. A circular array was designed in [10] for mobile TV reception applications, where three kinds of collinear subarrays are specially designed to be compatible with the curved edge, and an extra feed network is added to combine these subarrays together to provide a peak antenna gain of 27.4 dBi. A commercial product for mobile satellite communication in Ku-band, described in [13], adopts flat antenna boards to chamfer shapes so that the antenna can rotate mechanically in elevation without interfering with any

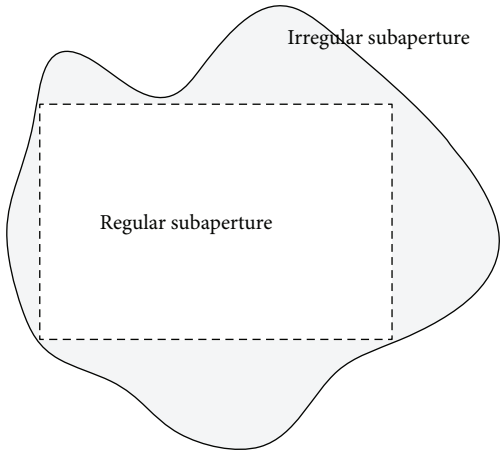

Figure 1: Layout of an arbitrarily shaped array.

radome of related structure. When combined together, the three panels produce a receive gain of 29.5 dBi. A hexagon-shaped 12-element array designed for dual polarizations was reported in [12], to have a gain of <17.5 dBi at a frequency of 15.4 GHz. In [14], a symmetrical feed network composed of multiple T-junctions was specially designed for a 3 × 2-element array to achieve a gain of 17 dBi. All these antenna design examples were based on the available system space, but they exhibit no universality in either irregularity in the geometry or employ complicated geometrical shapes. Therefore, it is useful to investigate an arbitrarily shaped antenna array for better utilizing the available space. In [15], the authors gave a feed network layout of an 8 × 8-element array; the array is divided into 32 2-element subarrays, which are combined by a parallel and serial technique. A curved microstrip line and 1 to 3 power dividers make this different from reference [9–14]. Nevertheless the approach cannot be used to design arbitrarily shaped arrays as the feed network would be very complicated and the loss therein would be significant. Another disadvantage of the available design methods is that they all employ a single method to design the whole array, which may contain both regular and irregular subapertures, as shown in Figure 1. The traditional symmetry method is preferred for a regular subaperture because the symmetry network is beneficial in cancelling out spurious radiation. However, a regular symmetrical network cannot be applied to an irregular subaperture design due to the constancy of its layout.

In this paper, we present a design technique for an arbitrarily shaped antenna array. The array itself has a fixed beam that is scanned mechanically. In contrast with existing design methods, the regular and the irregular subapertures are treated differently with alternative design methods in order to achieve overall maximum gain. Moreover, small subarrays are employed in the construction of the irregular subaperture so that depending on the application it can be integrated with the regular subaperture. The design technique is easy to be realized with planar circuit fabrication; hence it is applicable to most wireless communications systems.

The paper is organized as follows. Section 2 describes an arbitrarily shaped array design approach, where several basic modules are introduced. A design guideline is given in Section 3 for the combination of the modules. In Section 4 a circular array is constructed and fabricated using the described method. Measured results are then reported and discussed to assess the theoretical design. Our conclusion is given in the final Section.

2. Arbitrarily Shaped Array Design Principle

An arbitrarily shaped array can be divided into regular and irregular subapertures as shown in Figure 1. For the regular subaperture, the number of elements is chosen to be 2^N ($N = 1, 2, 3 \ldots$), which can be designed by conventional symmetrical methods. For example, in [9], a 4-element array was first designed as a sub-array and then a 16-element array was constructed by duplicating the sub-array twice with an appropriate feed network. An identical strategy can be employed to design a larger 2^N-element array. On the other hand, for an array in their regular subaperture, the antenna structure and the number of elements depend on the aperture size and shape. In common with symmetrical arrays, an irregular subaperture has two major attributes: element distribution and a corresponding feed network.

Consider now an array element layout for the shape in Figure 1. Assume that their regular subaperture contains M elements. Figure 2 shows several basic modules for one, two, and three elements. For a single element, there is only one case, denoted by M_1 (see Figure 2(a)). For two elements, two cases are possible based on the parallel and serial feeds, respectively, denoted by M_{2-1} and M_{2-2}, as shown in Figures 2(b) and 2(c). For three elements, there are two kinds of distributions: one is linear and the other is triangular. Moreover, each distribution has four structures of feed network, as shown in Figure 2(d) to 2(k), which are indicated by M_{3-1} to M_{3-8}.

The next module in the series, M_4, can be expressed as $M_4 = M_1 + M_3$ or $M_4 = M_2 + M_2$; hence, it is not difficult to construct M_4 using the previously mentioned modules M_1, M_2, and M_3. Using the same strategy, M_N can be expanded to $M_N = M_{(N-X)} + M_X$ ($N > X$).

The irregular subaperture of Figure 1 can also be formed from a combination of the basic modules shown in Figure 2 as will be described in the next Section.

3. Design of Feed Network

3.1. Typical Structures. In order to suggest a general approach, we describe firstly subapertures with notched and concave boundaries. Figures 3 and 4 show notched concave rectangular apertures, respectively. Both spaces capable of 19 elements, where the 3 elements (the irregular sub-aperture containing the missing elements) are located next to a 4 × 4-element square array (the regular sub-aperture). Each structure has two cases: a vertical and a horizontal polarization feed network. Here, we regard a 2 × 2-element array as the basic unit, and the conventional method of feeding the basic

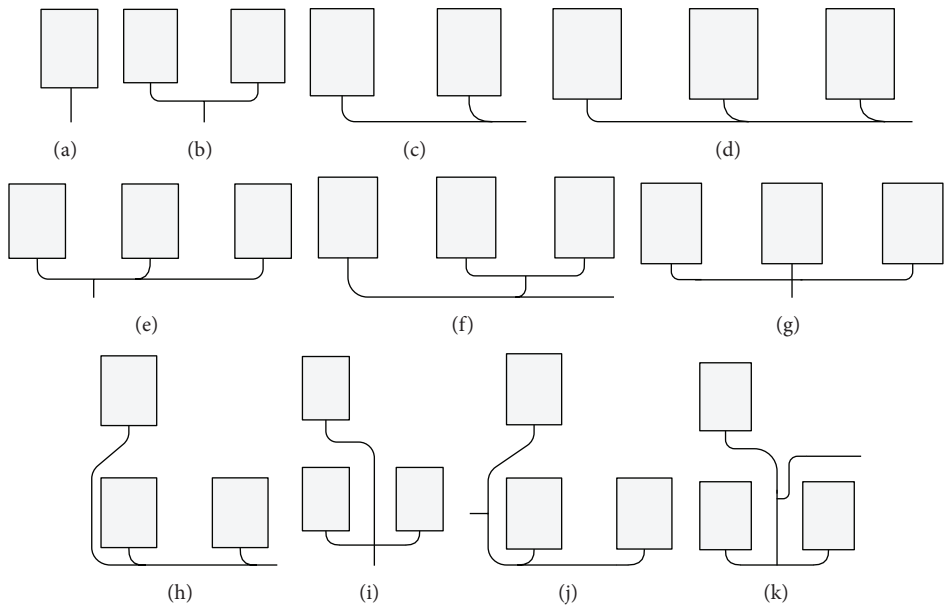

Figure 2: Configuration of the basic array element modules (a) M_1 (b) M_{2-1} (c) M_{2-2} (d) M_{3-1} (e) M_{3-2} (f) M_{3-3} (g) M_{3-4} (h) M_{3-5} (i) M_{3-6} (j) M_{3-7} (k) M_{3-8}.

unit is simply using the serial and parallel techniques, in which multiple T-shaped power dividers are used. For the irregular subaperture, the three special elements (denoted by the dotted line) are commonly neglected in conventional design.

To improve the efficiency of the antenna aperture, three special elements designs need to be considered. Figures 3 and 4 show the corresponding two designs, namely, irregular design 1 and irregular design 2. Design 1 confines the feed network inside the area between regular and irregular subapertures, whereas in design 2, it further divides the irregular subaperture into several smaller modules. The main differences between the two designs are the topology of the feed lines and the positions of feed junctions.

3.2. Simulated Results and Discussion. The array element designs were carried out with CST microwave studio (MWS). They were all modeled in the size indicated in Figures 3 and 4. Power is side fed through a waveguide port input. The adjustment of the microstrip network is now described. Firstly, all elements are tuned to have nearly uniform excitation. Secondly, the current travelling to the irregular subaperture is slightly reduced or increased until the gain of the complete array reaches its maximum value. During this process, the elements and the feed lines are matched throughout to maintain a reflection coefficient less than −15 dB as shown in Figure 5. For the notched array with vertical polarization, array 2 exhibits a better return loss and a higher gain than array 1. The feeding paths to module M_3 have almost the same length in both configurations; hence, it was concluded that in such cases the smaller module would be preferred. In both designs, the feed line used to connect the regular and irregular subapertures inevitably causes mutual coupling with the adjacent elements, and, further, the coupling effect is more severe as the currents become stronger. It is noted that the coupling will cancel out part of original currents on the element and cause the aperture efficiency to decrease. For array 1, unfortunately, the feed line from A1 to M_3 couples energy to adjacent elements along its path. Meanwhile, one section of the feed line carries a strong current; hence, the coupling is severe. By contrast, in array 2, M_3 is divided into small modules so that the feed line current to each module is reduced. Therefore, the feed line will have coupling with the elements only when it is in the regular subaperture. Hence, small modules help reduce coupling effects where high aperture efficiency is required, as shown in Table 1. The result for horizontal polarization is similar. Smaller modules in array 4 give a better performance than in array 3. It should be pointed out that in array 4 M_1 is not fed from the available junctions, but from newly created ones (B1, B2, and B3) in the feed lines, as illustrated in Figure 3(b). This is done to prevent changes at the higher level junctions in the basic unit so as to reduce the coupling effects.

For the concave array with vertical polarization, if M_3 is divided into the smaller modules, the feed network may be too complicated; hence the two designs differ only in feeding positions. Compared with array 5, array 6 has a little low aperture efficiency, as seen in Table 1. It is caused by three junctions in array 6, denoted by C1, C2, and C3, where the power ratios are 7 : 4, 2 : 5, and 1 : 1 : 3, respectively, according to the uniform distribution. It is difficult to realize these power ratios accurately using the microstrip line, and impedance matching will not be properly achieved with the result that the loss with feed line increases and aperture efficiency decreases. Instead, the elements in array

Figure 3: Designs of notched array (a) vertical and (b) horizontal polarization.

5 are distributed evenly which facilities the design of power dividers, where the power ratio in C4 is 3 : 4 : 4.

Similar to the notched array, array 7 has a crowded feed line inside the basic sub-array unit. The strong coupling decreases the antenna aperture efficiency. Array 8 has a higher gain than array 7, but at the lower frequency, its gain falls rapidly with frequency. This is because the modules M_1 and M_2 are serially fed from the basic unit. Nevertheless, it performs much better than the combined case with M_3.

Based on the simulated results, the array performances are compared in Table 1, where the total antenna efficiency is given by

$$\eta_{\text{eff}} = \frac{G_{\text{simulated}}}{G_{\text{max}}}. \quad (1)$$

$G_{\text{simulated}}$ is the simulated gain and $G_{\text{max}} = 4\pi A/\lambda^2$ is the maximum gain for a uniform aperture with the same aperture area A [16]. All irregular design arrays, containing 19 elements excited, have a gain of 0.5~0.7 dB higher than that of regular design array, which has only 16 elements excited, and hence the aperture efficiency is improved from 74% to 83~88.8%. The loss due to the feed line is determined by the length and the reflection coefficient of junctions. Based on the simulations the used substrate causes about 0.155 dB power loss per wavelength. The feed loss for each sub-array is estimated and the results have been compared. It is known that the differences of aperture efficiency mainly come from the aperture field distribution. For the regular design, the low aperture efficiency is mainly due to the three special elements that are not used although the remaining 16 elements are uniformly excited. For the irregular design, the array 2, array 4, and array 8 designs have a relatively high efficiency. The reason for this improvement was explained above. Not only the resulting array designs have a good performance, but also, as can be seen from the Figures, they have a very compact

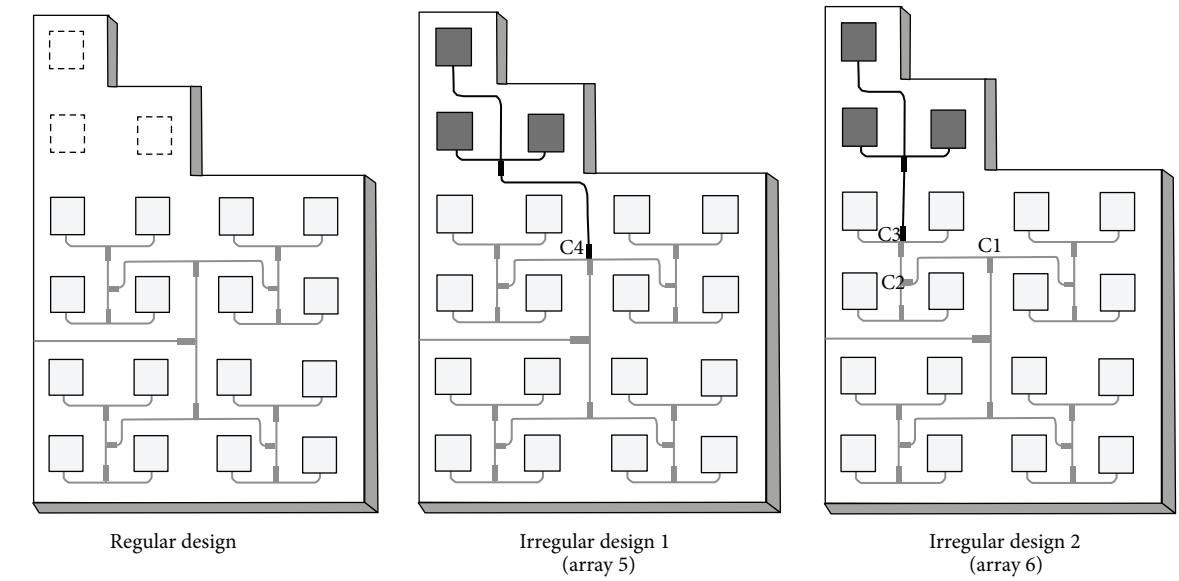

(a)

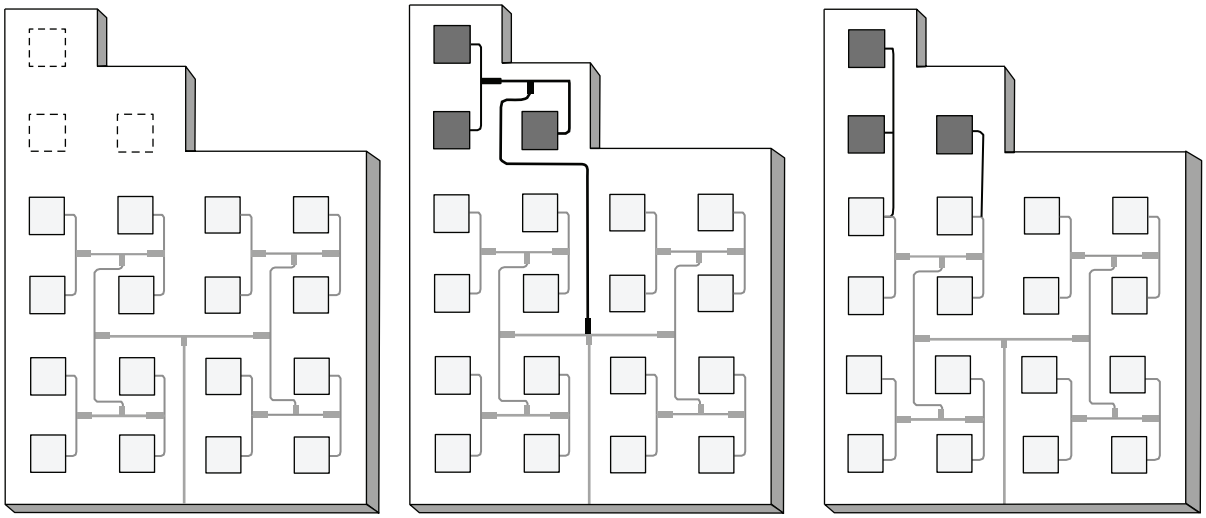

(b)

Figure 4: Designs of concave array (a) vertical and (b) horizontal polarization.

Table 1: Computed results of the subarrays.

Design	Gain (dBi)	S.L.L (dB)	Cross-Pol. (dB)	Loss with feed line (dB)	Aperture eff.	η_{eff}
Regular design	19.30	≤−13.4	≤−45	~−0.69	74%	63.1%
Array 1	19.90	≤−13.3	≤−38	~−0.70	85.4%	72.7%
Array 2	20.05	≤−13.4	≤−38	~−0.70	88.4%	75.3%
Array 3	19.80	≤−13.3	≤−39	~−0.70	83.5%	71.2%
Array 4	20.05	≤−13.4	≤−43	~−0.71	88.8%	75.4%
Array 5	19.90	≤−13.5	≤−38	~−0.70	85.5%	72.7%
Array 6	19.75	≤−13.6	≤−42	~−0.72	83.0%	70.8%
Array 7	19.85	≤−13.3	≤−38	~−0.71	84.9%	71.9%
Array 8	19.95	≤−13.5	≤−39	~−0.72	86.8%	73.6%

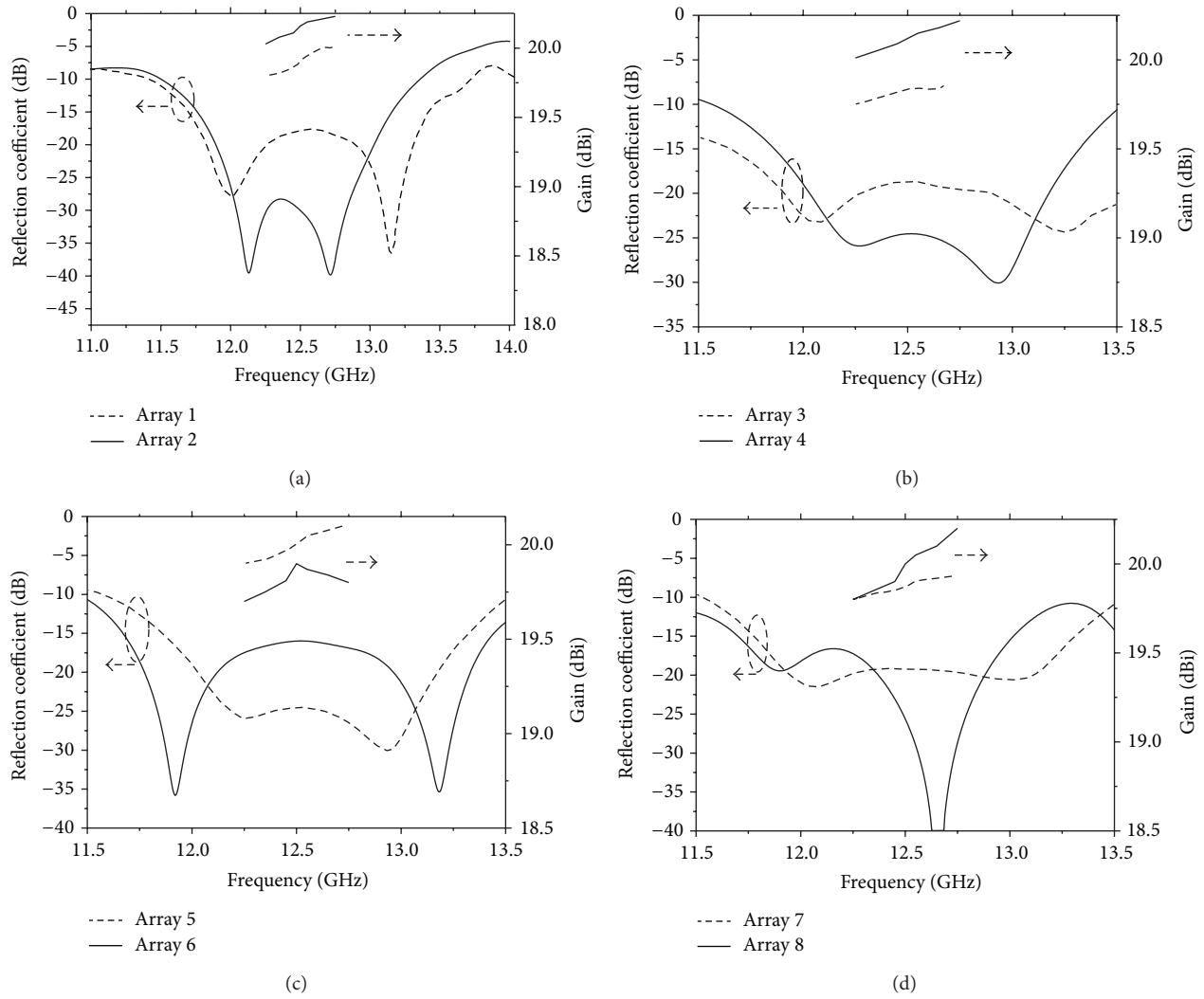

Figure 5: The simulated reflection coefficient and gain of the notched array (a) V-polarization, (b) H-polarization and concave array, (c) V-polarization, and (d) H-polarization.

layout, which is not constrained by the irregular shape of the array.

3.3. Design Guideline. From the illustration of the design and following discussion, it has been observed that all the irregular designs which exhibit a good performance have one trait in common; namely, the fewer changes to the main part of the feed network in the regular subaperture the better performance. In addition, the irregular subaperture should be considered an extension of the regular subaperture. This is reasonable because the regular subaperture plays the key role in radiation. Therefore, a general design guideline is that the layout must guarantee the performance of the regular subaperture, and then the potential of the irregular subaperture should be fully exploited without affecting the regular subaperture significantly.

A practical guideline can be described as follows: first, the arbitrarily shaped array is divided into two parts: a regular subaperture and an irregular one. The regular subaperture is designed using a symmetry technique. Then, according to the element distribution, the irregular subaperture is divided into several modules. Smaller modules are better. However, small modules often require a complicated feed network, so a tradeoff is needed to reach the highest antenna gain. The feed line to the modules is connected to the lower level junctions in basic unit of the regular subaperture to reduce unwanted coupling. The power distribution can be realized over a modest bandwidth (~20%) with a quarter wavelength transformer, which is adjusted as follows: the magnitude of current to the irregular modules is slightly increased or decreased until the gain of the array reaches its maximum value.

4. Practical Array Design

The design technique outlined above was applied to obtain a circular antenna array design over the bandwidth of 12.25–12.75 GHz. The diameter of the array is 325 mm. The design

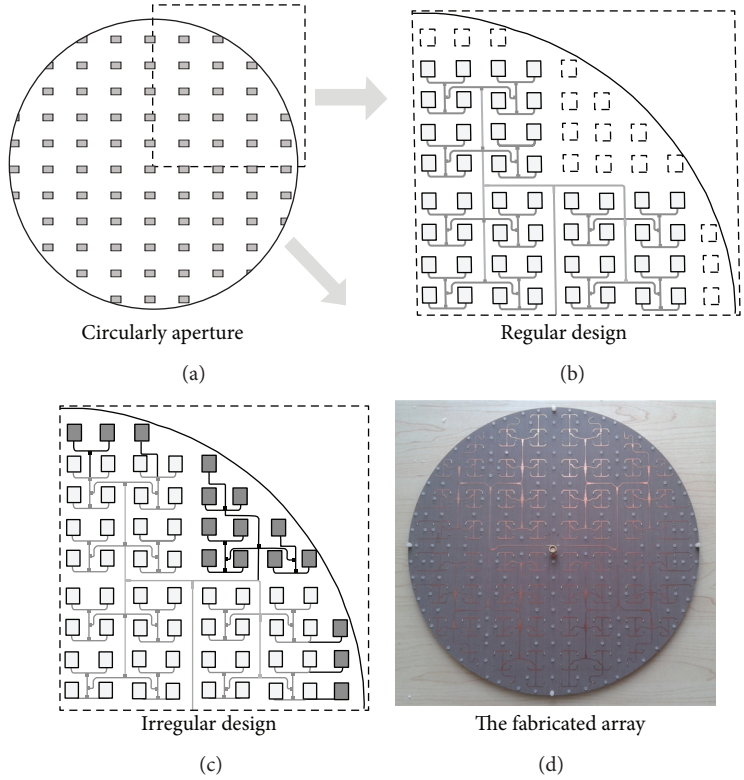

Figure 6: The layout of the circular array.

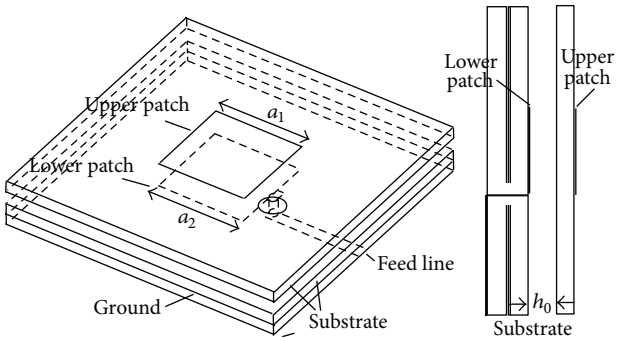

Figure 7: The array element design.

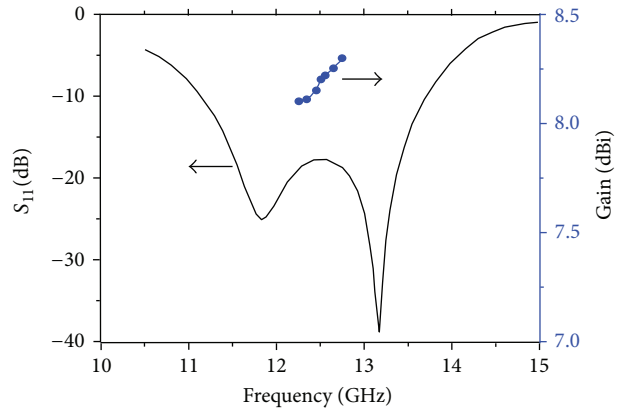

Figure 8: The reflection coefficient and gain of the element.

layout is illustrated in Figure 6. The aperture quadrant is divided into regular and irregular parts as shown. The regular subaperture was first filled based on a combination of parallel and serial feeding techniques to reduce the length of the feed line. The irregular subaperture was then composed of three modules: two M_3 and one M_{10}, and is further divided as follows: $M_3 = 3 \times M_1$, $M_3 = M_2 + M_1$, and $M_{10} = M_4 + M_3 + M_3$; the small modules such as M_1 and M_2 are individually connected to the regular subaperture, while the modules separated from module M_{10} are connected to each other since the M_{10} can be integrated with the 4×4-element array of the regular subaperture directly.

For simplicity, a stacked patch antenna was selected for the antenna element [17]. Figure 7 shows the configuration of the element, which consists of three substrate layers. All substrates have the same dielectric constant of $\varepsilon_r = 2.55$ and thickness h. The upper square patch with a side length of a_1 is printed on the upper substrate while the lower square patch with a side length of a_2 is on the middle substrate. The distance between these two substrates is h_0. The microstrip feed network is printed on the bottom side of the substrate and is isolated from the patches through a metal ground plane, which frees up the design of feed network. The final optimized geometry of the antenna element for the frequency band of 12.25~12.75 GHz is listed in Table 2. The substrate

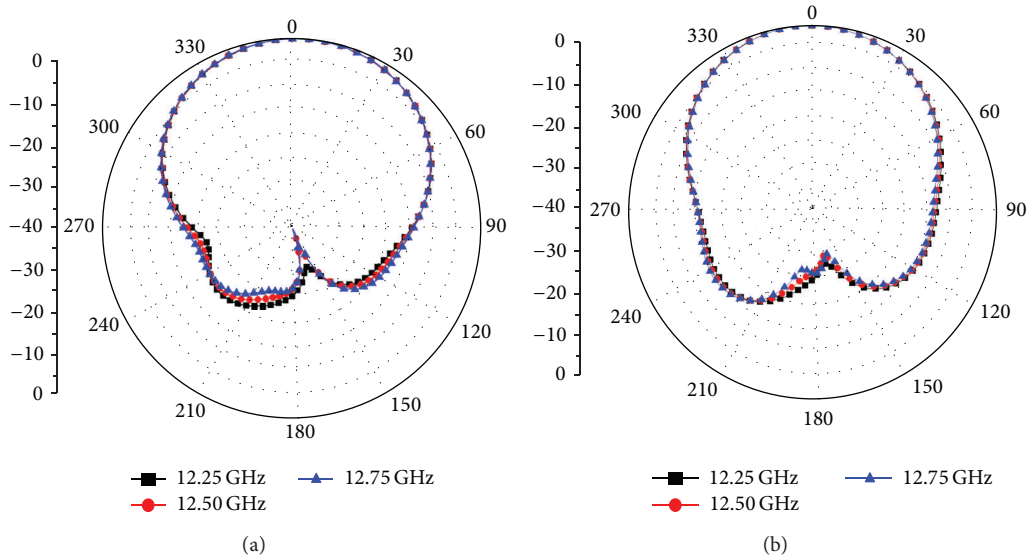

Figure 9: The normalized farfield patterns of the element at (a) E plane and (b) H plane.

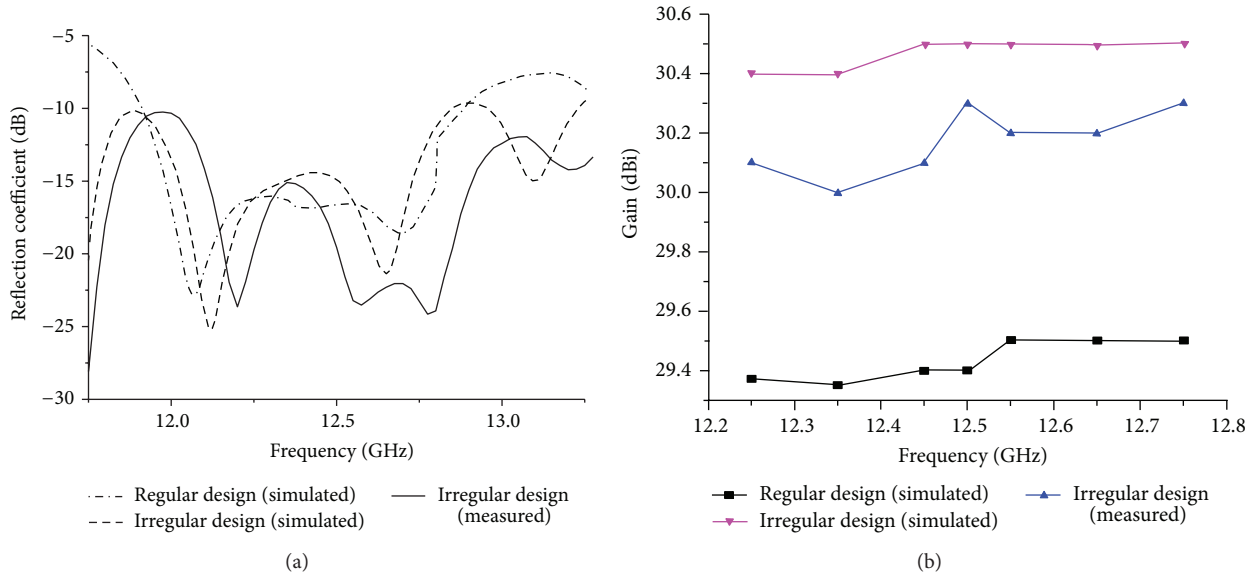

Figure 10: The (a) input reflection coefficient and (b) gain of the circular array.

Table 2: The parametric dimensions of the element (mm).

h	h_0	a_1	a_2
0.762	1.3	3.5	3.5

material used is from Arlon AD255. It has a loss tangent of 0.0018 at 10 GHz, and the conductor thickness is 0.035 mm.

The simulated reflection coefficient of the antenna element is better than −15 dB across the band as shown in Figure 8. The far-field patterns are plotted in Figure 9, and the half power beam widths are 66° and 73.5° for E and H planes, respectively. The antenna element gain is 8.1~8.3 dBi.

The antenna array spacing is 18 mm ($0.75\lambda_0$, where λ_0 is the wavelength in free space at 12.5 GHz). Mutual coupling between elements is low at this distance, usually better than −20 dB. Figure 10(a) shows the simulated reflection coefficient of the arrays. All the reflection levels are below −15 dB in the operational band. The simulated gains are shown in Figure 10(b).

It is seen that the array with the regular design, employing only 192 of the elements, has a gain about 29.4 dBi. The full array with the irregular sub-array that uses 256 elements has a gain about 30.5 dBi. The maximum gain of the circular array is about 32.6 dBi according to formula (1). As discussed above, the antenna efficiency is mainly limited by two aspects: the power loss of the feed network and the nonuniform aperture

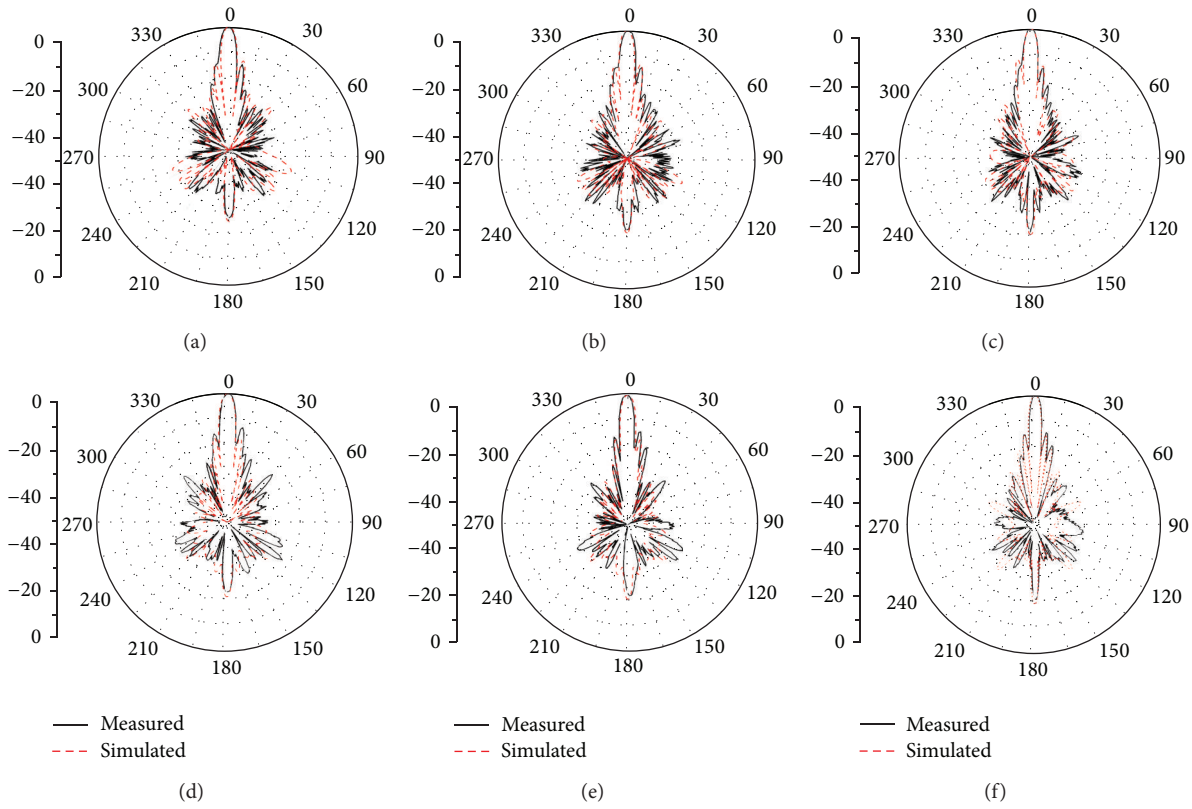

Figure 11: The measured far-field patterns at (a) 12.25 GHz, E plane (b) 12.5 GHz, E plane (c) 12.75 GHz, E plane (d) 12.25 GHz, H plane (e) 12.5 GHz, H plane (f) 12.75 GHz, H plane.

field distribution. The power loss of the whole feed network with parallel and serial techniques is estimated to be about 1.7 dB, and therefore the aperture efficiency is about 90%.

As can be seen, the irregular subaperture is divided into many small modules, and the topology of feed network is compact. It is noted that the contribution of the feed network is not only that it has a short feed line, but also it has mostly protected the feed network of the regular subaperture.

To verify the design approach and the calculated results, a circular array based on the irregular design was fabricated. The resulting structure is shown in Figure 6. The reflection coefficient was measured with an Agilent 8722ES vector network analyzer (VNA) and the results are also shown in Figure 10(a). Good agreement is observed between the computed and measured results. The slight discrepancy may be due to the imperfect fabrication and cable connections.

The radiation patterns of the experimental circular array are shown in Figure 11 at various frequencies across the band. It can be seen that the simulated and measured results are in good agreement, except that the measured side lobes at the low frequency (Figure 11(d)) are slightly higher than those predicted, and the sidelobes in the E plane tend to merge. Since the feed network is isolated by the ground, the merging may be due to imperfections in the feed network as well as imperfect antenna alignment in the measuring process. All the side lobes are 13.2 dB or more below the peak level. The array gain was also measured by comparison with a standard horn antenna. The results obtained are plotted in Figure 10(b) and it can be seen that the measured gain agrees well with the computed result. The variation between the two is thought due to fabrication tolerances, ohmic loss, and assembly tolerances. A maximum gain of 30.3 dBi was achieved at 12.5 GHz. Table 3 summarizes the radiation performance over the band where antenna efficiency is given by (1), except that $G_{\text{simulated}}$ is replaced by G_{measured}, the measured gain of the test array. The irregular design aperture efficiency is obviously higher than the regular design, and it causes very little cross-polarization component in the band.

5. Conclusion

A design technique for a high efficiency arbitrarily shaped planar microstrip antenna array is described. In this design technique, the shape of the array is treated as a combination of regular and irregular subapertures. For the regular subaperture, a conventional symmetry technique is used to obtain a high performance, and for the irregular subaperture, small modules are used to construct the array. The selection of modules as well as the topology of feed network is optimized to increase the antenna gain. Based on this decomposition of the array aperture, a circular aperture array was designed and fabricated to demonstrate the approach. The agreement between the computed and measured results verified the effectiveness of the design technique. The design approach for

Table 3: The performance of the circular array.

Frequency (GHz)	Simulated								Measured		
	Regular design				Irregular design				Irregular deign		
	Gain (dBi)	η_{eff}	X-Pol. (dB)	S.L.L (dB)	Gain (dBi)	η_{eff}	X-Pol. (dB)	S.L.L (dB)	Gain (dBi)	η_{eff}	S.L.L. (dB)
12.25	29.3	49.7%	≤−48	≤−13.7	30.4	63.0%	≤−45	≤−13.7	30.1	58.8%	≤−13.2
12.50	29.4	48.1%	≤−48	≤−13.9	30.5	61.9%	≤−43	≤−14.2	30.3	59.2%	≤−14.1
12.75	29.5	47.3%	≤−44	≤−13.7	30.5	59.5%	≤−40	≤−13.6	30.3	55.3%	≤−13.8

arrays ensures better utilization of the limited system space available. In addition, the design technique is simple and easily realized with planar circuit fabrication, making it very suitable to various wireless communications applications.

Acknowledgments

This work was supported by the National Science and Technology of Major Project (2011ZX03001-007-03), the National Natural Science Foundation (61201058), the Research and Innovation Project of Shanghai Education Commission (12Z112030001), and the Scientific Research Foundation for Returned Overseas Chinese Scholars, State Education Ministry, the Project of "SMC Excellent Young Faculty."

References

[1] Y.-B. Jung, S.-Y. Eom, and S.-I. Jeon, "Novel antenna system design for satellite mobile multimedia service," *IEEE Transactions on Vehicular Technology*, vol. 59, no. 9, pp. 4237–4247, 2010.

[2] S. Y. Eom, S. H. Son, Y. B. Jung et al., "Design and test of a mobile antenna system with tri-band operation for broadband satellite communications and DBS reception," *IEEE Transactions on Antennas and Propagation*, vol. 55, no. 11, pp. 3123–3133, 2007.

[3] J. M. Fernández González, P. Padilla, G. Expósito-Domínguez, and M. Sierra-Castañer, "Lightweight portable planar slot array antenna for satellite communications in X-band," *IEEE Antennas and Wireless Propagation Letters*, vol. 10, pp. 1409–1412, 2011.

[4] J. Hirokawa, M. Ando, N. Goto, N. Takahashi, T. Ojima, and M. Uematsu, "A single-layer slotted leaky waveguide array antenna for mobile reception of direct broadcast from satellite," *IEEE Transactions on Vehicular Technology*, vol. 44, no. 4, pp. 749–755, 1995.

[5] Y. Hase, N. Obara, H. Saitoh, and C. Ohuchi, "Slot array antenna system for COMETS advanced mobile satcom experiments," in *Proceedings of the IEEE 46th Vehicular Technology Conference (VTC '96)*, vol. 1, pp. 353–356, Atlanta, Ga, USA, May 1996.

[6] S. Vaccaro, F. Tiezzi, M. F. Rúa, and C. D. G. De Oro, "Ku-band low-profile Rx-only and Tx-Rx antennas for mobile satellite communications," in *Proceedings of the IEEE International Symposium on Phased Array Systems and Technology*, pp. 536–542, Waltham, Mass, USA, October 2010.

[7] J. Wang and J. H. Winters, "An embedded antenna for mobile DBS," in *Proccedings of the IEEE 60th Vehicular Technology Conference (VTC '04)*, vol. 6, pp. 4092–4095, Los Angeles, Calif, USA, September 2004.

[8] M. W. Shelley and J. Vazquez, "Low profile scanning antennas for sitcom 'on-the-move'," in *IEEE Military Communications conference*, vol. 2, pp. 705–709, 1993.

[9] E. Levine, G. Malamud, S. Shtrikman, and D. Treves, "A study of microstrip array antennas with the feed network," *IEEE Transactions on Antennas and Propagation*, vol. 37, no. 4, pp. 426–434, 1989.

[10] R. Azadegan, "A Ku-band planar antenna array for mobile satellite tv reception with linear polarization," *IEEE Transactions on Antennas and Propagation*, vol. 58, no. 6, pp. 2097–2101, 2010.

[11] M. E. Bialkowski and N. C. Karmakar, "A two-ring circular phased-array antenna for mobile satellite communications," *IEEE Antennas and Propagation Magazine*, vol. 41, no. 3, pp. 14–23, 1999.

[12] Y. Liu, L.-M. Si, M. Wei et al., "Some recent developments of microstrip antenna," *International Journal of Antennas and Propagation*, vol. 2012, Article ID 428284, 10 pages, 2012.

[13] Raysat Cyprus Limited, "Flat microwave antenna," World Intellectual Property Organization, WO2005/004284 A1.

[14] H. D. Chen, C.-Y.-D. Sim, J.-Y. Wu, and T.-W. Chiu, "Broadband high-gain microstrip array antennas for WiMAX base station," *IEEE Transactions on Antennas and Propagation*, vol. 60, no. 8, pp. 3977–3980, 2012.

[15] N. Herscovici, "New considerations in the design of micro strip antennas," *IEEE Transactions on Antennas and Propagation*, vol. 46, no. 6, pp. 807–812, 1998.

[16] C. L. Lin and Z. P. Nie, *Antenna Engineering Handbook*, Publishing House of Electronics Industry, Beijing, China, 2002.

[17] Z.-N. Chen, X.-L. Liang, S. Ye et al., "A novel dual-polarization microstrip antenna array with wideband and high gain in Ku band," *Chinese Journal of Radio Science*, vol. 26, no. 4, pp. 661–665, 2011.

Hindawi Publishing Corporation
International Journal of Antennas and Propagation
Volume 2013, Article ID 614754, 6 pages
http://dx.doi.org/10.1155/2013/614754

Research Article

A Compact Size 4–19.1 GHz Heart Shape UWB Antenna with Triangular Patches

Gokmen Isik[1] and Serkan Topaloglu[2]

[1] *Electrical-Electronics Engineering Department, Faculty of Engineering, Yeditepe University, 34755 Istanbul, Turkey*
[2] *TRON Elektronik Sist. San. ve Tic. A.S., 34776 Istanbul, Turkey*

Correspondence should be addressed to Serkan Topaloglu; serkantopaloglu77@gmail.com

Received 31 May 2013; Revised 19 November 2013; Accepted 20 November 2013

Academic Editor: Alistair P. Duffy

An ultrawideband antenna is designed, simulated, and realized. To overcome the narrow bandwidth characteristics of basic patch antennas, the structure of the radiation pattern is optimized by the aid of elliptical and rectangular patches. Also triangular patches are applied to the antenna edge in order to enhance the VSWR and gain properties. A typical VSWR of 1.5 (less than 2 in the whole frequency range) and a typical gain of 2 dBi (mainly above 1 dBi in the whole frequency range) are observed. The simulations present that the designed antenna has a bandwidth ratio of ~5 : 1 within the frequency range of 4–19.1 GHz with compact dimensions of $25 \times 26\,\text{mm}^2$. It is fabricated on a 0.5 mm thick, RO3035 substrate. The input impedance, gain, and radiation characteristics of the antenna are also presented. With these properties, it is verified that, with its novel shape, the proposed antenna can be used for various UWB applications.

1. Introduction

In last decades, the ultrawideband (UWB) technology is developed widely and rapidly. There are many applications employing UWB such as sensor networks [1], location tracking, and biomedical imaging [2]. UWB technology has also become very popular in high speed short range communication systems. Since antenna has a major effect on the performance of these systems, design of the compact antennas has become more important and critical. As a result of these, for broadband and ultrawideband (UWB) applications, patch antennas are an attractive candidate due to their light weight, low cost, wide bandwidth, compact size, and ease of fabrication [3–10].

Here it should be also noted that, since the transmission power in UWB is pretty low, the loss becomes an important issue. Moreover, power loss due to the dielectric and conductor losses needs to be minimized with the selection of a proper substrate.

In the work of Ojaroudi et al. [3], an ultrawideband monopole antenna with inverted T-shaped notch in the ground plane, operating from 3.12 GHz to 12.73 GHz, is presented with a compact size of $12 \times 18\,\text{mm}^2$. A monopole antenna with ladder-shaped resonant structures is also presented. This antenna has a dimension of $22 \times 22\,\text{mm}^2$ with a bandwidth of 19.3 GHz [4]. Liu and Yang [5] presented a hook-shaped UWB antenna operating from 3 GHz to 10.7 GHz with a dimension of $10 \times 10\,\text{mm}^2$. A microstrip-fed, hexagonal wide slot antenna having $30 \times 30\,\text{mm}^2$ area exhibited UWB performance from 2.9 GHz to 18 GHz [6]. A printed circular ring antenna operating from 2.54 GHz to 12.08 GHz is also presented in the literature [7]. In the work of Oudaya Coumar et al. [8], planar monopole antenna operating between 1.8 GHz and 10.6 GHz is studied with an area of $25 \times 30\,\text{mm}^2$. Symmetrical triangle-shaped [9] and tapered-shaped slot antennas [10] with areas of $12 \times 38\,\text{mm}^2$ and $22 \times 24\,\text{mm}^2$ presented operation frequencies from 2.77 GHz to 10.64 GHz and from 3 GHz to 11.2 GHz, respectively.

To overcome the narrow bandwidth property of patch antennas, different techniques have been investigated and applied to cover the entire UWB frequency range [11–14].

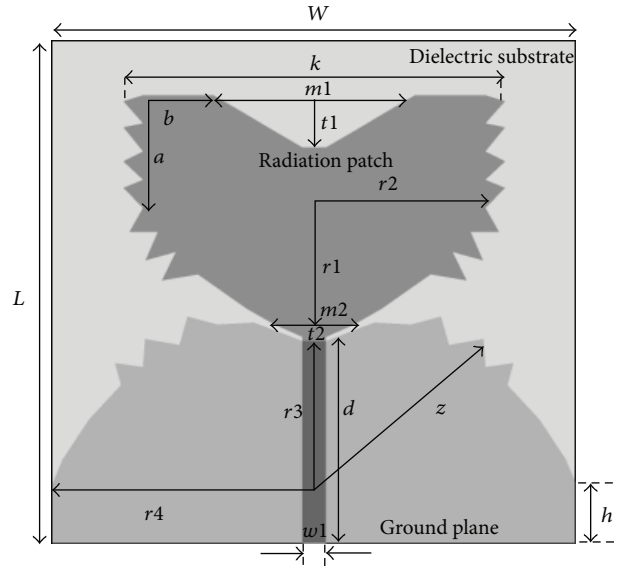

Figure 1: Geometry of the proposed UWB antenna. ($w1$ = 1.16 mm, $m1$ = 10 mm, $m2$ = 6 mm, $t1$ = 0.6 mm, $t2$ = 2.1 mm, z = 13 mm, h = 3 mm, a = 5.6 mm, b = 3.5 mm, $r1$ = 6.4 mm, $r2$ = 8.5 mm, $r3$ = 12 mm, $r4$ = 12.5 mm, k = 19 mm, d = 11.9 mm, W = 25 mm, and L = 26 mm.)

In this work, a "heart shape" slot antenna with enhanced impedance bandwidth has been designed and fabricated. The objective of the work is to enlarge the bandwidth of the antenna while reducing the antenna dimensions to make it appropriate for portable systems and electronic devices. With the help of triangular patch and small segment of arc (as shown in Figure 1 as "m2") at the middle of the ground plane [15–20], wide input impedance matching is achieved over the entire 4–19.1 GHz band. The simulation and measurement for the return loss and VSWR indicate that the proposed structure exhibits an ultrawideband impedance matching and offers an antenna gain greater than 1 dBi.

2. Antenna Configuration

UWB operation is basically defined as the operating frequencies of 3.1 GHz to 10.6 GHz and as 6 GHz to 8.5 Ghz with the definition of U.S. FCC [21] and European regulations (2007/131/EC) [22], respectively. On the other hand, a general definition is also given with the equation

$$\frac{2(f_H - f_L)}{(f_H + f_L)} > 0.2, \quad (1)$$

where f_H and f_L are the upper and lower frequencies, respectively [23].

The basic structure of a heart shape antenna consists of a radiation element and modified ground plane as given in Figure 1. The radiating element of the presented antenna is designed with rectangular and elliptical patch. Rectangular and elliptical shapes are well known antenna types, and they have UWB characteristics with a wide frequency range. "V" slot notch is one of the techniques which augments the gain

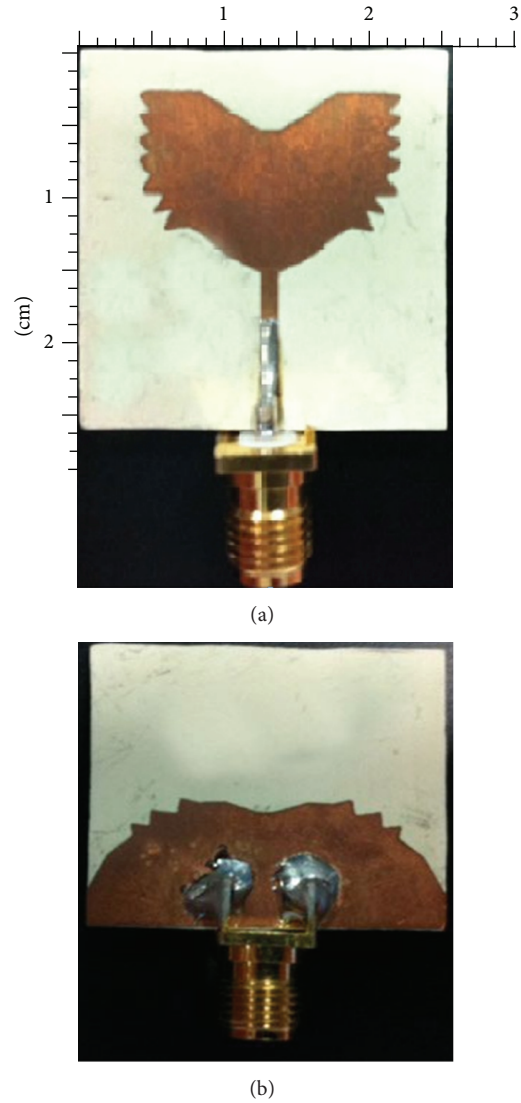

Figure 2: Fabricated prototype (radiating patch (a), ground plane (b)).

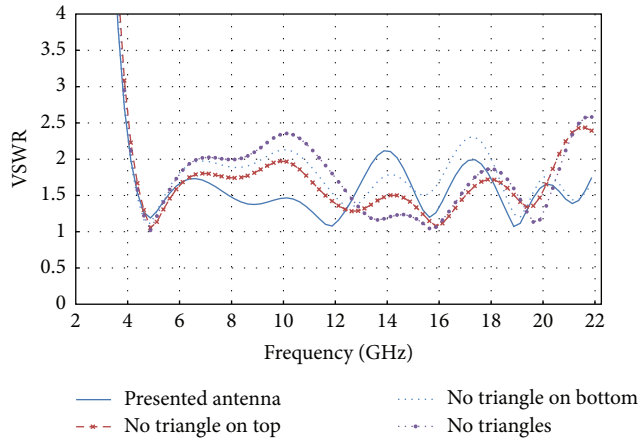

Figure 3: Comparison of VSWR for w/out triangular patches.

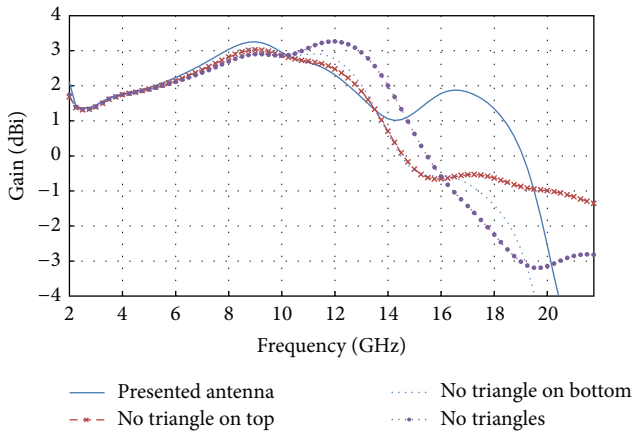

Figure 4: Comparison of gain for w/out triangular patches.

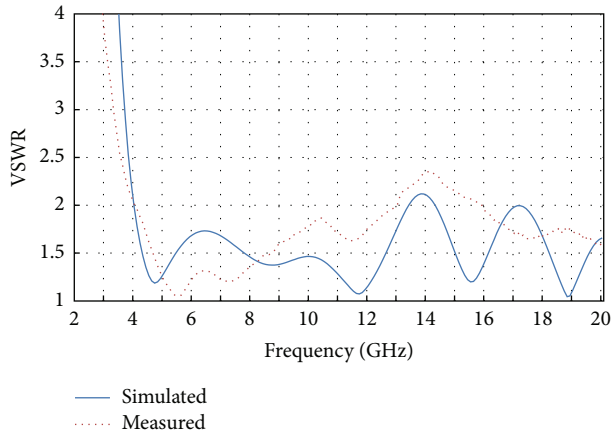

Figure 5: Comparison of simulated and measured VSWR.

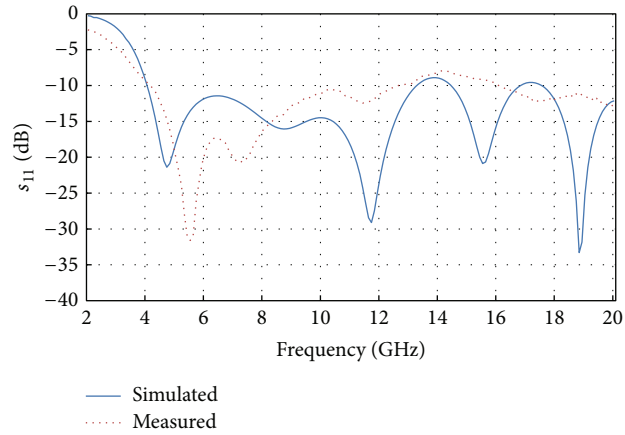

Figure 6: Comparison of simulated and measured return loss.

Table 1: Comparison of the proposed antenna with the recently published selected antennas.

Work	Bandwidth (GHz)	Size (mm × mm)	Gain (dBi)
[3]	3.12–12.73	12 × 18	—
[4]	2.7–20	22 × 22	—
[5]	3–10.7	10 × 10	~1
[6]	2.9–18	30 × 30	~3
[7]	2.54–21.08	39 × 40	~0
[8]	1.8–10.6	25 × 30	—
[9]	2.77–10.64	12 × 38	~1
[10]	3–11.2	22 × 24	~2
This work	4–19.1	25 × 26	~1

and improves the impedance matching of the antenna. On the other hand, triangular-shaped patches are also used at the edge of rectangular patch in order to improve the impedance matching. When we consider the whole frequency range of the presented antenna, more than 100% BW improvement is achieved in comparison to the UWB frequency range defined by FCC [17].

The ground plane used here is also similar to the radiating patch and it also consists of rectangular and elliptical patches. The gain and bandwidth of the antenna are improved by adding a small segment of arc at the middle of the ground plane as also applied in the work of Liu et al. [15]. Modified ground plane of the heart shape UWB antenna is shown in Figure 2. The dimension and the alignment of the ground plane and radiation element are also considered. The proposed antenna has compact dimension of $25 \times 26\,\text{mm}^2$ which is printed on RO 3035 substrate from Rogers Corp. having 0.5 mm thickness and relative dielectric constant of 3.50. Since the dielectric substrate thickness is 0.5 mm, antenna is flexible. Therefore, it may be also suitable for applications where flexibility is necessary, for example, wearable electronics.

3. Results and Discussion

In order to analyze the impact of the triangular patches on radiation element and ground plane, a serial of simulations are performed. It is clear from Figures 3 and 4 that triangles on the radiating element (on top) and the ground plane (on bottom) influence the antenna performance in terms of VSWR and gain. A better performance is achieved when triangles are applied to both sides. Briefly, the designed antenna presents VSWR below 2 and gain above 1 dBi from 4 GHz and up to 19.1 GHz.

For the measurement and the characterization of the antenna performance, a vector network analyzer from Agilent is used. The simulated and measured VSWR and return loss of the antenna are given in Figures 5 and 6. These results illustrate impedance matching bandwidth between 4 GHz and 19.1 GHz range. As given in Figures 5 and 6, measurement result is roughly similar to the simulation results. The slight discrepancy is due to not only the effect of the SMAs used but also the tolerances during fabrication. The VSWR is measured to be below 2 (partially the measured VSWR is 2.3 close to the 14 GHz), whereas the gain is achieved above 1 dBi, typically.

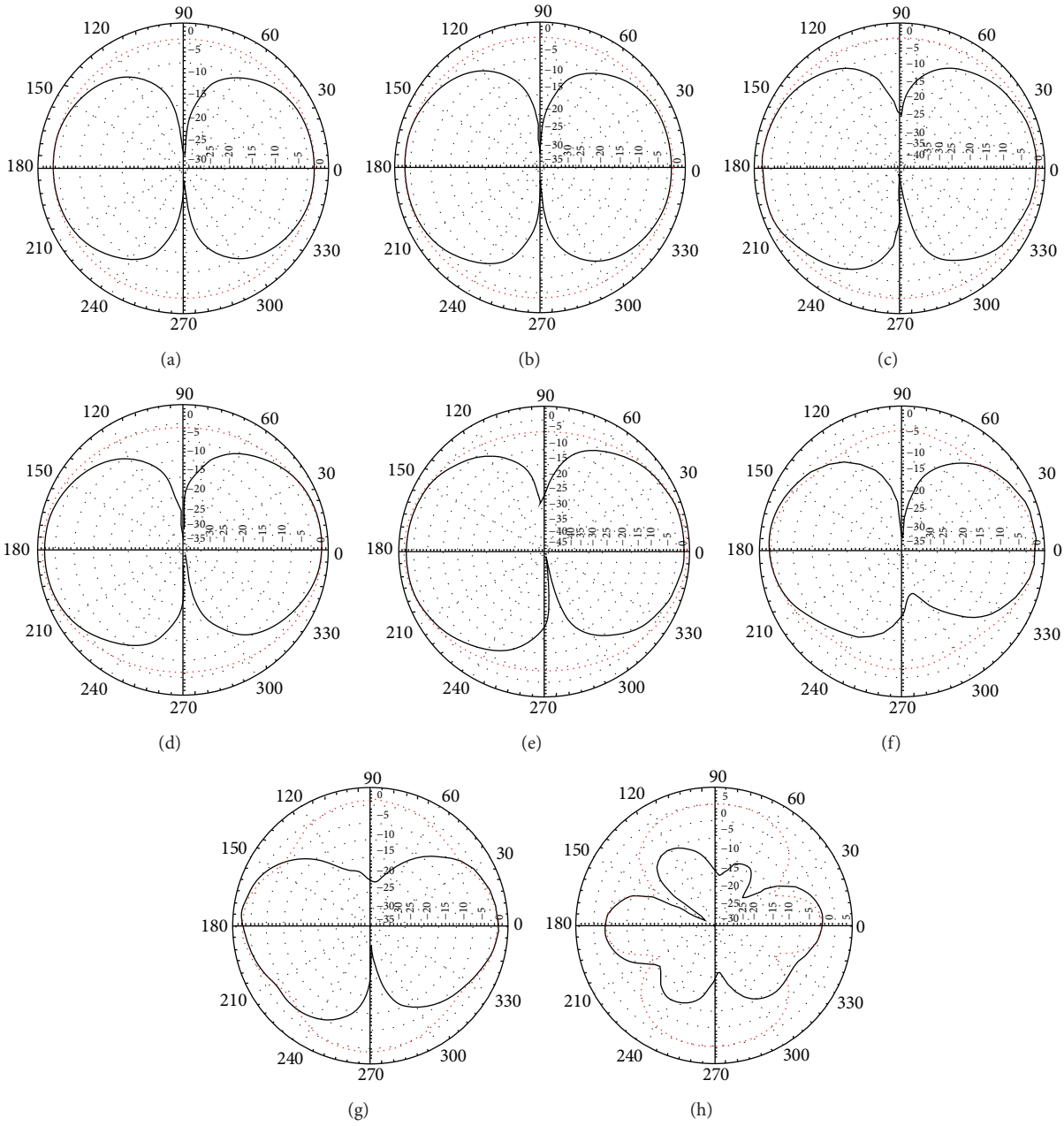

Figure 7: Normalized simulated radiation patterns of the antenna at (a) 3 GHz, (b) 4.5 GHz, (c) 6 GHz, (d) 7.5 GHz, (e) 9 GHz, (f) 10.5 GHz, (g) 12 GHz, and (h) 14 GHz.

The presented antenna in this paper is compared with the recently published antennas in Table 1 in terms of mainly bandwidth and size and also gain and the radiation pattern.

The proposed antenna in this work exhibits a pretty high bandwidth with its comparable size. It presents a moderate gain with a uniform the radiation pattern.

The simulated and measured radiation patterns in the X–Z and Y–Z planes, for frequencies 3, 4.5, 6, 7.5, 9, 10.5, 12, and 14 GHz, are presented in Figures 7 and 8, respectively.

These radiation patterns show a reasonably good agreement between simulations and measurements.

4. Conclusion

In this paper, a novel ultrawideband antenna named by us as heart shape antenna was designed, simulated, fabricated, and characterized. The structure of the radiation part is designed with elliptical and rectangular patches. Also triangular patches used at the edge of the antenna are analyzed to enhance the VSWR and gain of the antenna. In addition, modified ground of the presented antenna also consists of elliptical patches with a small segment of arc at the middle of the ground. With the help of the triangular patch on the modified ground, enhanced gain and impedance matching

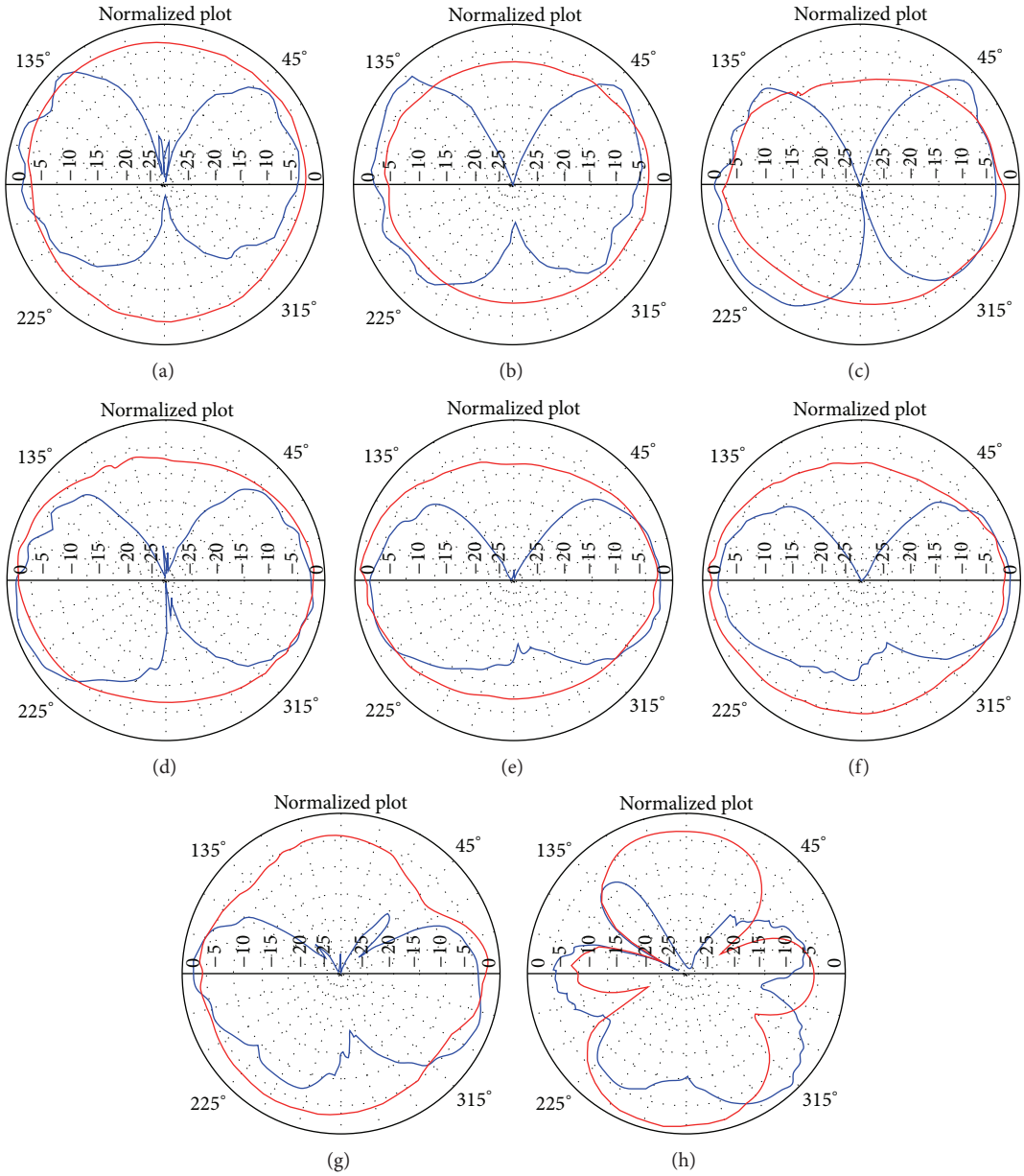

FIGURE 8: Normalized measured radiation patterns of the antenna at (a) 3 GHz, (b) 4.5 GHz, (c) 6 GHz, (d) 7.5 GHz, (e) 9 GHz, (f) 10.5 GHz, (g) 12 GHz, and (h) 14 GHz.

characteristics are achieved. Numerical simulation shows that the antenna has a bandwidth ratio of 5 : 1 within the frequency range of 4 GHz–19.1 GHz with a 25 × 26 mm^2 heart shape UWB antenna.

Briefly, a novel-shaped, flexible UWB antenna providing a VSWR less than 2 and gain of more than 1 dBi is achieved and fabricated with a compact size of 25 × 26 mm^2 which makes it attractive for mobile systems.

Acknowledgments

The authors would like to thank Scientific and Technological Research Council of Turkey (TUBITAK), Center of Research for Advanced Technologies of Informatics and Security (BİLGEM), Electromagnetics and Antenna Systems (EAS) Department—Antenna Design and Research Center, and Spherical Near Field Measurement Laboratory for providing measurement support.

References

[1] J. R. Verbiest and G. A. E. Vandenbosch, "A novel small-size printed tapered monopole antenna for UWB WBAN," *IEEE Antennas and Wireless Propagation Letters*, vol. 5, no. 1, pp. 377–379, 2006.

[2] H. Deng, X. He, B. Yao, and Y. Zhou, "A compact square-ring printed monopole ultra wideband antenna," in *Proceedings of*

the International Conference on Microwave and Millimeter Wave Technology (ICMMT '08), pp. 1644–1646, Nanjing, China, April 2008.

[3] M. Ojaroudi, C. Ghobadi, and J. Nourinia, "Small square monopole antenna with inverted T-shaped notch in the ground plane for UWB application," *IEEE Antennas and Wireless Propagation Letters*, vol. 8, pp. 728–731, 2009.

[4] R. A. Sadeghzadeh-Sheikhan, M. Naser-Moghadasi, E. Ebadi-fallah, H. Rousta, M. Katouli, and B. S. Virdee, "Planar monopole antenna employing back-plane ladder-shaped resonant structure for ultra-wideband performance," *IET Microwaves, Antennas and Propagation*, vol. 4, no. 9, pp. 1327–1335, 2010.

[5] H.-W. Liu and C.-F. Yang, "Miniature hook-shaped monopole antenna for UWB applications," *Electronics Letters*, vol. 46, no. 4, pp. 265–266, 2010.

[6] M. R. Ghaderi and F. Mohajeri, "A compact hexagonal wide-slot antenna with microstrip-fed monopole for UWB application," *IEEE Antennas and Wireless Propagation Letters*, vol. 10, pp. 682–685, 2011.

[7] R. Azim, M. T. Islam, and N. Misran, "Printed circular ring antenna for UWB application," in *Proceedings of the 6th International Conference on Electrical and Computer Engineering (ICECE '10)*, pp. 361–363, Dhaka, Bangladesh, December 2010.

[8] S. Oudaya Coumar, R. Nakkeeran, and G. Ashwath, "Development of compact monopole antenna for UWB applications," in *Proceedings of the 3rd International Conference on Computing, Communication and Networking Technologies (ICCCNT '12)*, Coimbatore, India, July 2012.

[9] H.-C. Tang and K.-H. Lin, "Miniaturized asymmetrical triangle UWB antenna for WUSB dongle applications," in *Proceedings of the IEEE International Symposium on Antennas and Propagation and USNC/URSI National Radio Science Meeting (APSURSI '11)*, pp. 1467–1469, Washington, DC, USA, July 2011.

[10] R. Azim, M. T. Islam, and N. Misran, "Compact tapered-shape slot antenna for UWB applications," *IEEE Antennas and Wireless Propagation Letters*, vol. 10, pp. 1190–1193, 2011.

[11] L. Giauffret, J.-M. Laheurte, and A. Papiernik, "Study of various shapes of the coupling slot in cpw-fed microstrip antennas," *IEEE Transactions on Antennas and Propagation*, vol. 45, no. 4, pp. 642–647, 1997.

[12] A. B. Constantine, *Antenna Theory, Analysis and Design*, John Wiley & Sons, 3rd edition, 2005.

[13] R. Garg and P. Bhatia, *Microstrip Antenna Design Handbook*, Artech House, Norwood, Mass, USA, 2001.

[14] W. L. Stutzman and G. A. Thiele, *Antenna Theory and Design*, John Wiley & Sons, New York, NY, USA, 2nd edition, 1998.

[15] J. Liu, S. Zhong, and K. P. Esselle, "A printed elliptical monopole antenna with modified feeding structure for bandwidth enhancement," *IEEE Transactions on Antennas and Propagation*, vol. 59, no. 2, pp. 667–670, 2011.

[16] M. Al-Husseini, Y. Tawk, A. El-Hajj, and K. Y. Kabalan, "A low-cost microstrip antenna for 3G/WLAN/WiMAX and UWB applications," in *Proceedings of the International Conference on Advances in Computational Tools for Engineering Applications (ACTEA '09)*, pp. 68–70, Beirut, Lebanon, July 2009.

[17] W. Peng, W. Anguo, and D. Jiawei, "Design of the UWB antenna using fractal concept," in *Proceedings of the 8th International Symposium on Antennas, Propagation and EM Theory (ISAPE '08)*, pp. 189–192, Kunming, China, November 2008.

[18] O. M. H. Ahmed and A. R. Sebak, "A novel maple-leaf shaped UWB antenna with a 5.0–6.0 GHz band-notch characteristics," *Progress in Electromagnetics Research C*, vol. 11, pp. 39–49, 2009.

[19] D. Azzeddine, N. Mourad, D. A. Tayeb, and H. M. Adnane, "Design of UWB triangular slot antenna," in *Proceedings of the IEEE International Symposium on Antennas and Propagation and USNC/URSI National Radio Science Meeting (APSURSI '11)*, pp. 1456–1458, Spokane, Wash, USA, July 2011.

[20] M. Koohestani, M. N. Moghadasi, and B. S. Virdee, "Miniature microstrip-fed ultra-wideband printed monopole antenna with a partial ground plane structure," *IET Microwaves, Antennas and Propagation*, vol. 5, no. 14, pp. 1683–1689, 2011.

[21] Federal Communication Commision, *FCC Report and Order on Ultra Wideband Technology*, 2002.

[22] Commission of the European Communities, "Commission decision on allowing the use of the radio spectrum for equipment using ultra-wideband technology in a harmonized manner in the community," *Official Journal of the European Union*, vol. 50, 2007.

[23] W. Wiesbeck, G. Adamiuk, and C. Sturm, "Basic properties and design principles of UWB antennas," *Proceedings of the IEEE*, vol. 97, no. 2, pp. 372–385, 2009.

Hindawi Publishing Corporation
International Journal of Antennas and Propagation
Volume 2013, Article ID 215681, 12 pages
http://dx.doi.org/10.1155/2013/215681

Research Article

Zero Index Metamaterial for Designing High-Gain Patch Antenna

Yahong Liu, Xiaojing Guo, Shuai Gu, and Xiaopeng Zhao

Smart Materials Laboratory, Department of Applied Physics, Chang'an Campus, Northwestern Polytechnical University, Xi'an 710129, China

Correspondence should be addressed to Xiaopeng Zhao; xpzhao@nwpu.edu.cn

Received 16 April 2013; Revised 12 August 2013; Accepted 14 August 2013

Academic Editor: Alistair P. Duffy

A planar wideband zero-index metamaterial (ZIM) based on mesh grid structure is studied. It is demonstrated that the real part of the index approaches zero at the wideband covering from 9.9 GHz to 11.4 GHz. Two conventional patch antennas whose operating frequencies are both in the range of zero-index frequencies are designed and fabricated. And then, the ZIM is placed in the presence of the conventional patch antennas to form the proposed antennas. The distance between the antenna and the ZIM cover is investigated. Antenna performances are studied with simulations and measurements. The results show that the more directional and higher gain patch antennas can be obtained. The measured results are in good agreement with the simulations. Compared to the conventional patch antenna without the ZIM, it is shown that the beamwidth of antenna with the ZIM cover becomes more convergent and the gain is much higher.

1. Introduction

In recent years, artificial electromagnetic metamaterials have attracted growing interests. Based on the effective medium theory, electromagnetic metamaterials can be characterized by electric permittivity and magnetic permeability. Pendry realized the artificially electric plasma using a metallic wire whose permittivity is negative [1]. And then, Pendry discovered the artificially magnetic plasma whose permeability is negative [2]. Metamaterials open a door to realize all possible material properties by designing different cellular architectures and using different substrate materials [3–6]. Among the various, unusual material parameters provided by metamaterials, zero permittivity/permeability/index is a singular material parameter, which can lead to many interesting phenomena and applications [7–22]. Jiang et al. [7] and Jin and He [8] demonstrated that effective zero index metamaterial (ZIM) can enhance uniform fields. Silveirinha et al. [9–12] proposed that the electromagnetic wave can tunnel through a zero electric permittivity metamaterial. Nguyen et al. [13] and Hao et al. [14] investigated that ZIM with defects can realize the total transmission or reflection of the impinging electromagnetic wave. Therefore, ZIM structure can offer advances in shielding or cloaking technologies without restricting the object's viewpoint.

Recent studies show that ZIM may have paved a new way for designing novel high-gain antennas due to its unique properties. Based on Snell's law, it is considered an incident ray on an interface of the ZIM with grazing incidence that comes from a source inside ZIM. A near-zero index ray in the media will be refracted in a direction that is very close to the normal. The lower the optical index is, the closer the normal direction is. Enoch et al. [15] is the first to realize high directive radiation by employing monopole source embedded in ZIM, thus confining the radiated energy to a small solid angle. After the work of Enoch, Wu et al. [16] proposed a left-handed metamaterial as a substrate for designing directional radiation. Through the control of the structure's geometry, the zero index frequency can be tuned to the desired specification to produce directional emission. In addition, other works about directive radiations employing ZIM were also studied [17–19]. However, in the previous references, the directive antennas based on ZIM operate at a single frequency or a narrowband frequency.

Inspired by Enoch, in this paper, a planar wideband ZIM is fabricated firstly. The resonant electromagnetic properties present in the bandwidth of the planar ZIM can be up to 1.5 GHz. And then, two high-gain patch antennas (narrowband patch antenna and wideband patch antenna) based on the ZIM cover are studied. The antennas' performances are studied with simulations and measurements. It is demonstrated that gain and directivity of the proposed antennas can be improved at the wideband frequencies compared to the conventional patch antennas without the ZIM. In addition, the electric field distributions are presented for explaining physically the improvement of antenna performance. A simple method for achieving a wideband high-gain patch antenna is provided in the present work.

2. Zero Index Metamaterial

2.1. ZIM Design Principle. Pendry discovered that electromagnetic behaviors of arrays of periodical wires are similar to those of metal [1]. Plasma is a system composed of a large number of charged particles, which shows neutral. The effective permittivity can be expressed as

$$\varepsilon(\omega) = 1 - \frac{\omega_p^2}{\omega^2}, \tag{1}$$

where ω_p is the plasma frequency and ω is the frequency of the propagating electromagnetic wave. The plasma frequency ω_p of the metal can be expressed as

$$\omega_p^2 = \frac{n_e e^2}{\varepsilon_0 m_{\text{eff}}}, \tag{2}$$

where n_e is the charge density, e is the electric quantity, m_{eff} is the effective mass, and ε_0 is the permittivity in free space. The plasma frequency ω_p of the metal is in the frequency of ultraviolet. Pendry proposed a mechanism for the depression of the plasma frequency ω_p to microwave by employing arrays of wires. Wires can depress n_e and increase m_{eff}, resulting in lowering the plasma frequency ω_p. The plasma frequency ω_p of the wires can be expressed as

$$\omega_p^2 = \frac{2\pi c_0^2}{a^2 \ln(a/r)}, \tag{3}$$

where r is the radius of the wires, a is the lattice constant, and c_0 is the speed of light in the free space. From (3), the plasma frequency ω_p can be lowered by optimizing the lattice constant a and the radius r of the wires. It can be concluded that the permittivity is negative when the frequency is below the plasma frequency.

Based on Pendry's thought, we design the mesh grid structure whose plasma frequency can be in the microwave band by optimizing the parameters of the mesh grid structure. When operating at the plasma frequency, the effective permittivity is zero, and hence it yields a zero index.

2.2. Fabrication and Experiment. Figure 1 shows the planar ZIM consisting of arrays of mesh grid on each side of the substrate with the thickness of 1.5 mm and the effective dielectric constant ε_r of 2.65 ($tg\theta = 0.009$). The design idea is inspired by [15]. However, in the present paper, we utilize single-layer microstrip technology for realizing the planar ZIM. Geometrical dimension of the unit cell presented in Figure 1(a) are line width w and lattice constant l. Zero index frequency can be controlled by constructing the parameters w and l. In the present paper, the simulations were employed by using German commercial software package CST Microwave Studio on the basis of the finite integration method. Electromagnetic resonant behaviors of the planar ZIM for different parameters w and l are studied. Figure 2 shows the resonant behaviors for $w = 0.2$ mm, 0.4 mm, 06 mm, and 0.8 mm with constant $l = 14$ mm. Figures 2(a) and 2(b) show the transmission spectrums and reflection spectrums. The calculated permeability, permittivity, and index by using S-parameters retrieval method [23] are presented in Figures 2(c), 2(d), 2(e), 2(f), 2(g), and 2(h). It is presented that the cutoff near-zero index is 9.9 GHz, 10.9 GHz, 11.7 GHz, and 12.39 GHz corresponding to $w = 0.2$ mm, 0.4 mm, 06 mm, and 0.8 mm. The near-zero index shifts the higher frequency with the increase of the parameter w. Meanwhile, the results show that the imaginary parts of the permeability, permittivity, and index are all small at the near-zero index. The electromagnetic behaviors of the planar ZIM versus the parameter l are also investigated. The study shows that the near-zero index shifts the lower frequency with the increase of l (not shown here).

The planar ZIM structure was fabricated by using a shadow mask/etching technique in this paper. The geometrical dimensions of the unit cell are chosen as follows: line width $w = 0.6$ mm and lattice constant $l = 14$ mm. Deposited copper thickness is 35 μm. The fabricated planar ZIM sample is shown in Figure 1(b). The experiments composed of two standard horn antennas (8.2–12.4 GHz) were carried out with an AV3618 network analyzer (50 MHz–20 GHz) in an anechoic chamber. The measured refractive index is shown in Figure 2(g), where the real part of the index is near-zero at the wideband frequencies.

3. High-Gain Patch Antennas with the ZIM Cover

3.1. Antennas' Design and Fabrication. Based on the wideband zero index, besides a conventional narrowband patch antenna, a wideband patch antenna has also been designed and fabricated. Antennas' design is employed by CST Microwave Studio and the fabrication is by using a shadow mask/etching technique on the 1.5 mm thickness substrate with an effective dielectric constant ε_r of 2.65 ($tg\theta = 0.009$). The dimension of the radiation patch is 9.7 mm × 7.8 mm. The ground plane size and substrate size are both 56 mm × 56 mm. A 50 Ω coaxial probe which is used to feed the antenna was situated at the centre of a rectangular patch along the y-axis, and 2.3 mm away from the x-axis in the cartesian coordinate. The fabricated narrowband antenna sample is shown in Figure 3(a). The simulated and measured antenna reflections are presented in Figure 3(c). It shows that the simulated −10 dB bandwidth is 0.846 GHz covering

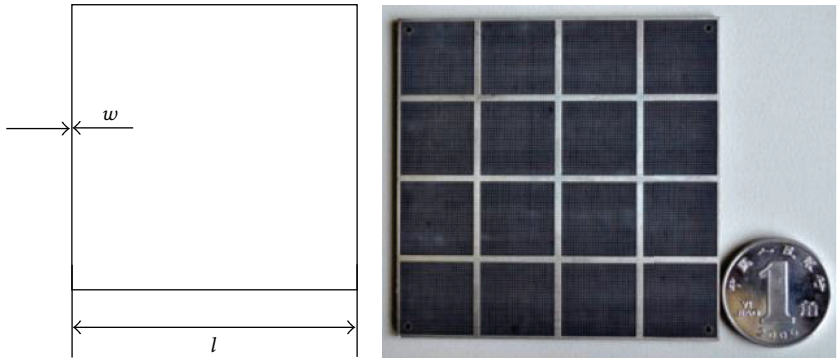

(a) (b)

Figure 1: Zero index metamaterial, (a) the unit cell and (b) the sample.

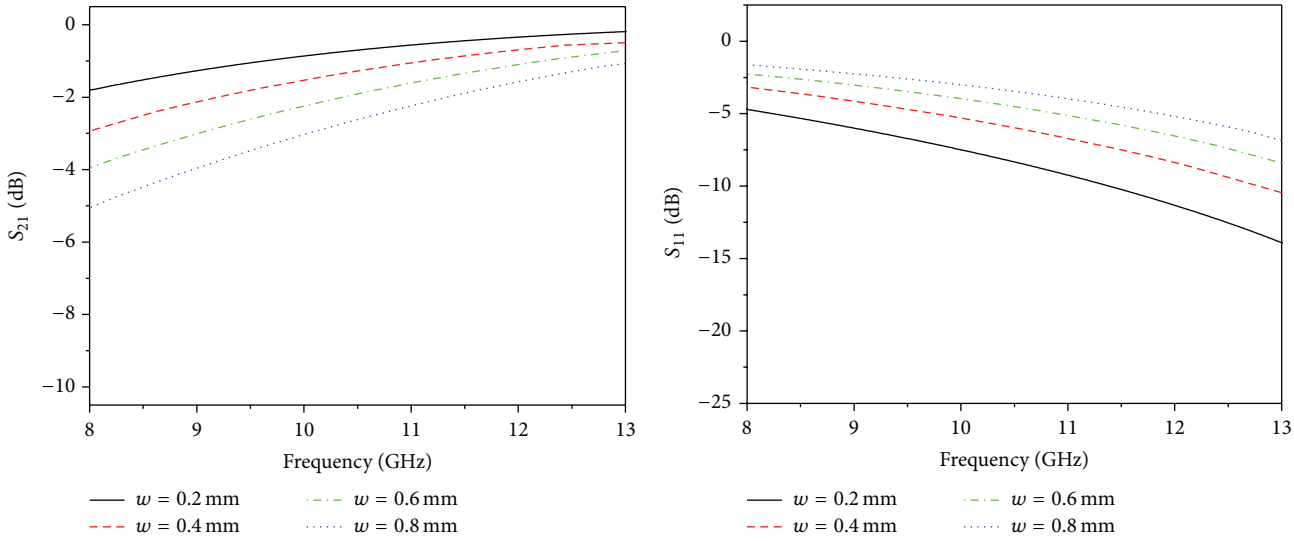

(a)

(b)

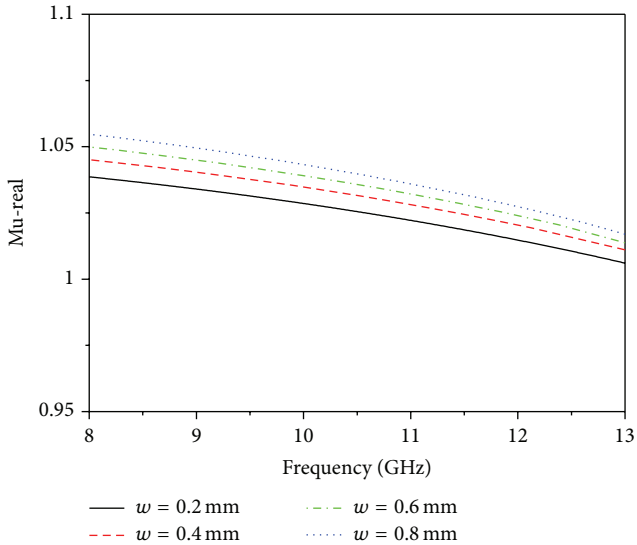

(c)

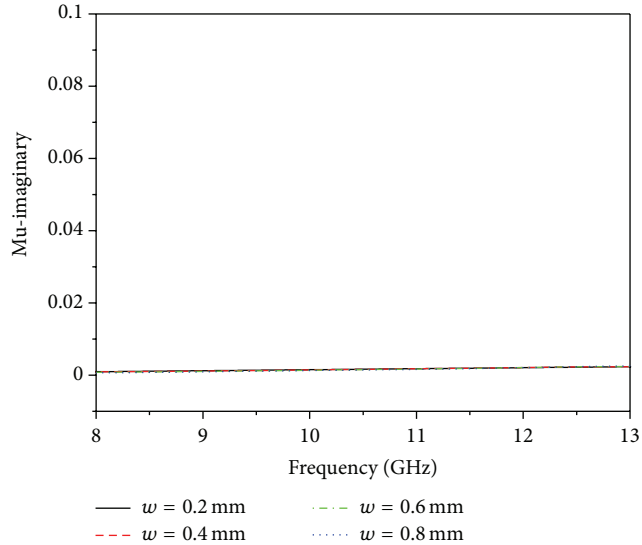

(d)

Figure 2: Continued.

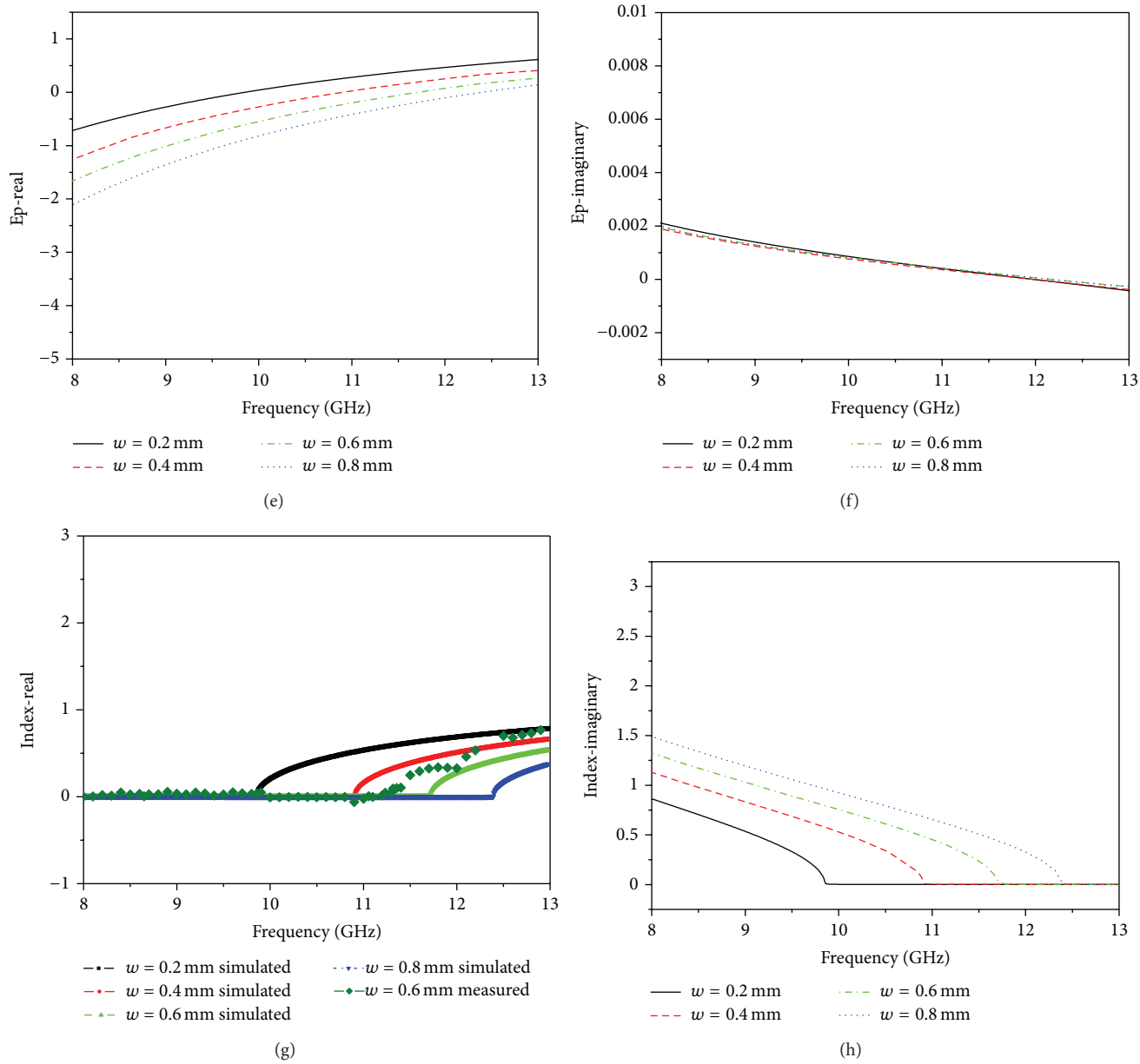

FIGURE 2: The results for $w = 0.2$ mm, 0.4 mm, 0.6 mm, and 0.8 mm with $l = 14$ mm, (a) the simulated transmission spectrums, (b) the simulated reflection spectrums, (c) the simulated real parts of the permeability, (d) the simulated imaginary parts of the permeability, (e) the simulated real parts of the permittivity, (f) the simulated imaginary parts of the permittivity, (g) the simulated and measured real parts of the index, and (h) the simulated imaginary parts of the index.

from 9.914 GHz to 10.76 GHz, with the relative bandwidth of 8.184%. Whereas the measured −10 dB bandwidth is 0.8 GHz covering from 10.14 GHz to 10.94 GHz, with the relative bandwidth of 7.6%. The measured frequency is slightly higher than the simulated one. This discrepancy may be due to the fabrication tolerance and the substrate material where the actual dielectric constant is a little different from the value used in the simulations.

In order to broaden antenna bandwidth, four parasitic patches [24] with the dimension of 2.3 mm × 7.8 mm surrounded by the radiation patch are added. The wideband patch antenna prototype is shown in Figure 3(b). The simulated −10 dB bandwidth is 1.212 GHz covering from 9.884 GHz to 11.096 GHz, with the relative bandwidth of 11.55%. Whereas the measured −10 dB bandwidth is 1.2 GHz covering from 10.05 GHz to 11.25 GHz, with the relative bandwidth of 11.3%. The antenna bandwidth is wider by 0.4 GHz than that of the narrowband patch antenna. The operation frequency of the wideband antenna is still in the range of zero index of the ZIM.

The prototype of the proposed antenna with the ZIM cover is shown in Figure 4. It is demonstrated that

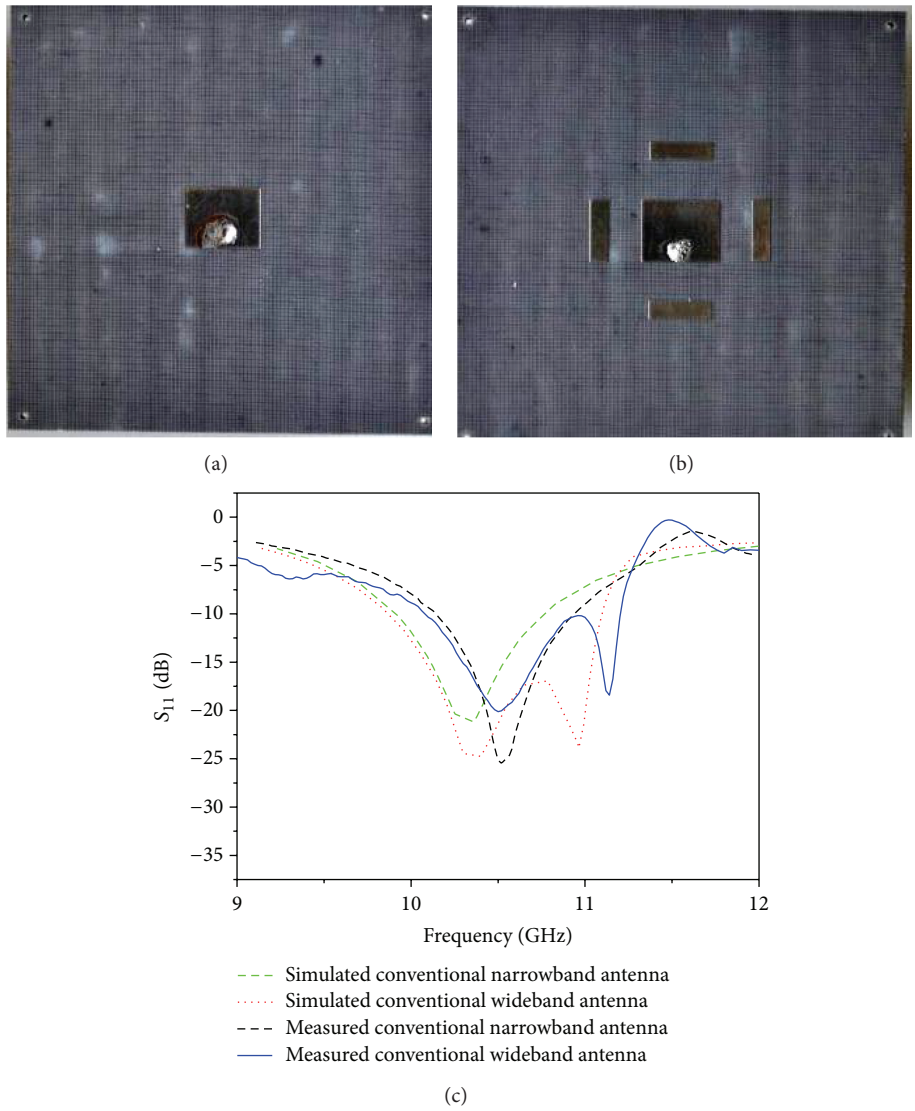

Figure 3: The conventional patch antennas, (a) the prototype of the conventional narrowband antenna, (b) the prototype of the conventional wideband antenna, and (c) the reflection coefficients.

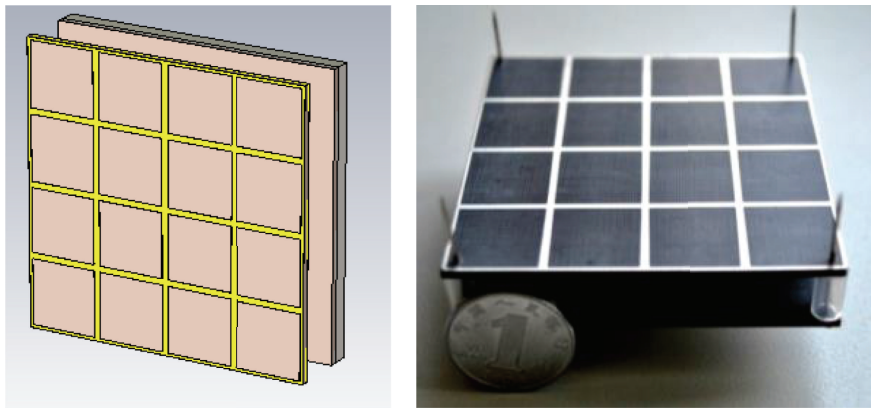

Figure 4: The prototype of the proposed wideband antenna with the ZIM cover, (a) the setup for the numerical simulations and (b) the proposed antenna sample.

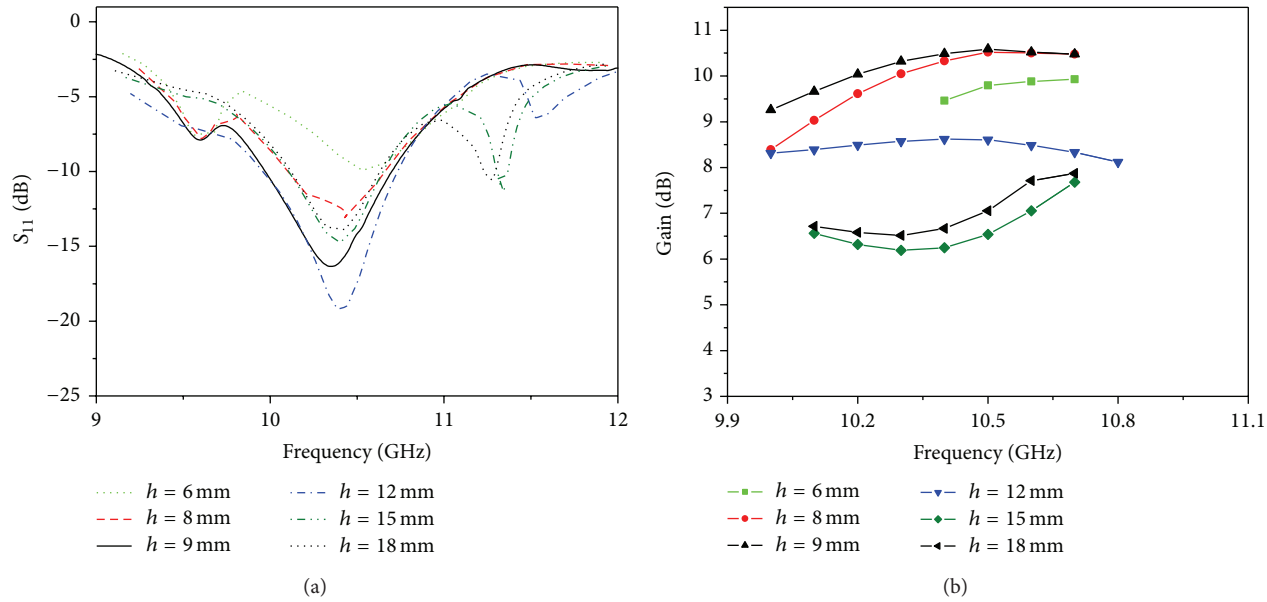

FIGURE 5: The performance of the proposed narrowband antenna with the ZIM cover for different distances h, (a) the reflection coefficients and (b) the antenna gains.

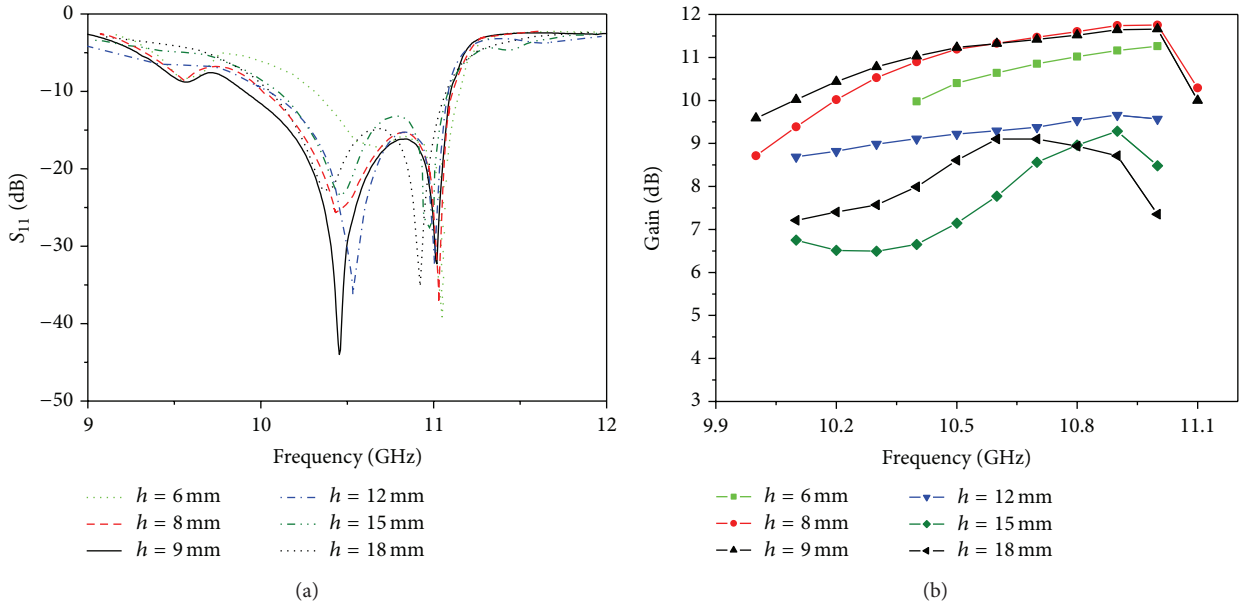

FIGURE 6: The performance of the proposed wideband antenna with the ZIM cover for different distances h, (a) the reflection coefficients and (b) the antenna gains.

the distance h between the patch antenna and ZIM cover influences the antenna performances. Figure 5 gives the simulated performances of the narrowband patch antenna with the ZIM cover, which presents the optimum distance $h = 9$ mm. The average gain of the narrowband antenna with the ZIM is 10.17 dB at the working frequencies, and the peak gain can be up to 10.59 dB at 10.5 GHz. Figure 6 gives the simulated performances of the wideband antenna with the ZIM cover. The optimum distance is also $h = 9$ mm. The average gain of the proposed wideband antenna with ZIM is 10.9 dB at the working frequencies, and the peak gain is 11.6 dB at 10.9 GHz. Therefore, in the present paper, we fabricate the antenna samples with the optimum distance $h = 9$ mm. In addition, the number of the ZIM layers versus antenna performances is also investigated. The antenna performances are listed in Table 1. The results show that the antenna gain is improved with the increase of the ZIM layers. When one layer ZIM is placed above the conventional patch antenna, antenna beamwidth is convergent and the gain is improved greatly. When two layers ZIM or much more layers

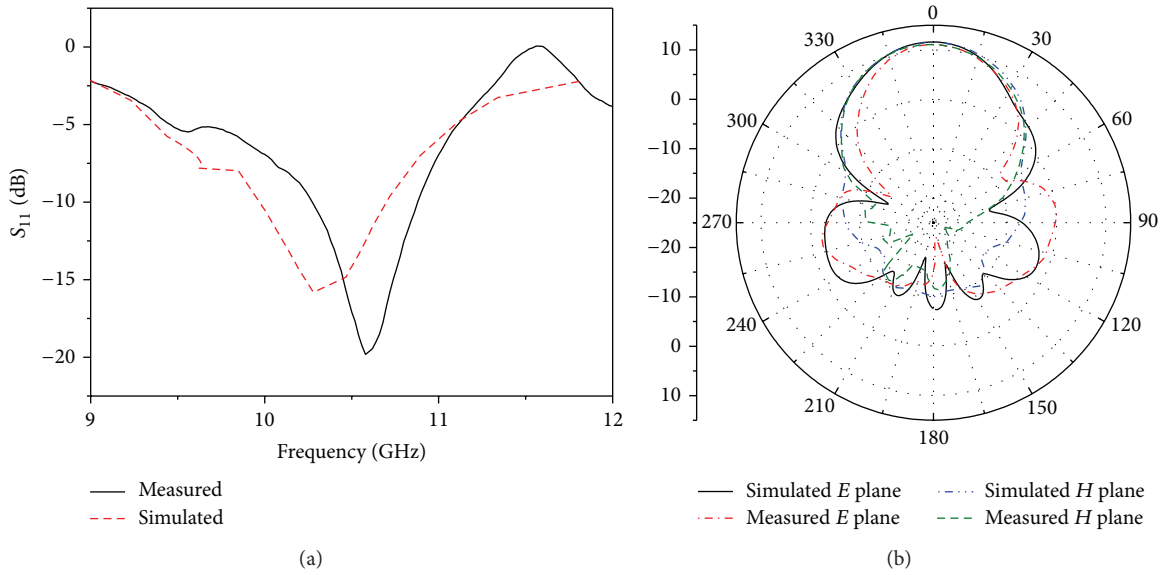

Figure 7: The performances of the proposed narrowband antenna with the ZIM cover, (a) the reflection coefficients and (b) the radiation patterns.

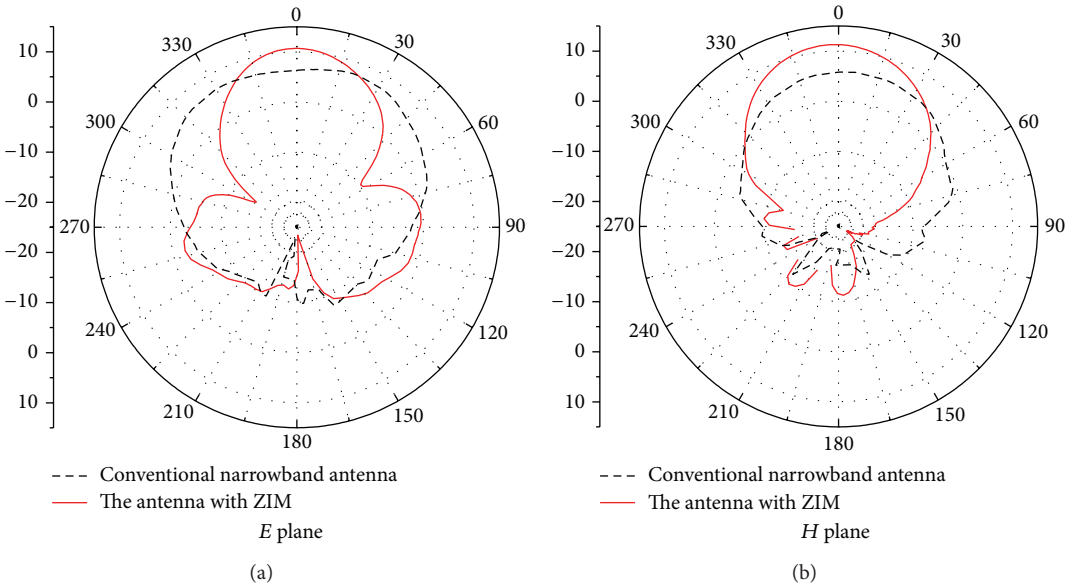

Figure 8: The measured radiation patterns for the conventional narrowband antenna and the antenna with the ZIM cover.

ZIM are utilized, antenna gain is improved slowly. When the ZIM cover is increased to seven layers, the antenna gain is almost stable. In order to design the antenna with compact volume and improved gain, the antenna based on one layer ZIM with the optimum distance $h = 9$ mm is fabricated in the present paper.

3.2. Performances of the Narrowband Patch Antenna with the ZIM Cover. Figure 7 presents the performances of the proposed narrowband high-gain antenna. The simulated and measured antenna reflection coefficients are shown in Figure 7(a), where the simulated −10 dB bandwidth is 0.71 GHz covering from 9.98 GHz to 10.69 GHz and the measured −10 dB bandwidth is 0.63 GHz covering from 10.26 GHz to 10.89 GHz. The proposed antenna radiation patterns are shown in Figure 7(b). It shows that the simulated half-power beamwidth (HPBW) in the E plane and H plane are 45° and 51°, respectively. The measured HPBW in the E plane and H plane are 41° and 49°, respectively. The simulated gain is 10.48 dB and the measured one by using the gain comparison method is 10.6 dB. The simulated and measured aperture efficiencies are 24% and 23.7%, respectively. The measured results are in good agreement with the simulated ones.

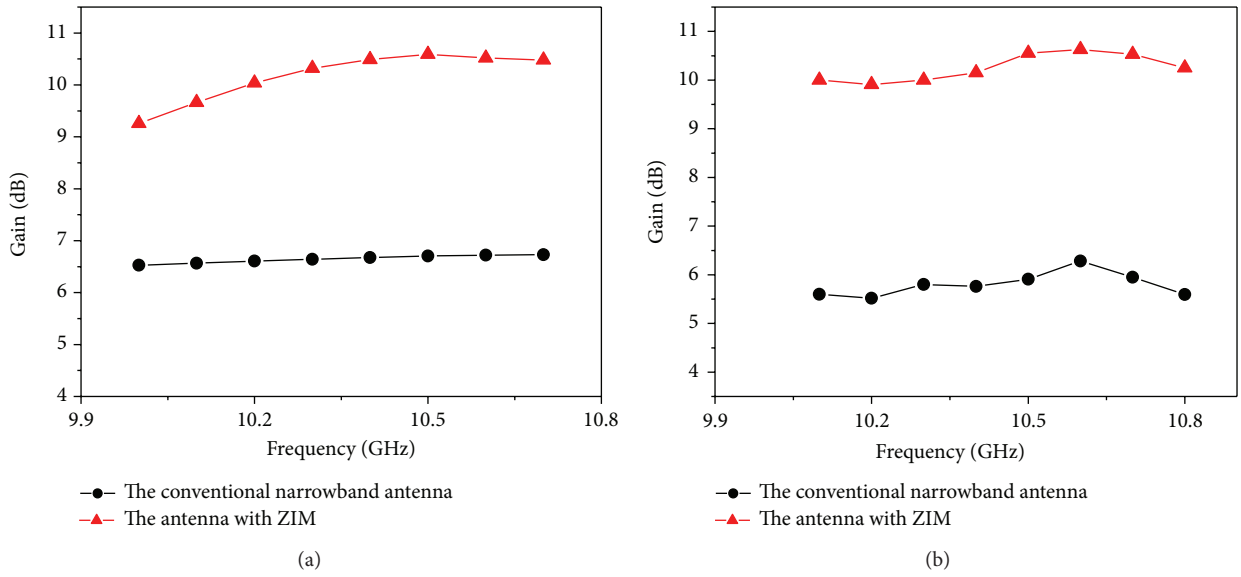

FIGURE 9: The comparative gains of the conventional narrowband antenna and the proposed antenna, (a) simulations and (b) measurements.

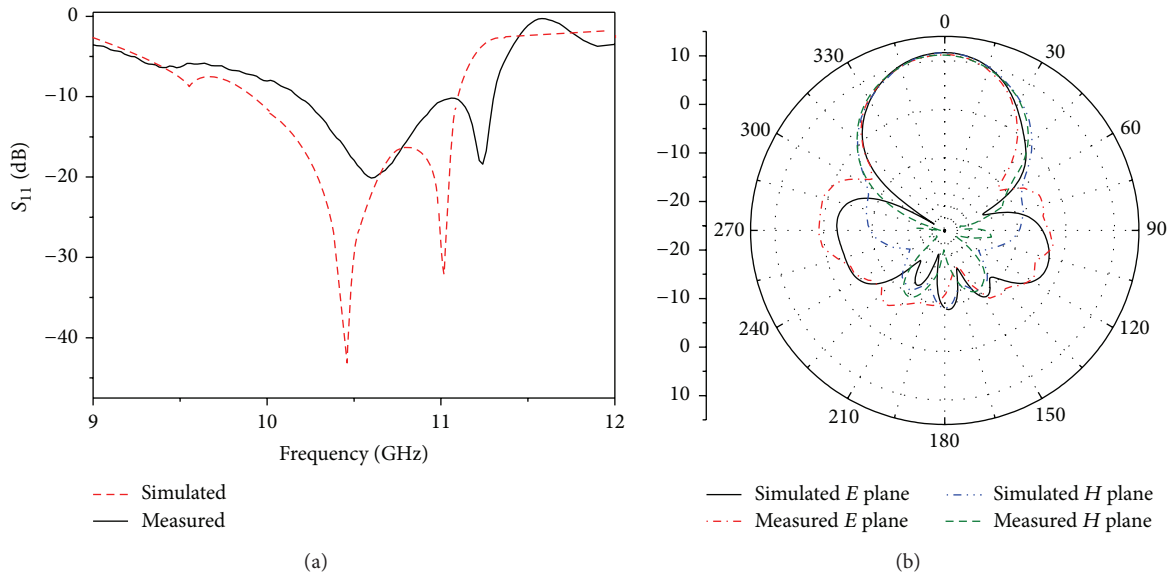

FIGURE 10: The performances of the proposed wideband antenna with the ZIM cover, (a) the reflection coefficients and (b) the radiation patterns.

To demonstrate the ZIM cover for improving antenna performance, the comparative radiation patterns between the conventional patch antenna and the proposed antenna are presented in Figure 8. It shows that the measured HPBW in the E plane is reduced by 42°, and HPBW in the H plane is reduced by 15° compared to the conventional patch antenna without the ZIM. The side lobe is reduced and the forward radiation is enhanced. As a result, the gain is improved. The comparative gains are shows in Figure 9, which presents that the measured average gain is improved by 4.23 dB compared to the conventional antenna without the ZIM.

3.3. Performances of the Wideband Patch Antenna with the ZIM Cover. Figure 10 presents the performances of the proposed wideband antenna. The simulated and measured antenna reflection coefficients are shown in Figure 10(a), where the simulated −10 dB bandwidth is 1.192 GHz covering from 9.908 GHz to 11.1 GHz and the measured −10 dB bandwidth is 1.18 GHz covering from 10.14 GHz to 11.32 GHz. The proposed antenna radiation patterns are shown in Figure 10(b). It shows that the simulated HPBW in the E plane and H plane are 36.4° and 37.2°, respectively. The measured HPBW in the E plane and H plane are 38° and

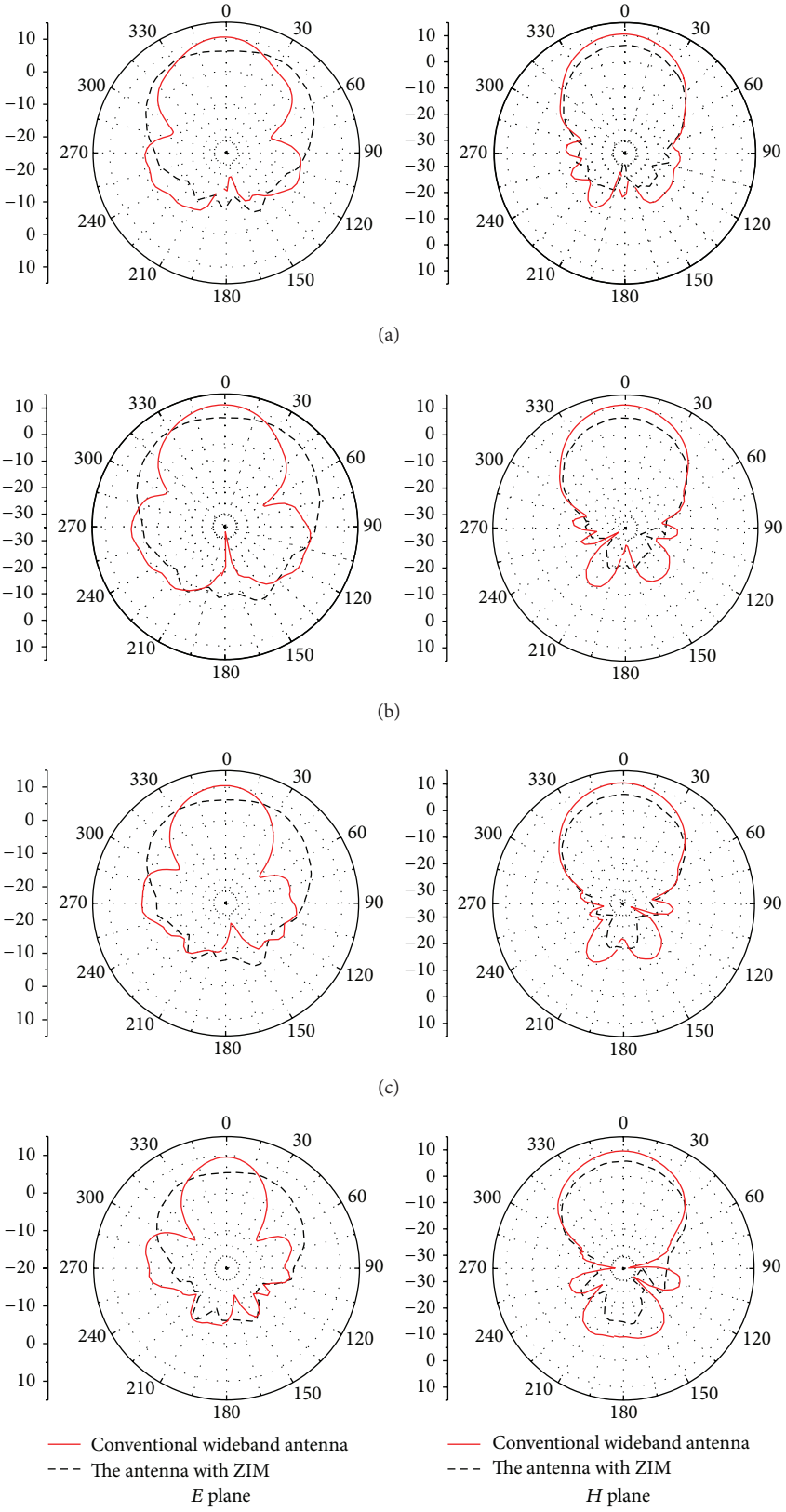

Figure 11: The measured radiation patterns for the conventional wideband antenna and the proposed antenna at the frequencies of (a) 10.15 GHz, (b) 10.6 GHz, (c) 10.8 GHz, and (d) 11.3 GHz.

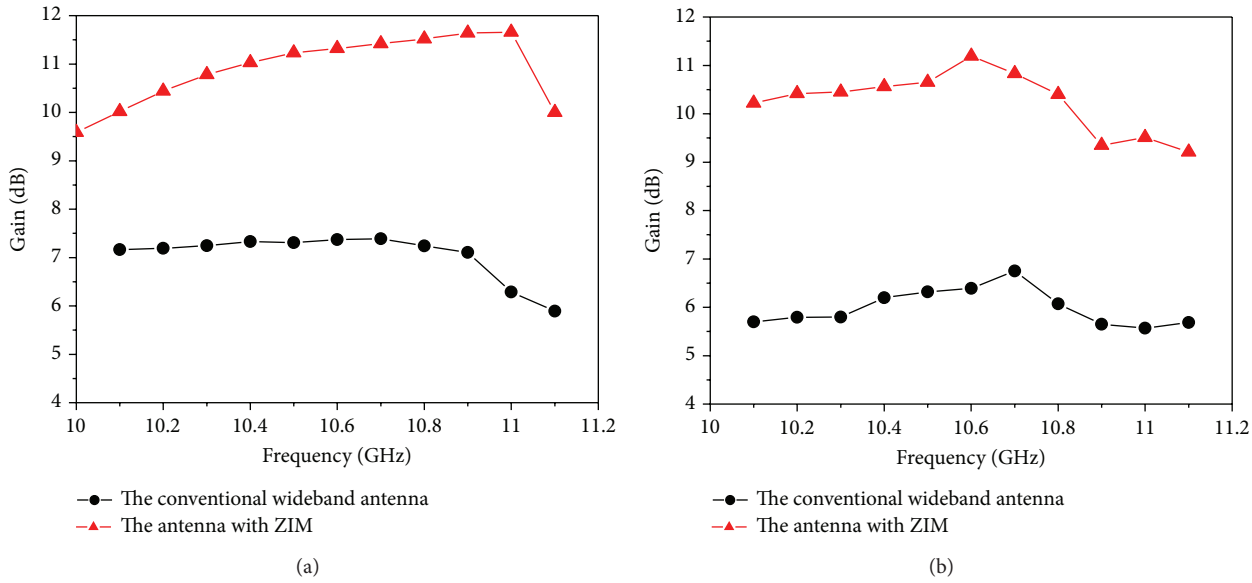

Figure 12: The comparative gains of the conventional wideband antenna and the proposed antenna, (a) simulations and (b) measurements.

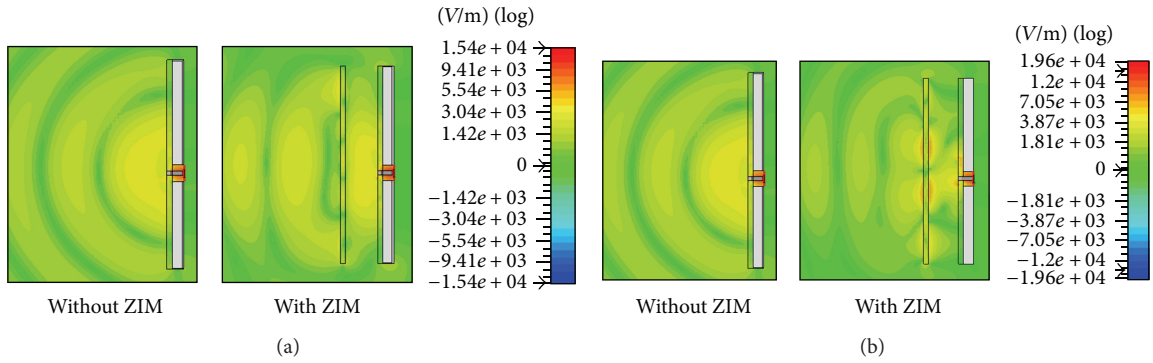

Figure 13: The comparative electric field magnitude distributions of the antennas, (a) 10 GHz and (b) 11.1 GHz.

Table 1: The performances of the antenna based on the different ZIM layers.

Antennas	Parameters		
	HPBW (θ_E)	HPBW (θ_H)	Gain (dB)
Patch antenna without ZIM	106°	90°	6.643
Antenna with 1 layer ZIM	45°	51°	10.33
Antenna with 2 layers ZIM	35°	40°	10.8
Antenna with 3 layers ZIM	31°	36°	11.3
Antenna with 4 layers ZIM	28°	32°	12.4
Antenna with 5 layers ZIM	26°	28°	13.0
Antenna with 6 layers ZIM	23°	24°	13.7
Antenna with 7 layers ZIM	20°	20°	13.9

43°, respectively. The simulated gain is 11.63 dB and the measured one is 11.3 dB at the center frequency. The simulated and measured aperture efficiencies are 30.4% and 28.7%, respectively.

The comparative antenna radiation patterns between the conventional wideband patch antenna and the proposed antenna are presented in Figure 11. The radiation patterns at the frequencies of 10.15 GHz, 10.6 GHz, 10.8 GHz, and 11.3 GHz are all given in order to demonstrate that the antenna performs good performances at the wideband frequencies. It shows that HPBW in the E plane is reduced by 49° and HPBW in the H plane is reduced by 22° compared to the conventional wideband patch antenna without the ZIM cover. The comparative gains are presented in Figure 12, which shows that the measured average gain is improved by 4.37 dB compared to the conventional wideband antenna without the ZIM cover.

3.4. Discussion. In order to explore physically the improvement of antenna performance, simulated electric field distributions for the conventional wideband antenna and the antenna with the ZIM cover at the lower frequency (10 GHz) and the upper frequency (11.1 GHz) are given in Figure 13. The electromagnetic wave front presents a spherical wave for

the conventional antenna without the ZIM cover at these two frequencies. However, the electromagnetic wave front shows a plane wave for the antenna with the ZIM cover. The planar ZIM cover plays a role in controlling the electromagnetic wave propagation direction, changing the spherical wave radiated by the conventional antenna to the plane wave. In the far-field view, the sideward radiation will be reduced, and forward radiation can be enhanced in the radiation patterns. As a result, a more directional and higher gain antenna can be obtained. The similar electric field distributions can be obtained for the conventional narrowband antenna and the antenna with the ZIM cover.

It is known that the propagation phase can be defined as $\Delta\phi = nk_0d$ when the electromagnetic wave transmits the distance d in the medium. For the ZIM, the index is zero. Therefore, propagation phase is independent of propagation distance. It is expected that the propagation phase is the same at the interface between the medium and the free space whenever excitation of radiation source in the ZIM is the spherical wave or the plane wave. Hence, the form of the electromagnetic wave front depends on the curvature of the emergent surface when the electromagnetic wave transmits through the ZIM. In this paper, the planar ZIM can be employed for changing the spherical wave radiated by the conventional antenna to the plane wave. As a result, the directivity and gain of the antenna with the ZIM cover can be enhanced.

In the present paper, the high-gain patch antennas based on the ZIM cover are proposed. The planar ZIM structure in our paper is fabricated by using a single-layer shadow mask/etching microstrip technology, resulting in the merits of simple and planar structure, low profile, low weight, compact size, and easy fabrication. In addition, compared to the reported patch antennas [25, 26], our proposed patch antenna has the compact volume and a much better aperture efficiency. In summary, the proposed antenna has the advantages of more compact volume, better gain, and higher aperture efficiency. Hence, we provide a method to solve some limitations (low gain, low radiation efficiency) of the conventional patch antenna. It is regarded that using the planar ZIM to improve the gain of the conventional patch antenna is significant in this paper.

4. Conclusions

In this work, a wideband planar ZIM is investigated. According to the zero index, two high-gain patch antennas based on the ZIM cover are designed and fabricated. The optimal distance between the patch and the ZIM cover and the number of the ZIM layers are demonstrated. The antenna performances are studied with simulations and measurements. The results show that the energy radiated by the ZIM cover antennas becomes more concentrate. As a result, the more directional and higher gain antennas are obtained. The average gain for the narrowband proposed antenna is improved by 4.23 dB. Besides the narrowband antenna, the antenna performance is improved at the wideband frequencies when the ZIM cover is placed above the wideband patch antenna. The average gain for the proposed wideband antenna is improved by 4.37 dB as compared with the antenna without the ZIM cover.

It is significant that the wideband high-gain planar patch antenna based on the ZIM cover is realized. It is expected that the proposed high-gain antenna can be applied in the fields of high-rate data transmission, high-resolution radar systems, and among other fields. In addition, the ZIM has the merits of simple structure, compact size, and most importantly it can improve the antenna performances greatly at the wideband frequency. Furthermore, the planar ZIM cover can also be used with the other antennas such as monopoles, dipole antennas, leak-wave antennas, and aperture antennas.

Acknowledgments

This work is supported by the National Natural Science Foundation of China under Grants 11204241, 50936002, and 51272215, and by the NPU Foundation for Basic Research under Grants JC201154 and JC201153, and by the NPU Aoxiang Star Project.

References

[1] J. B. Pendry, A. J. Holden, W. J. Stewart, and I. Youngs, "Extremely low frequency plasmons in metallic mesostructures," *Physical Review Letters*, vol. 76, no. 25, pp. 4773–4776, 1996.

[2] J. B. Pendry, A. J. Holden, D. J. Robbins, and W. J. Stewart, "Magnetism from conductors and enhanced nonlinear phenomena," *IEEE Transactions on Microwave Theory and Techniques*, vol. 47, no. 11, pp. 2075–2084, 1999.

[3] H. S. Chen, L. X. Ran, J. T. Huangfu et al., "Left-handed materials composed of only S-shaped resonators," *Physical Review E*, vol. 70, no. 5, Article ID 057605, 2004.

[4] E. Kim, Y. R. Shen, W. Wu et al., "Modulation of negative index metamaterials in the near-IR range," *Applied Physics Letters*, vol. 91, no. 17, Article ID 173105, 2007.

[5] J. Zhou, L. Zhang, G. Tuttle, T. Koschny, and C. M. Soukoulis, "Negative index materials using simple short wire pairs," *Physical Review B*, vol. 73, no. 4, Article ID 041101, 2006.

[6] X. Zhou, Y. Liu, and X. P. Zhao, "Low losses left-handed materials with optimized electric and magnetic resonance," *Applied Physics A*, vol. 98, no. 3, pp. 643–649, 2010.

[7] H. T. Jiang, Z. L. Wang, Y. Sun et al., "Enhancement of (nearly) homogeneous fields in a (effective) zero-index cavity," *Journal of Applied Physics*, vol. 109, no. 7, Article ID 073113, 2011.

[8] Y. Jin and S. He, "Enhancing and suppressing radiation with some permeability-near-zero structures," *Optics Express*, vol. 18, no. 16, pp. 16587–16593, 2010.

[9] M. Silveirinha and N. Engheta, "Tunneling of electromagnetic energy through subwavelength channels and bends using ε-near-zero materials," *Physical Review Letters*, vol. 97, no. 15, Article ID 157403, 2006.

[10] R. Liu, Q. Cheng, T. Hand et al., "Experimental demonstration of electromagnetic tunneling through an epsilon-near-zero metamaterial at microwave frequencies," *Physical Review Letters*, vol. 100, no. 2, Article ID 023903, 2008.

[11] B. Edwards, A. Alù, M. E. Young, M. Silveirinha, and N. Engheta, "Experimental verification of epsilon-near-zero metamaterial coupling and energy squeezing using a microwave waveguide," *Physical Review Letters*, vol. 100, no. 3, Article ID 033903, 2008.

[12] Y. Jin, P. Zhang, and S. He, "Squeezing electromagnetic energy with a dielectric split ring inside a permeability-near-zero metamaterial," *Physical Review B*, vol. 81, no. 8, Article ID 085117, 2010.

[13] V. C. Nguyen, L. Chen, and K. Halterman, "Total transmission and total reflection by zero index metamaterials with defects," *Physical Review Letters*, vol. 105, no. 23, Article ID 233908, 2010.

[14] J. Hao, W. Yan, and M. Qiu, "Super-reflection and cloaking based on zero index metamaterial," *Applied Physics Letters*, vol. 96, no. 10, Article ID 101109, 2010.

[15] S. Enoch, G. Tayeb, P. Sabouroux, N. Guérin, and P. Vincent, "A metamaterial for directive emission," *Physical Review Letters*, vol. 89, no. 21, Article ID 213902, 2002.

[16] B. I. Wu, W. Wang, J. Pacheco, X. Chen, and J. A. Kong, "A study of using metamaterials as antennasubstrate to enhance gain," *Progress in Electromagnetics Research*, vol. 51, pp. 295–328, 2005.

[17] Z. B. Weng, Y. Song, Y. C. Jiao, and F. S. Zhang, "A directive dual-band and dual-polarized antenna with zero index metamaterial," *Microwave and Optical Technology Letters*, vol. 50, no. 11, pp. 2902–2904, 2008.

[18] H. Zhou, Z. Pei, S. Qu et al., "A novel high-directivity microstrip patch antenna based on zero-index metamaterial," *IEEE Antennas and Wireless Propagation Letters*, vol. 8, pp. 538–541, 2009.

[19] Y. L. Lv, F. Y. Meng, J. Hua, and M. L. Chen, "A wideband zero index metamaterial lens for directive emission based on Z-shaped meta-atom," in *Proceedings of the 5th Global Symposium on Millimeter Waves (GSMM '12)*, pp. 418–421, 2012.

[20] Q. W. Hou, H. F. Tang, Y. H. Liu, and X. P. Zhao, "Dual-frequency and broadband circular patch antennas with a monopole-type pattern based on epsilon-negative transmission line," *IEEE Antennas and Wireless Propagation Letters*, vol. 11, pp. 442–445, 2012.

[21] Y. H. Liu, S. Gu, C. R. Luo, and X. P. Zhao, "Ultra-thin broadband metamaterial absorber," *Applied Physics A*, vol. 108, pp. 19–24, 2012.

[22] Y. Yao, X. Wang, and J. Yu, "Multiband planar monopole antenna for LTE MIMO systems," *International Journal of Antennas and Propagation*, vol. 2012, Article ID 890705, 6 pages, 2012.

[23] D. R. Smith, D. C. Vier, T. Koschny, and C. M. Soukoulis, "Electromagnetic parameter retrieval from inhomogeneous metamaterials," *Physical Review E*, vol. 71, no. 3, Article ID 036617, 2005.

[24] R. Garg, R. Bhartia, I. Bahl, and A. Ittipiboon, *Microstrip Antenna Design Handbook*, Artech House, Boston, Mass, USA, 2001.

[25] A. P. Feresidis, G. Goussetis, S. Wang, and J. C. Vardaxoglou, "Artificial magnetic conductor surfaces and their application to low-profile high-gain planar antennas," *IEEE Transactions on Antennas and Propagation*, vol. 53, no. 1 I, pp. 209–215, 2005.

[26] F. M. Zhu, Q. C. Lin, S. L. He, J. Hu, and Z. N. Ying, "A high directivity patch antenna using a PBG cover together with a PBG substrate," in *Proceeding of the 6th International Symposium on Antennas, Propagation and EM Theory*, pp. 92–95, November 2003.

Hindawi Publishing Corporation
International Journal of Antennas and Propagation
Volume 2013, Article ID 149296, 6 pages
http://dx.doi.org/10.1155/2013/149296

Research Article

Printed Modified Bow-Tie Dipole Antenna for DVB/WLAN Applications

Ching-Chih Hung, Chia-Mei Peng, and I-Fong Chen

Department of Electronic Engineering, Institute of Computer and Communication Engineering, Jinwen University of Science and Technology, No. 99 An-Chung Road, Hsintien City 23154, Taipei, Taiwan

Correspondence should be addressed to I-Fong Chen; ex0206@just.edu.tw

Received 28 April 2013; Revised 24 June 2013; Accepted 27 June 2013

Academic Editor: Bal Singh Virdee

A printed modified bow-tie dipole antenna which consists of asymmetric-feed and inserted slots is presented to apply to the DVB and WLAN systems. This antenna combines omnidirectional radiation pattern, broad bandwidth, and band rejection in an easy way to fabricate. Experimental results of the constructed prototype indicate that the VSWR 2.5 : 1 bandwidths achieve 166.7%, 28.57%, and 23.63% at 660 MHz, 2450 MHz, and 5500 MHz, respectively.

1. Introduction

An increasingly popular paradigm for wireless communications considers clusters of cooperating networks, which offer the user seamless access through a range of technologies such as digital video broadcasting (DVB, UHF band: 470–862 MHz) and wireless local area network (WLAN, ISM bands: 2.4–2.4835 GHz and 5.15–5.825 GHz) [1]. The interworking wireless technologies, such as WLAN with DVB networks, provide the user with a return link for interactive TV and high bandwidth asymmetric downlink for data transfer to terminals operating in the heterogeneous roaming environment. Therefore, the desired antenna design must be able to cover both DVB and WLAN systems at the same time and to include dual-band/broad bandwidth, simple impedance matching to the feed line, and low profile. The bow-tie dipole antenna has become the main candidate for the above application since its bandwidth performances are reasonably better than other alternatives [2]. However, it is difficult for the traditional printed bow-tie dipole antenna to meet multiband operation for respective communication systems. The solution is to design a dual- or multiband integrated antenna for wireless product applications. For this purpose, in this paper, we introduce a printed modified bow-tie dipole antenna which combines band-rejection slots and asymmetric-feed structure to yield three operating bands [3]. The printed modified bow-tie dipole arms adjustable in position will yield an asymmetrical structure. The impedance matching is obtained through tuning the shifted distance of the arms [4]. The band rejection is obtained by inserting some slots in the dipole arms [5–9]. Details of the specification of the proposed designs and the experimental results of constructed prototype are presented and discussed in the following sections.

2. Antenna Structure and Design

Figure 1 shows the proposed asymmetric modified bow-tie dipole antenna for DVB and WLAN applications. The presented antenna structure is composed of a modified bow-tie dipole radiating element section of length L, width W, flare angle θ, and shifted distance D, which is printed on a 1.6 mm thick FR4 glass epoxy substrate (the relative permittivity is 4.3). The fundamental resonant mode of modified bow-tie dipole is designed to occur at about 660 MHz (the center frequency of the lower operating band: 470–862 MHz). The dipole length and width can be determined from the half- and quarter-wave lengths of the resonant frequencies. Note that the flare angle of modified bow-tie dipole is a function of operating bandwidth. In general, the bandwidth of the lower operating band increases with an increase in the flare angle. By determining appropriate dimensions (L, W, D, and θ)

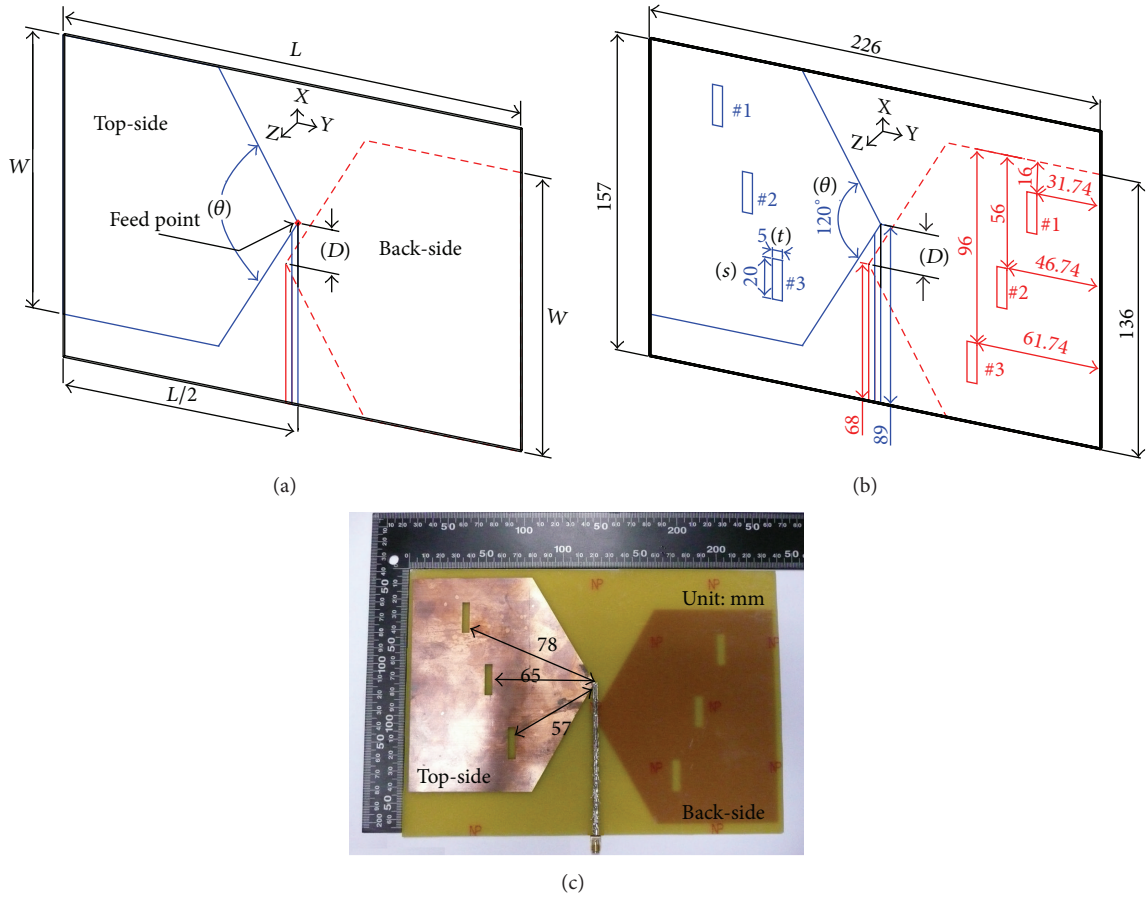

FIGURE 1: (a) Geometry of the original antenna. (b) Geometry of the proposed antenna. (c) Implemented prototype of the proposed antenna.

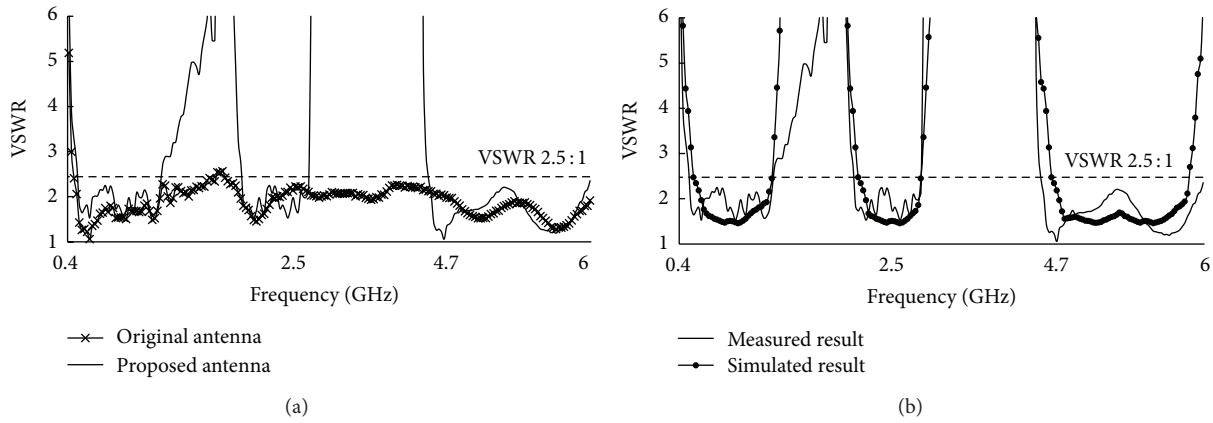

FIGURE 2: (a) Measured VSWR against frequency of the original and proposed antenna. (b) Measured and simulated VSWR against frequency of the proposed antenna.

of the antenna structure, good impedance matching of the printed modified bow-tie dipole can be obtained across an extended bandwidth. A parallel-strip feed excites the modified bow-tie dipole arms with shifted distance D to be of asymmetric structure as shown in Figure 1(a), denoted as the original antenna. The shape of the original antenna is designed for wideband operation. For fitting in with a 50 Ω feed system and to obtain an extended bandwidth, the shifted distance D should be $\lambda/20$ [4]. The band rejection of the dipole structure is obtained by inserting some slots in the dipole arms. Note that the size and number of the slots are not identical. The impedance matching at UHF band (470–862 MHz) and dual ISM band (2.4 GHz and 5.8 GHz) can be tuned by adjusting the size of the slots on the dipole arms.

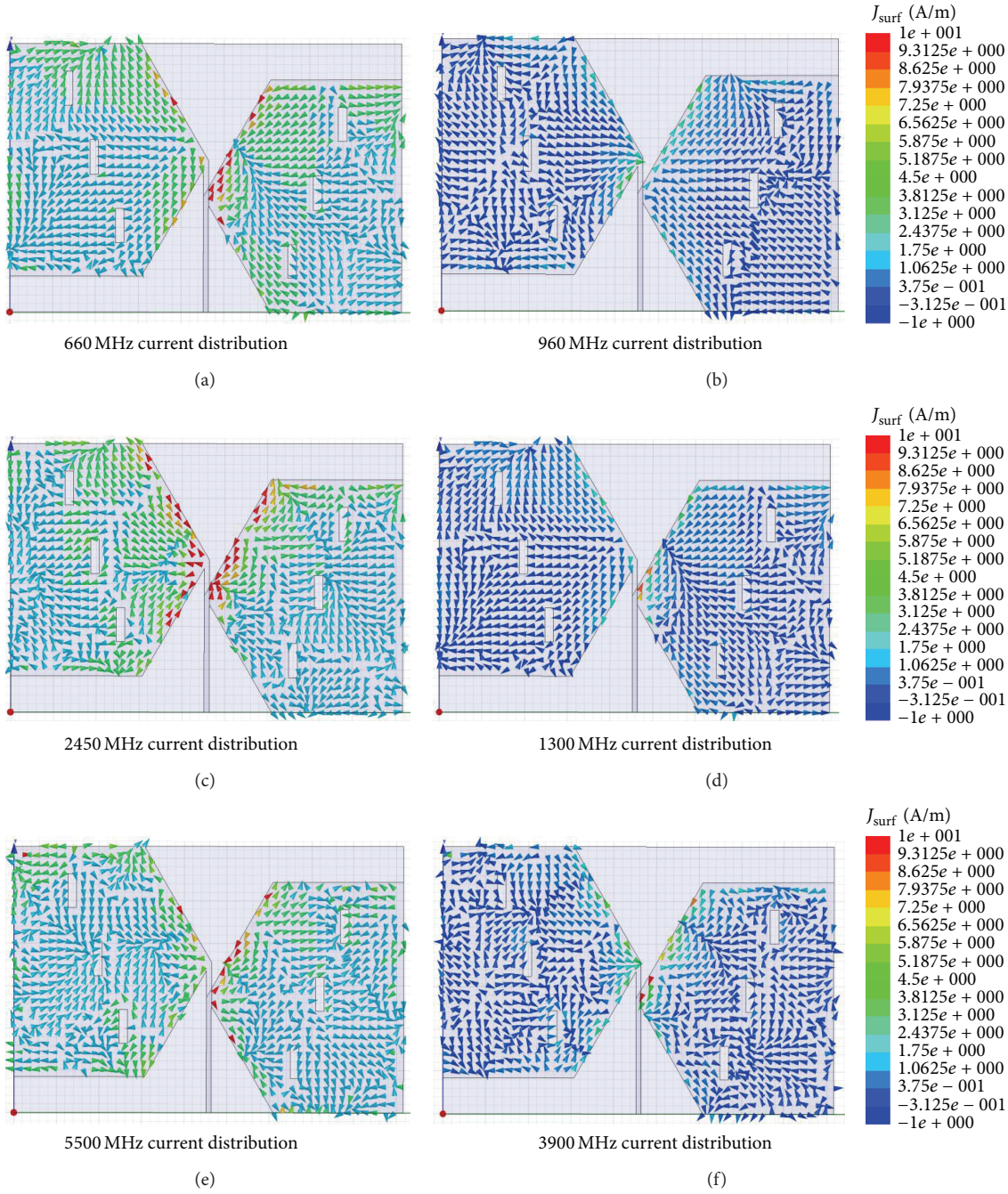

FIGURE 3: Simulated current density versus frequency on the modified bow-tie dipole arms.

3. Experimental Results and Discussion

In the experiment, the parallel-strip feed of the proposed antenna is connected to a 50 Ω SMA connector. By using the described design procedure, the original antenna is constructed to operate the VSWR ≤2.5 in the range of 450 MHz to 6 GHz, as shown in Figure 2(a), with modified bow-tie dipole-arm's size: length L = 22.6 cm, width W = 13.6 cm, flare angle θ = 120°, and shifted distance D = 2.1 cm [4]. Based on the experimental studies, the effects of key parameters (e.g., slots location, slots sizes, and slots numbers) are tested and optimized. In this paper, there are three same size insertion slots on the dipole arms. The slots are located at quarter-wave length of the undesired frequencies from the feed point (i.e., about 78 mm, 65 mm, and 57 mm, resp., at 960 MHz, 1150 MHz, and 1300 MHz). The optimal length (s) and width (t) of the slots are 20 mm and 5 mm, respectively. Figure 2(a) also shows the VSWR plot of the multiband antenna as a result of this design. Figure 2(b) shows the measured and simulated VSWR plot of the proposed antenna and the VSWR ≤2.5 bandwidths are 1100 MHz (166.71%), 700 MHz (28.57%), and 1300 MHz

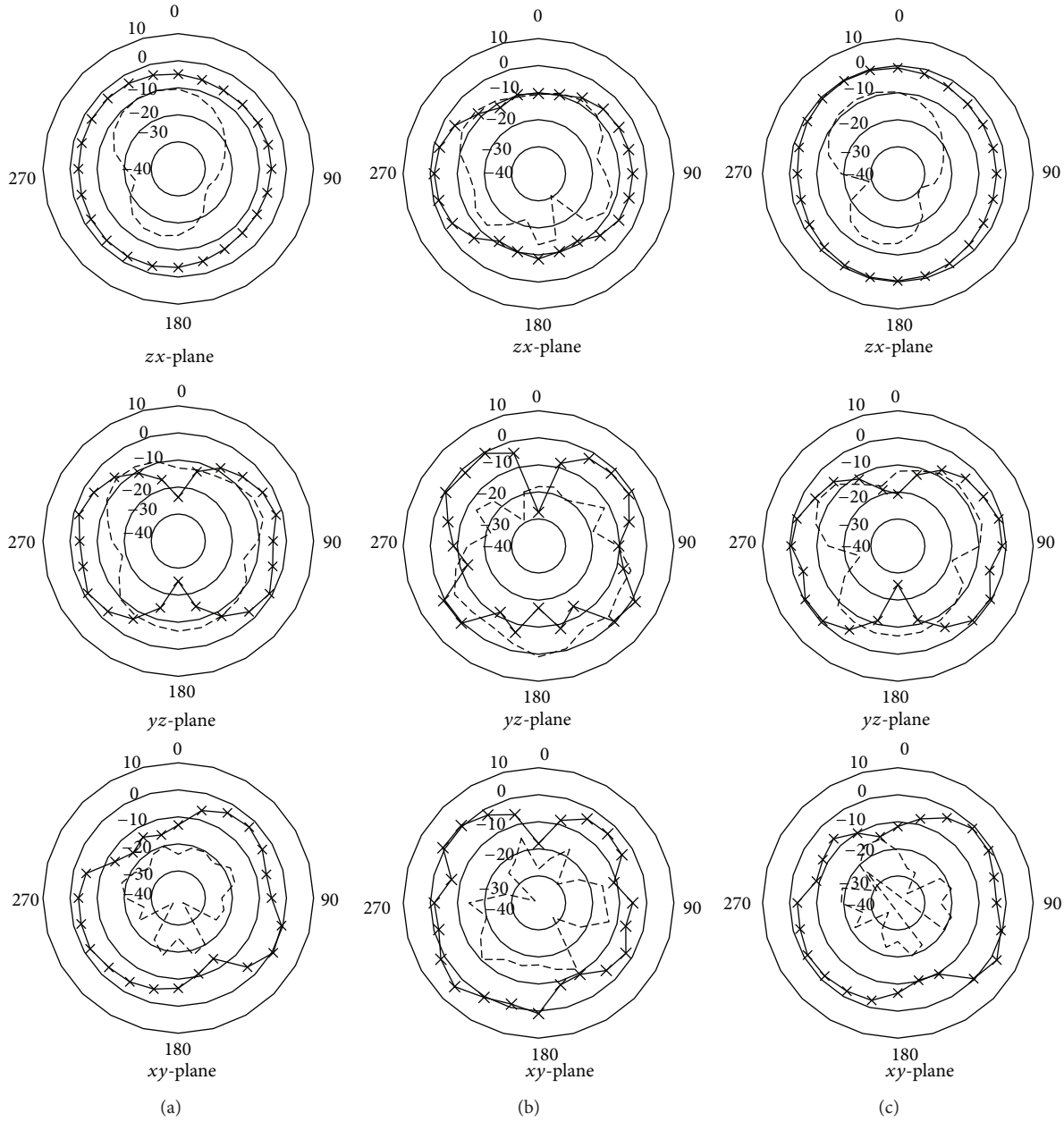

Figure 4: Measured radiation patterns for the proposed antenna (-×- copolar.—cross-polar.). (a) 660 MHz, (b) 2450 MHz, and (c) 5500 MHz.

(23.63%) at 660 MHz, 2450 MHz, and 5500 MHz, which meet the required bandwidths of the DVB and WLAN systems. The simulated results are obtained by using the Ansoft HFSS. We can also find that a good agreement between the simulation and the measurement is obtained. The simulation results of the current density on the proposed antenna are shown in Figure 3. Because the impedance mismatching at 960 MHz, 1300 MHz, and 3900 MHz results in the surface current density being lower than 660 MHz, 2450 MHz, and 5500 MHz, the slots are located at quarter-wave length of the undesired frequencies from the feed point that has also been verified.

Figure 4 presents the measured radiation patterns for free space in the yz-plane (E-plane) and the zx-plane (H-plane). The maximum gains in the E-plane and H-plane are 0.13 dBi, 1.27 dBi, and 1.04 dBi and 0.09 dBi, 0.04 dBi, and 0.11 dBi, respectively, at 660 MHz, 2450 MHz, and 5500 MHz. The gain response with frequency is shown in Figure 5, indicating that the effect of band rejection is remarkable. Table 1 shows the measured antenna gains and 3D pattern efficiency within the operating bands of the proposed antenna. Stable radiation patterns are observed. The total 3D pattern efficiency is defined as (gain/directivity) × 100%, which was done by using pattern integration employing the ETS-Lindgren anechoic chamber. Acceptable radiation characteristic for the practical applications is obtained for the proposed antenna. The omni-directional feature of the proposed antenna can also be observed from the horizontal plane. The operating

Table 1: The measured antenna gains within the operating bandwidth of the proposed antenna.

Frequency (MHz)	*H*-plane (*zx*-plane)		*E*-plane (*yz*-plane)	3D pattern
	Max. gain	Avg. gain	Max. gain	Efficiency (%)
470	−2.37	−4.43	0.19	51.22
660	0.09	−3.77	0.13	56.56
860	0.91	−3.03	0.94	58.71
2400	0.06	−3.76	0.43	66.45
2450	0.04	−3.61	1.27	65.52
2500	0.06	−3.15	1.43	68.72
5150	1.01	−2.76	0.93	69.71
5500	0.11	−3.31	1.04	71.23
5850	1.09	−3.05	1.76	70.52

Max.: maximum and Avg: average.

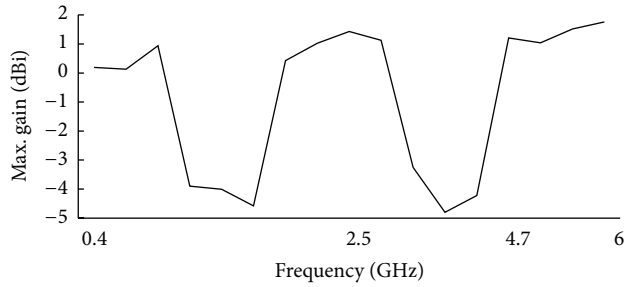

Figure 5: Measured antenna gain versus frequency.

bandwidth of the proposed antenna with usable broadside radiation patterns is consistent with the specification of DVB and WLAN systems.

The effect on the antenna performance by varying the insertion-slot numbers and dimensions has been studied, and the results are described below. The structure of insertion slot is a rectangular slot, as shown in Figure 1(b). The corresponding characteristics of resonant frequency, input impedance, and bandwidth are a function of the geometrical parameters of the insertion-slot structure. The experimental results of varying insertion-slot numbers and sizes were obtained by measurement, as shown in Figure 6. According to the above analyses, it is obvious that the inserted slots are used for the band rejection. Figure 6(a) shows impedance characteristics with various numbers of inserted slots, which control the operating bands. Measurement results show that by inserting three slots, the desired operating bands can be obtained. In the UHF band, an increase in the insertion-slot length (s) leads to an increase in impedance bandwidth. Contrarily, the insertion-slot length (s) has a negative effect on impedance bandwidth in the dual-ISM band; the measurement results are shown in the Figure 6(b). On the other hand, an increase in the insertion-slot width (t) leads to a decrease in impedance bandwidth in the UHF band, while in the dual-ISM band, there is a positive relation between insertion-slot width (t) and impedance bandwidth, as shown in Figure 6(c). The optimal slot sizes of length (s) and width (t) are 20 mm and 5 mm, which will provide the appropriate operating band for DVB and WLAN system applications.

4. Conclusion

It has been demonstrated that a printed modified bow-tie dipole provides multiband operation. By correctly choosing the width of the slots, three bandwidths, defined for a VSWR lower than 2.5, achieving 166.71%, 28.57%, and 23.63%, respectively, at 660 MHz, 2450 MHz, and 5500 MHz, can be obtained. The contribution of this paper is to implement a simple and easy fabrication antenna for practical DVB and WLAN applications. The locations of the inserted slots on the dipole arms have been confirmed. The slots are located at quarter-wave length of the undesired frequencies from the feed point. Measurement results show that the structure indeed offers broad bandwidth and band rejection characteristics. Although this antenna was designed for DVB and dual ISM-band applications, its design concept can be extended to other frequency bands of interest.

Acknowledgments

This work was sponsored by the National Science Council, Taiwan, under the Contract no. 100-2221-E-228-001 and Wieson Corp. Tech. (http://www.wieson.com/), Taiwan,

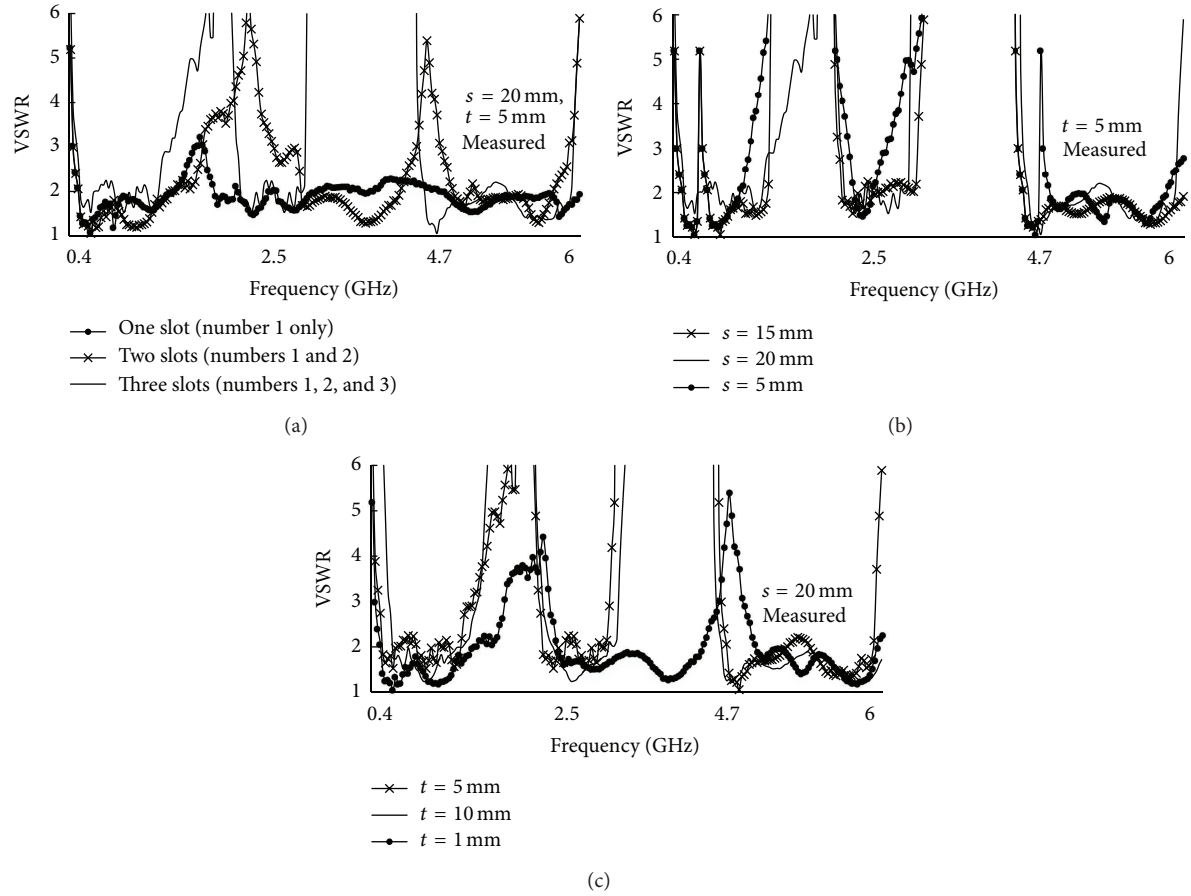

Figure 6: Measured VSWR as a function of (a) the inserting-slot numbers, (b) the inserting-slot length (s), and (c) the inserting-slot width (t). Other dimensions are the same as given in Figure 1.

under Contract no. JW100-F-411-148. The authors also appreciate the reviewer's comments that improved the quality of this paper.

References

[1] D. Morris, P. Pangalos, and A. H. Aghvami, "Mobile terminal location discovery schemes for a "Beyond 3G" inter-worked network," in *Proceedings of the sixth IEEE International Symposium on WoWMom*, pp. 401–406, June2005.

[2] J. D. Kraus and R. J. Marhefka, *Antennas*, McGraw-Hill, New York, NY, USA, 2002.

[3] R. Jordan and C. T. Abdallah, "Wireless communications and networking: an overview," *IEEE Antennas and Propagation*, vol. 44, no. 1, pp. 185–193, 2002.

[4] C.-M. Peng, I.-F. Chen, C.-C. Hung, and H.-C. Chen, "Printed modified bow-tie dipole antenna for multi-band applications," *IEICE Transactions on Communications*, vol. 92, no. 4, pp. 1404–1405, 2009.

[5] Q.-X. Chu and Y.-Y. Yang, "3.5/5.5 GHz dual band-notch ultra-wideband antenna," *Electronics Letters*, vol. 44, no. 3, pp. 172–174, 2008.

[6] K. Chung, S. Hong, and J. Choi, "Ultrawide-band printed monopole antenna with band-notch filter," *IET Microwaves, Antennas and Propagation*, vol. 1, no. 2, pp. 518–522, 2007.

[7] D.-O. Kim, N.-I. Jo, H.-A. Jang, and C.-Y. Kim, "Design of the ultrawideband antenna with a quadruple-band rejection characteristics using a combination of the complementary split ring resonators," *Progress in Electromagnetics Research*, vol. 112, pp. 93–107, 2011.

[8] H. H. Yong, M. S. Deokong, and C. Kyoung:, "Wideband bow-tie monopole antenna having an improved band rejection characteristic," Korea Patent: KR 20080858969 B1, 2008.

[9] A. A. Gheethan and D. E. Anagnostou, "Dual band-reject UWB antenna with sharp rejection of narrow and closely-spaced bands," *IEEE Transactions on Antennas and Propagation*, vol. 60, no. 4, pp. 2071–2076, 2012.